ADVANCED LECTURES 1986

DYNAMICAL PROCESSES IN OCEANOGRAPHY

DR M J DAVEY

Advanced lectures on dynamical processes

Meteorological Office, Bracknell, September 15-19, 1986

M. K. Davey

Met. Office Unit

Hooke Institute for Atmospheric Research

Clarendon Laboratory

Oxford

Overview

The aim of these five lectures is to describe the application of simple models to the dynamics of the tropical oceans and atmosphere.

The major El Nino event in 1982-83 is a recent example of substantial ocean-atmosphere interaction, when large departures from climatology occurred. Some of these are shown in Fig. 1.1, adapted from Gill & Rasmusson (1983). (Further details are given in lecture 5.) Fig. 1.1a shows a large negative anomaly in outgoing longwave radiation (OLR) moving eastward across the tropical Pacific. This is associated with deep convection and precipitation, and represents a heat source for the atmosphere through latent heating. This pattern is related to underlying anomalously warm sea surface temperature. In lecture 4 a model is used to explain how the atmosphere reacts to such a heat source.

Fig. 1.1b similarly shows a westerly low-level wind anomaly, and lecture 3 includes the response of an ocean model to such changes in surface wind stress.

The anomalies shown occur together: evidently the atmosphere drives the ocean while the ocean drives the atmosphere. The precise nature of this

strong coupling is not yet well understood: in lecture 5 some simple mechanisms are investigated. (Work on much more complex coupled general circulation models to simulate, and hopefully predict, El Nino events is in progress within Met. O. 20.)

Equatorial waves are essential to an understanding of the dynamics, and the properties of such waves and the effects of boundaries are described in lecture 2.

The simple models to be described are based on the linear shallow water equations, and they have been particularly useful for tropical regions where the propagation speed of equatorially-trapped waves is relatively fast. (Linear theory is better for larger wave-speed/particle-speed ratio.) Although linear models usually only qualitatively represent observed behaviour, a linear shallow-water ocean model has been surprisingly good at reproducing the observed interannual variability in equatorial Pacific sea level when driven by the observed wind stress (Busalacchi & O'Brien 1980, 1981 and Busalacchi at. al. 1983).

The shallow-water equations are reviewed in lecture 1, with an introduction to Kelvin waves.

Throughout this lecture series reference will often be made to papers by Adrian Gill (especially to his book on Ocean-Atmosphere Dynamics), who made an enormous contribution to this field by explaining apparently complex phenomena with simple models.

Lecture 1: The shallow-water equations

In this lecture linear shallow-water equations (SWE) are reviewed in the context of a shallow sea, then used to introduce the coastally-trapped Kelvin wave. The SWE are then related to vertical normal modes, for continuous and discrete stratification.

A frame of reference with constant rotation rate (f-plane) is assumed for this lecture.

1.1 Homogeneous shallow sea

Consider a homogeneous ocean with constant depth H at rest, density ρ, and surface displacement η, as illustrated in Fig. 1.2 . We restrict attention to motion with a horizontal scale much greater than H, so the hydrostatic balance

$$p_z = -\rho g \tag{1.1}$$

is assumed. Then the horizontal pressure gradient is independent of depth and is related to the surface displacement by

$$\nabla p = \rho g \nabla \eta \quad , \tag{1.2}$$

where $\nabla = \left(\frac{\partial}{\partial x}, \frac{\partial}{\partial y} \right)$.

Consequently the horizontal flow $\underline{u} = (u,v)$ driven by this pressure gradient is also depth-independent.

The total depth of water is

$$h = H + \eta \tag{1.3}$$

and mass conservation requires

$$h_t + \nabla.(h\underline{u}) = 0 \quad . \tag{1.4}$$

For small disturbances with $\eta << H$ the approximate linear form that we will use is

$$\eta_t + H \nabla.\underline{u} = 0 \quad . \tag{1.5a}$$

The linear form of the momentum equations on an f-plane is

$$u_t - f_0 v = -\frac{1}{\rho} p_x = -g \eta_x \quad , \tag{1.5b}$$

$$v_t + f_0 u = -\frac{1}{\rho} p_y = -g \eta_y \quad . \tag{1.5c}$$

Equations (1.5) constitute the linear shallow-water equations.

These equations have plane-wave solutions of the form

$$\exp \{ i(kx+ly-\omega t) \} \tag{1.6}$$

On substitution, the dispersion relation for Poincare waves is obtained:

$$\omega^2 = f_0^2 + (k^2 + l^2) c^2 \tag{1.7}$$

where

$$c = (gH)^{1/2} \tag{1.8}$$

is the speed of gravity waves in the absence of rotation (i.e. when $f_o=0$).

Eq. (1.8) can be rewritten as

$$(\omega/f_o)^2 = 1 + (k^2+l^2)a^2 \qquad (1.9)$$

where

$$a = c/f_o \qquad (1.10)$$

is the Rossby radius of deformation. Beacuse $2\pi a$ is the distance a gravity wave would travel in a rotation period, this is the scale on which rotation effects become significant. For length scales << a, waves are little affected by rotation, but for length scales >> a rotation dominates and $\omega \tilde{=} f_o$. Gravity has no effect on these long waves, which are known as inertial waves. The group velocity c_g of such waves is nearly zero (compared with $c_g = c$ for the short gravity waves), so such waves do not transmit information away from their source region.

1.2 The response to uniform wind stress

Suppose the ocean is at rest, and a spatially uniform surface wind stress F>0 is switched on at time t=0. The depth averaged effect is as though the wind were a uniform body force throughout the depth H (Ekman spiral details are not relevant here), and with no horizontal pressure gradient the momentum equations are

$$u_t - f_o v = \frac{1}{\rho}\frac{F}{H}, \qquad (1.11a)$$

$$v_t + f_o u = 0. \qquad (1.11b)$$

The subsequent motion consists of a steady current (Ekman drift) to the right of the wind (northern hemisphere) given by

$$v_E = -\frac{F}{\rho H f_0} \tag{1.12}$$

plus an inertial oscillation. (With no pressure gradient there are no gravity waves.) With $\underline{u}=0$ at $t=0$ we find

$$u = -v_E \sin(f_0 t) \quad , \tag{1.13a}$$

$$v = v_E \left[1 - \cos(f_0 t) \right] \quad . \tag{1.13b}$$

The path of a particle starting at (x_0, y_0) at $t=0$ is

$$x = x_0 + \frac{v_E}{f_0} \cos(f_0 t) \tag{1.14a}$$

$$y = y_0 + v_E t - \frac{v_E}{f_0} \sin(f\ t) \tag{1.14b}$$

taking the cycloidal shape shown in Fig. 1.3 . (See also Gill book, Fig. 9.2.)

1.3 The effect of a coastline

Suppose there is a coast, represented by a vertical wall, along $y=0$ as in Fig. 1.4, and there is a longshore wind stress F as before. The coast now blocks the Ekman drift v_E so water tends to pile up at the coast and an offshore pressure gradient develops. Neglecting transient effects associated with initial conditions, the response is a steady onshore current decaying to zero at the coast:

$$v = v_E \left[1 - \exp\{-y/a\} \right] \quad , \qquad (1.15a)$$

rising sea level near the coast:

$$\eta = \frac{F}{\rho c} \exp\{-y/a\}\, t \quad , \qquad (1.15b)$$

and an increasing geostrophic longshore current:

$$u = -g\eta_x / f_o = -v_E \exp\{-y/a\}\, f_o t \quad . \qquad (1.15c)$$

The important feature here is that the effect of the coast is confined to a region which has the Rossby radius as a width scale.

Example:

A shallow sea of depth 50m at 50 N has a = 230 Km. A longshore wind stress F = 2 N m-2 would cause a sea level rise of 1m in 3 hours at the coast.

1.4 The coastal Kelvin wave

One effect limiting the amplitude of the above response is the finite space and time scale of the wind. To simplify the algebra in this case, suppose the longshore scale of the wind is L >> a, as is usually the case. Then the longshore current is in geostrophic balance, the onshore wind component can be neglected, and wind far from the coast can be neglected. Then the SWE set reduces to

$$u_t - f_o v = -g\eta_x + \frac{F(x,t)}{\rho H} \quad , \qquad (1.16a)$$

$$f_0 u = -g \eta_y \quad , \tag{1.16b}$$

$$\eta_t + H \nabla \cdot \underline{u} = 0 \quad . \tag{1.16c}$$

This leads to

$$v = v_{\infty} [\, 1 - \exp\{-y/a\} \,] \tag{1.17}$$

(as before), and

$$\eta / H = u/c = A(x,t) \exp\{-y/a\} \tag{1.18}$$

where the amplitude A at the coast is governed by

$$A_t + c A_x = \frac{F}{\rho H c} \quad . \tag{1.19}$$

(Note that $u \ll c$ when $\eta \ll H$.) This is the equation for a forced wave travelling with speed c in the +x direction. That is, the coast is on the right (northern hemisphere) when looking in the direction of propagation of this wave.

Example: consider

$$F(x,t) = F_0 \begin{cases} \frac{1}{2}\pi \sin(\pi t/\tau) & 0 \le t \le \tau, \quad 0 \le x \le L \\ 0 & \text{otherwise} \end{cases} \quad . \tag{1.20}$$

(F_0 is the average wind stress for $0<t<\tau$; $L=c\tau$ is chosen for

convenience.) Then for $0 \leq x/L \leq 1$:

$$A = A_0 \begin{cases} 1 - \cos[\pi t/\tau] & 0 \leq t/\tau \leq x/L \\ \cos[\pi(t/\tau - x/L)] - \cos[\pi t/\tau] & x/L \leq t/\tau \leq 1 \\ 1 + \cos[\pi(t/\tau - x/L)] & 1 \leq t/\tau \leq 1 + x/L \\ 0 & 1 + x/L \leq t/\tau \end{cases} \quad (1.21a)$$

where $A_0 = \dfrac{F_0}{2\rho H c}$, and for $1 \leq x/L$:

$$A = A_0 \begin{cases} 0 & 0 \leq t/\tau \leq x/L - 1 \\ 1 + \cos[\pi(t/\tau - x/L)] & x/L - 1 \leq t/\tau \leq x/L + 1 \\ 0 & x/L + 1 \leq t/\tau \end{cases} \quad (1.21b)$$

The response A can be seen more clearly in the time-longshore map in Fig. 1.5a. After time $t/\tau = 1$ there is no forcing and the response is a free wave travelling along the coast at speed c, trapped near the coast. This is a coastal Kelvin wave. The spatial structure (1.18) is shown in Fig. 1.5b for time $t/\tau = 2$: remember that L>>a.

Features of the free Kelvin wave:

- it is a solution of the full SWE set (1.5)
- $v = 0$, so flow is alongshore only
- $f_0 u = -g \eta_y$, longshore geostrophy
- group velocity $c_g = c$, so the wave is non-dispersive and will travel along the coast without change of shape
- the wave propagates at the gravity wave speed, so it allows rapid transmission of information alongshore away from the source
- coastally trapped, with decay scale a offshore
- unidirectional propagation with the coast on the right (northern hemisphere; vice-versa for southern hemisphere)

In a section parallel to the coast, this Kelvin wave looks like a non-rotating gravity wave travelling in the +x direction. Why not in the -x direction? This would require u and η to have opposite signs, and longshore geostrophy would require $|\eta|$ increasing offshore without bound. So what happens in a channel? See Gill book, chapter 10.

The coastal Kelvin wave is clearly an important component in storm surge prediction: it is essential to know when and where a (perhaps remotely) forced surge may coincide with a high tide, for example. In practice, a quantitative model needs to take into account other factors such as coastline shape, dissipation, and nonlinearity.

1.5 Kelvin wavesin the atmosphere

'Coastal' Kelvin waves also occur in the atmosphere, being trapped against high ground rather than coastlines. Fig. 1.6 from Gill (1977) shows a region of low surface pressure following a high escarpment around southern Africa (keeping the high ground on the left, for this is in the

southern hemisphere). In his paper, Gill describes a simple model of this event, similar to the simple model above.

The waves can be highs as well as lows: Fig. 1.7a shows high ground in south-eastern Australia, and in Fig. 1.7b a ridge can be seen forming and moving northward (again with the high ground on the left). Further details can be seen in Holland & Leslie (1986).

1.6 Stratification

The preceding atmospheric observations were in a stratified medium, rather than the homogeneous shallow sea described earlier. The SWE can easily be applied to stratified flow, however, by separating out the vertical structure.

Fig. 1.8a is a sketch of a typical vertical profile of density in the deep ocean: a mixed layer of nearly uniform density overlying a thermocline region of rapidly changing density overlying a deep region of slowly increasing density.

(a) Discrete stratification and the 'shallow-water ocean'

In ocean modelling it is common to represent the vertical density structure by two or more layers of constant density, such as in Fig. 1.8b. The flow calculated in each layer then represents a vertical average of the corresponding flow in the continuous case.

The linear continuity equation in layer j of depth h_j is

$$h_{jt} + H_j \nabla . \underline{u}_j = 0 \qquad (1.22)$$

where, for a two layer example,

$$h_1 = H_1 + \eta_1 - \eta_2 \qquad (1.23a)$$

$$h_2 = H_2 + \eta_2 \qquad (1.23b)$$

(We shall assume flat bottom topography.) Using the hydrostatic balance (1.1) the linear momentum equations can be written

$$\underline{u}_{1t} + f_o \underline{k} \times \underline{u}_1 = -g \nabla \eta_1 \qquad (1.24a)$$

$$\underline{u}_{2t} + f_o \underline{k} \times \underline{u}_2 = -g \nabla \eta_1 - g' \nabla \eta_2 \qquad (1.24b)$$

where

$$g' = g \frac{\rho_2 - \rho_1}{\rho_2} \qquad (1.25)$$

acts as a reduced gravity. For an ocean, g' is typically 10^{-3} g, and $H_1 << H_2$.

The equations (1.22) and (1.24) can be rewritten in terms of two vertical modes (see Gill book): a barotropic mode with

$$\underline{u}_1 \approx \underline{u}_2 \qquad (1.26a)$$

$$\eta_1 \approx \frac{H_1 + H_2}{H_2} \eta_2 \qquad (1.26b)$$

and gravity wave speed

$$c_o = [\, g (H_1 + H_2) \,]^{1/2} \qquad (1.26c)$$

(typically 200 m sec-1 for the major oceans); and a baroclinic mode with

$$H_1 \underline{u}_1 + H_2 \underline{u}_2 \approx \underline{0} \quad , \qquad (1.27a)$$

$$g \eta_1 \approx -g' \frac{H_2}{H_1 + H_2} \eta_2 \quad , \qquad (1.27b)$$

and gravity wave speed

$$c \approx \left[\frac{g' H_1 H_2}{H_1 + H_2} \right]^{1/2} , \qquad (1.27c)$$

(typically 2 m sec-1). The horizontal structure of each mode is governed by the SWE.

For baroclinically dominated cases (such as the tropical oceans) a further simplification is often made when $\underline{u}_2 \ll \underline{u}_1$ and $\eta_1 \ll \eta_2$. We assume the deep ocean is at rest (i.e. $\underline{u}_2 \equiv \underline{0}$) and set the lower layer pressure gradient to zero. From (1.24b) this requires (using $H_1 \ll H_2$)

$$g \eta_1 = - g' \eta_2 \quad . \tag{1.28}$$

Further, is neglected in (1.23a) and we obtain

$$\underline{u}_{1t} + f_0 \underline{k} \times \underline{u}_1 = - g' \nabla h_1 \quad , \tag{1.29a}$$

$$h_{1t} + H_1 \nabla . \underline{u}_1 = 0 \quad . \tag{1.29b}$$

This is the SWE set again, with reduced gravity g' and depth H_1 giving a gravity wave speed

$$c = (g' H_1)^{1/2} \quad . \tag{1.29c}$$

The depth change is due to variations in the interface between the two layers. The sea-level change η_1 can be obtained as a diagnostic from (1.28).

The model governed by (1.29) is variously known as a 'reduced gravity' or 'one-and-a-half layer' or 'shallow-water' ocean.

(b) Continuous stratification

An alternative to prescribing discrete layers of fixed density is to

prescribe a stratification $\rho_0(z)$ in the absence of motion and to consider small perturbations.

Incompressibility is assumed (compressibility has negligible effect on the atmospheric internal waves of interest):

$$u_x + v_y + w_z = 0 \quad . \tag{1.30a}$$

From (1.1)

$$p'_z = -\rho' g \tag{1.30b}$$

where p' and ρ' are perturbations from the rest state. The linearised density equation is

$$\rho'_t + w \frac{d\rho_0}{dz} = 0 \tag{1.30c}$$

and the linearised momentum equations are

$$\underline{u}_t + f_0 \underline{k} \times \underline{u} = -\frac{1}{\rho_0} \nabla p' \quad . \tag{1.30d}$$

To separate out the vertical structure we put

$$u = \psi(z)\, \hat{u}(x, y, t) \tag{1.31a}$$

$$v = \psi(z)\, \hat{v}(x, y, t) \tag{1.31b}$$

$$p' = \rho_0(z)\, g\, \psi(z)\, \hat{\eta}(x, y, t) \tag{1.31c}$$

$$w = \phi(z)\, \hat{w}(x, y, t) \tag{1.31d}$$

where ψ and ϕ are non-dimensional functions to be determined. Note that $\hat{\eta}$ has the dimension of vertical displacement.

The hydrostatic equation requires

$$\rho' = -(\rho_0 \psi)_z \hat{\eta} \tag{1.32a}$$

With

$$\psi = He\, \phi_z \tag{1.33a}$$

and

$$(\rho_0 \psi)_z = \frac{d\rho_0}{dz} \phi \tag{1.33b}$$

the equations (1.30) reduce to

$$\hat{\underline{u}}_t + f_0 \underline{k} \times \hat{\underline{u}} = -g \nabla \hat{\eta} \tag{1.34a}$$

$$\hat{\eta}_t + He\,(\hat{u}_x + \hat{v}_y) = 0 \tag{1.34b}$$

i.e. to the SWE form (1.6) with effective depth He and gravity speed $c=(gHe)^{1/2}$. The separation constant He (also referred to as equivalent depth) can be found from (1.33), e.g. by solving the eigenvalue problem

$$\frac{1}{\rho_0}(\rho_0 \phi_z)_z + \frac{N^2}{g\,He} \phi = 0 \tag{1.35}$$

with suitable boundary conditions. Here

$$N^2 = -\frac{g}{\rho_0} \frac{d\rho_0}{dz} .$$

(An infinite series of values for He is usually thus produced, each associated with a different vertical structure ϕ .) Note that from (1.33b) the density perturbation (1.32a) can also be written as

$$\rho' = -\frac{\alpha \rho_*}{\alpha z}\ \phi\ \hat{\eta} \quad . \qquad (1.32b)$$

For baroclinic modes in the ocean, suitable boundary conditions are $w = 0$ (hence $\phi = 0$) at the flat ocean floor and at a 'rigid-lid' surface. However this requires ρ' = 0 at z=0 according to (1.32b), so the surface density [and hence sea-surface temperature (SST)] must remain fixed.

The sets of modes ϕ and ψ are orthogonal in some sense, and any prescribed forcing can easily be projected onto these modes to obtain equivalent forcing terms for the corresponding SWE. However, thermal forcing thus expressed must vanish at the sea surface, so SST still cannot change for each vertical mode.

1.7 Diffusion and dissipation

Some representation of diffusion and dissipation is needed if a realistic long-time response to forcing is to be obtained. Terms with linear horizontal operators, such as $\rho_{xx} + \rho_{yy}$. can easily be added because the extra complexity is merely transferred in the same form to the SWE. Vertical transfers are often more important though, and unfortunately these are not easy to incorporate. The simplest representation is to use linear damping terms (Rayleigh friction and Newtonian 'cooling') to damp out perturbations, but these are not physically well-founded.

Terms like $(\nu u_z)_z$ can be included, but a particular form of $\nu(z)$ is needed. For later reference (lecture 3) a form used by McCreary (1981) for an ocean model is described below.

As is common for ocean models, density is replaced by the constant ρ_{oo} except where derivatives occur, so the continuous equations are

$$\underline{u}_t + f_o \underline{k} \times \underline{u} = -\frac{1}{\rho_{oo}} \nabla p' + (\nu \underline{u}_z)_z \tag{1.36a}$$

$$\rho'_t + w \frac{\alpha \rho_o}{\alpha z} = (K \rho')_{zz} \tag{1.36b}$$

$$p'_z = -\rho' g \tag{1.36c}$$

$$u_x + v_y + w_z = 0 \tag{1.36d}$$

Note the different vertical derivative forms in (1.36a,b) needed for separation to work. The separation is almost as before, with (1.31c) slightly altered to

$$p' = \rho_{oo} g \Psi(z) \hat{z} \tag{1.37}$$

and (1.33b) changes to

$$\Psi_z = \frac{1}{\rho_{oo}} \frac{\alpha \rho_o}{\alpha z} \phi \tag{1.38}$$

The coefficients K(z) and $\nu(z)$ must take the form

$$\nu = A_m / N_o^2 , \qquad K = A_T / N_o^2 \tag{1.39}$$

where A_m and A_T are constants and

$$N_o^2 = -\frac{g}{\rho_{oo}} \frac{\alpha \rho_o}{\alpha z} .$$

Thus K and ν are larger where stratification is weaker, which seems physically reasonable. In particular, there can be no vertical gradients in a well-mixed surface layer where $N_o = 0$. (However, this form is not

reasonable in regions where internal wave breaking and absorbtion are important mechanisms, so it should be regarded as primarily a mathematical convenience which allows analytic progress.)

The SWE with this separation are

$$\hat{\underline{u}}_t + f_o \underline{k} \times \hat{\underline{u}} = -g \nabla \hat{\eta} - \frac{A_m}{g H_e} \hat{\underline{u}} \quad , \qquad (1.40a)$$

$$\hat{\eta}_t + H_e (\hat{u}_x + \hat{v}_y) = - \frac{A_T}{g H_e} \hat{\eta} \quad . \qquad (1.40b)$$

The dissipative and diffusive terms again take the form of Rayleigh friction and Newtonian 'cooling' for each mode, but now higher-order modes with smaller H_e are more strongly damped, which physically can be attributed to their smaller vertical scale. This scale-selective damping can be a qualitatively important feature --- see lecture 3.

The restriction to constant surface density remains. Rothstein (1984) has developed an inverse technique to incorporate a heat flux boundary condition, thus allowing sea-surface density perturbations to be prescribed.

References (lecture 1)

Busalacchi, A.J. & J.J.O'Brien (1980)
The seasonal variability in a model of the tropical Pacific
J. Phys. Oceanog., 10, 1929-1951

Busalacchi, A.J. & J.J. O'Brien (1981)
Interannual variability of the equatorial Pacific in the 1960's
J. Geophys. Res., 86, 10901-10907

Busalacchi, A.J., K. Takeuchi, & J.J. O'Brien (1983)
Interannual variability of the equatorial Pacific---revisited
J. Geophys. Res., 88, 7551-7562

Gill, A.E. (1977)
Coastally trapped waves in the atmosphere
Q. J. Roy. Met. Soc., 103, 431-440

Gill, A.E. (1982)
Atmosphere-Ocean Dynamics
Academic Press, 662pp

Gill, A.E. & E.M. Rasmusson (1983)
The 1982-83 climate anomaly in the equatorial Pacific
Nature, 306, 229-234

Holland, G.J. & L.M. Leslie (1986)
Ducted coastal ridging over S.E. Australia
Q. J. Roy. Met. Soc., 112, 731-748

McCreary, J.P. (1981)
A linear stratified ocean model of the equatorial undercurrent
Phil. Trans. Roy. Soc. London, 298, 603-635

Rothstein, L.M. (1984)
A model of the equatorial sea surface temperature field and associated circulation dynamics
J. Phys. Oceanog., 14, 1875-1892

Fig. 1.1 Monthly mean values along the Pacific equator in 1982-1983
(a) outgoing longwave radiation anomaly in Watts m-2
(b) westerly wind anomaly (5°S-5°N) in m sec-1
(from Gill & Rasmusson 1983)

Fig. 1.2 Vertical section of a homogeneous shallow sea

Fig. 1.3 The path of a particle driven by a wind stress F>0 switched on at time t=0. This path is the superposition of a steady Ekman drift and an inertial oscillation.

Fig. 1.4 Geometry of a shallow sea with a coast
(a) plan view
(b) vertical section looking alongshore

Fig. 1.5a Longshore-time map of the amplitude A at the coast of sea-level change η/H and longshore current u/c in response to a longshore wind stress imposed for $0 < t < \tau$, $0 < x < L$, with $L=c\tau$. Longshore sections for $t/\tau = 0.5$ and 1 are shown on the right.

Fig. 1.5b Plan view of the response $\eta/H = u/c$ at time $t/\tau = 2$, which is a free coastal Kelvin wave. Note the different longshore and offshore scales: L>>a.

Fig. 1.6 Surface pressure maps for August 2-6 197? around southern Africa. Land over 1000m high is shaded in the August 2 map. (From Gill 1977)

Fig. 1.7 (a) Land over 900m high in Australia, shown black.
(b) Mean sea-level isobars for November 10 and 11, 1982
(From Holland & Leslie 1986)

Fig. 1.8 (a) A typical vertical density profile for a deep ocean
(b) Geometry of a two-layer model.

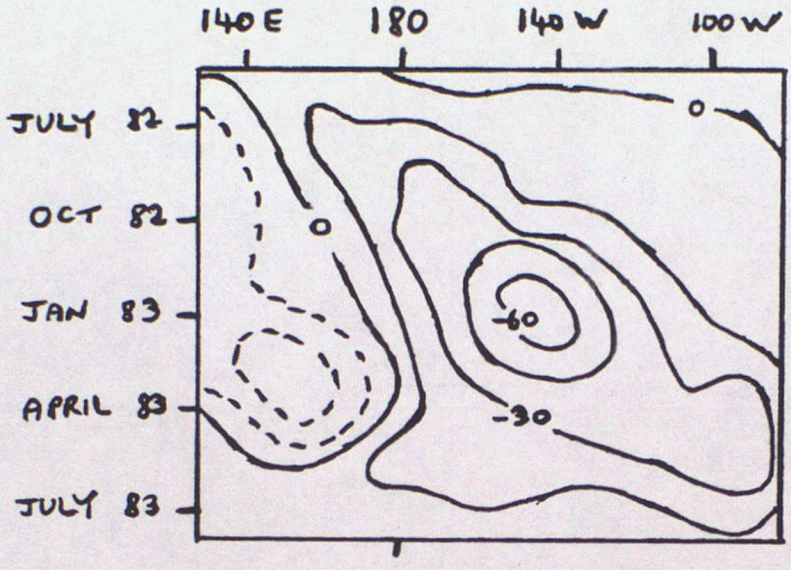
140 E
180
140 W
100 W
JULY 82
OCT 82
JAN 83
APRIL 83
JULY 83
0
0
-60
-30

(a)

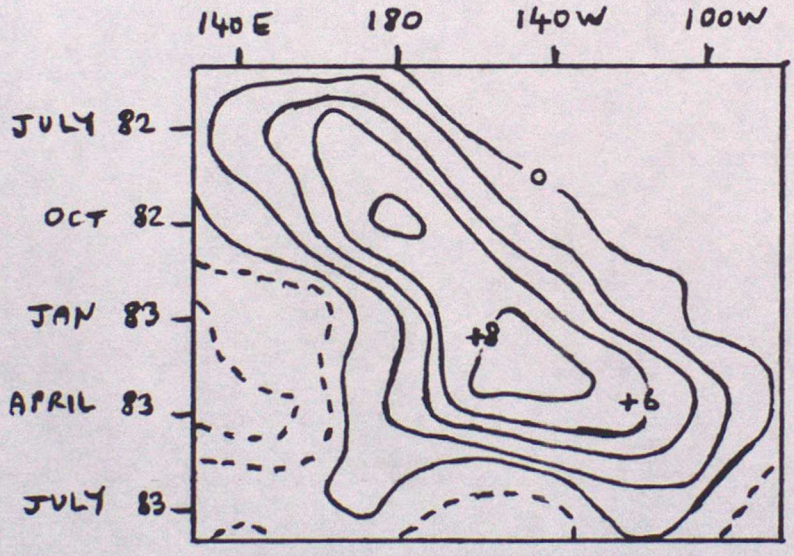
140 E
180
140 W
100 W
JULY 82
OCT 82
JAN 83
APRIL 83
JULY 83
0
+8
+6

(b)

Fig. 1-1

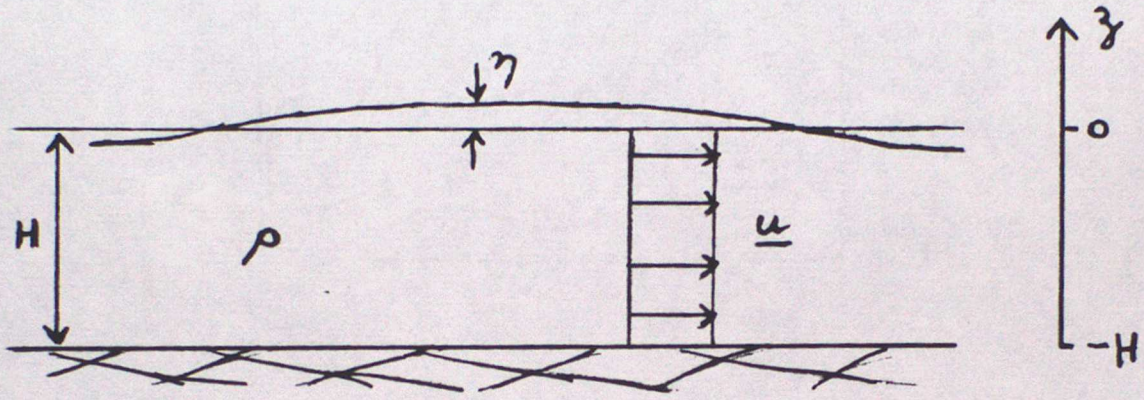

Fig. 1-2

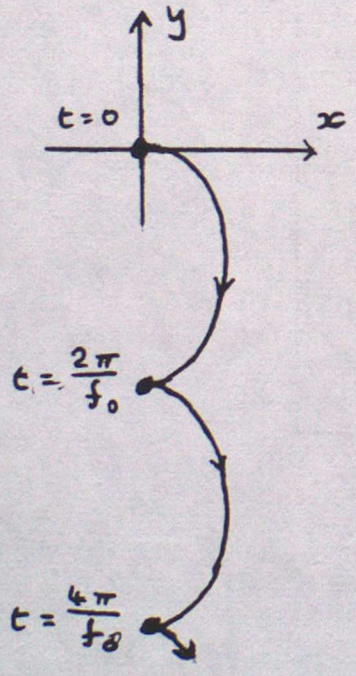

Fig. 1-3

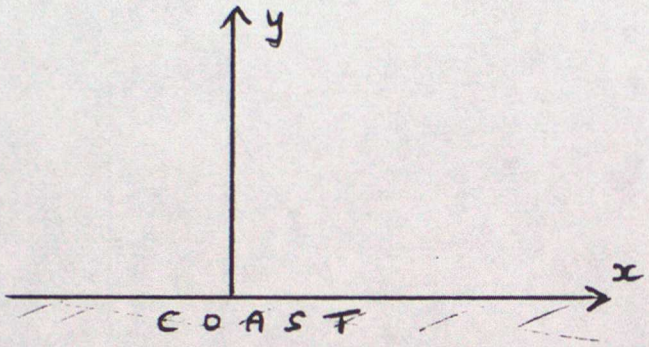

(a)

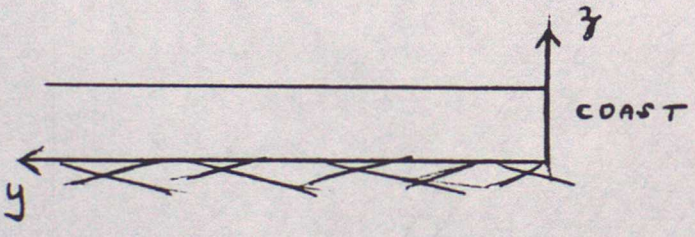

(b)

Fig. 1-4

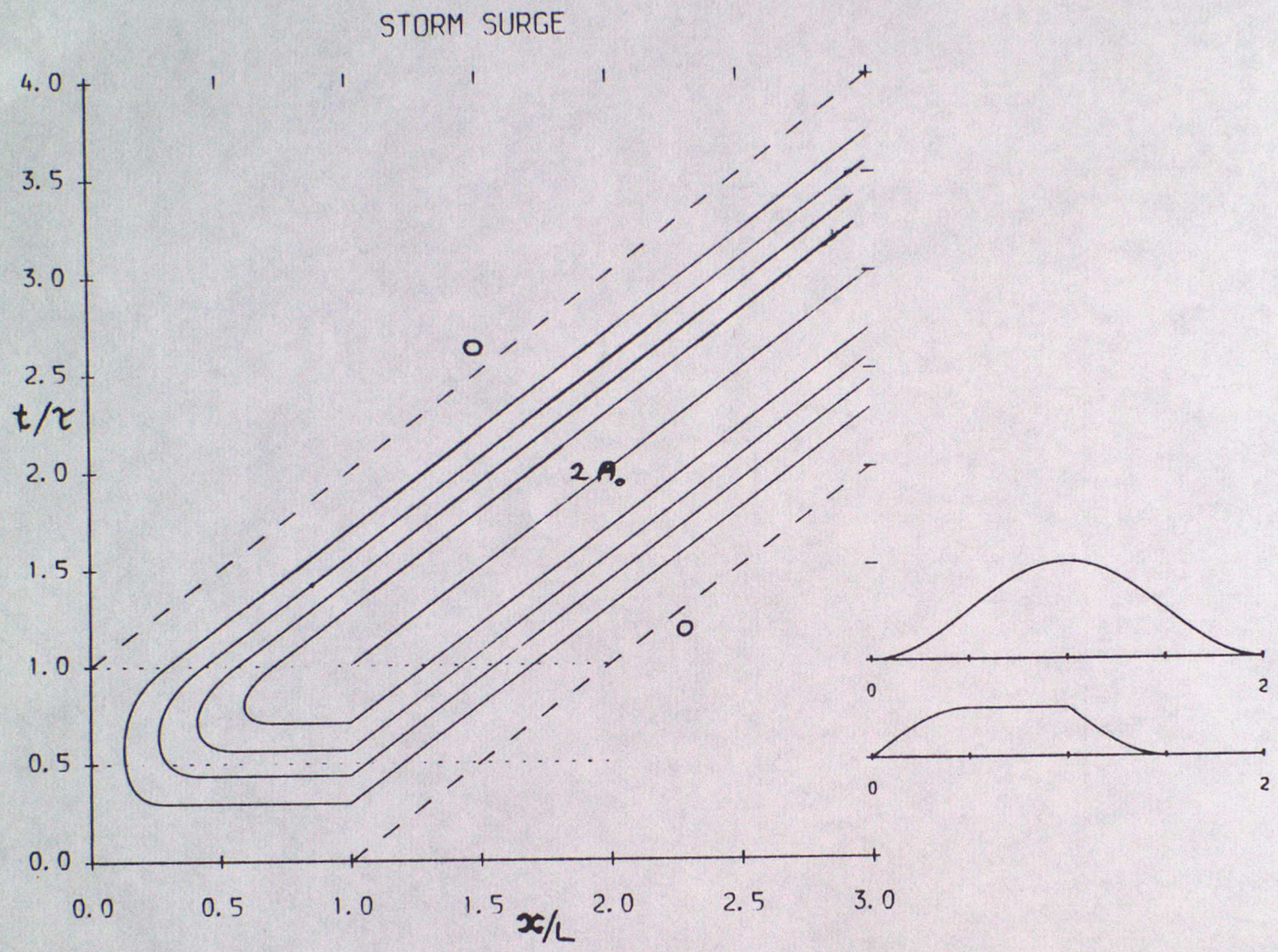
STORM SURGE
4.0
3.5
3.0
2.5
2.0
1.5
1.0
0.5
0.0
t/τ
0
2A₀
0
0.0
0.5
1.0
1.5
2.0
2.5
3.0
x/L
0
2
0
2

Fig. 1-5a

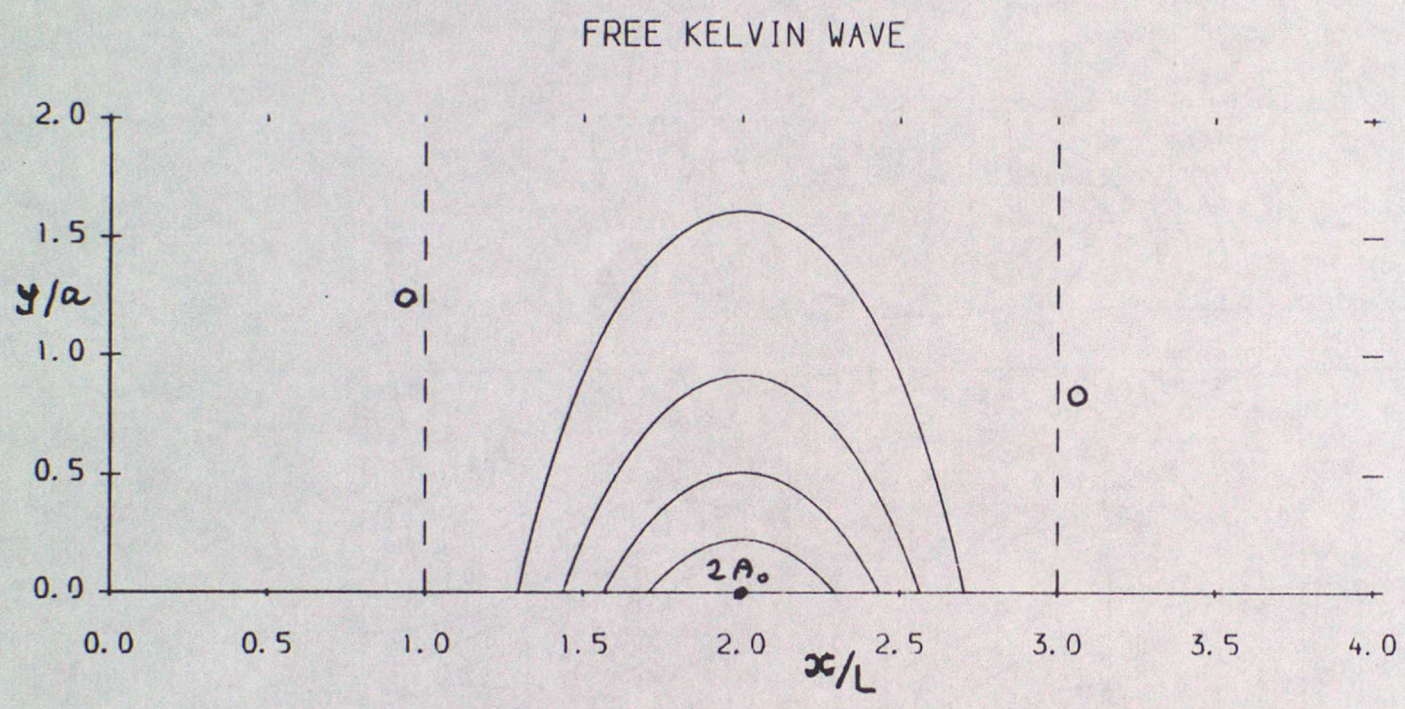
FREE KELVIN WAVE
2.0
1.5
y/a
1.0
0.5
0.0
0
0
2A₀
0.0
0.5
1.0
1.5
2.0
2.5
3.0
3.5
4.0
x/L

Fig. 1-5 b

AUGUST

2

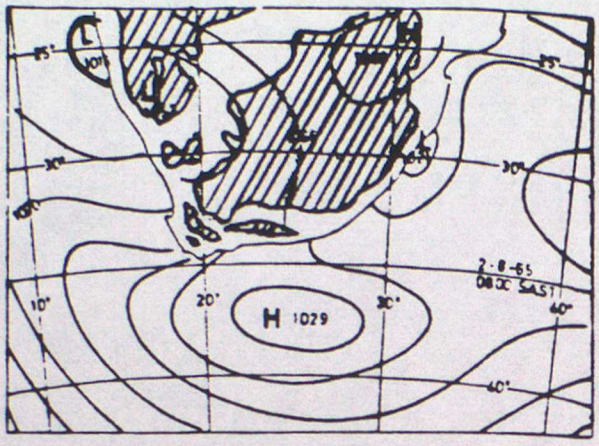

3

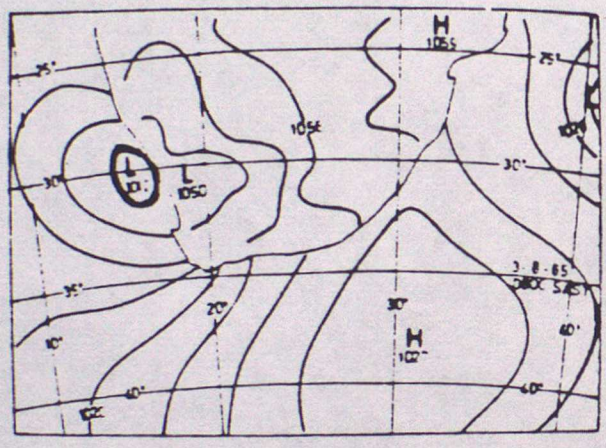

4

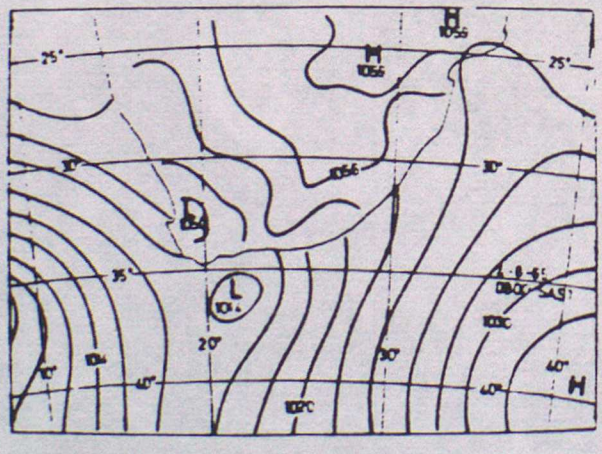

5

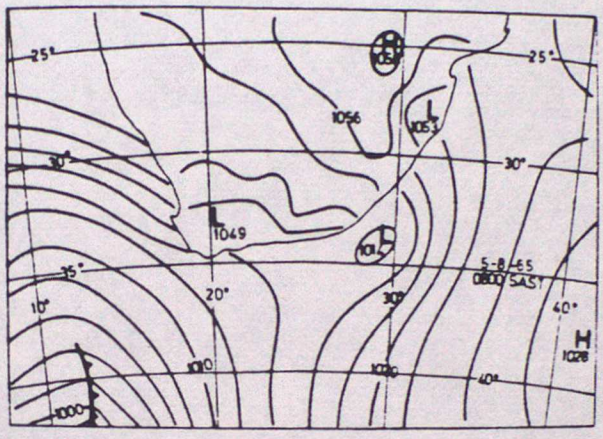

6

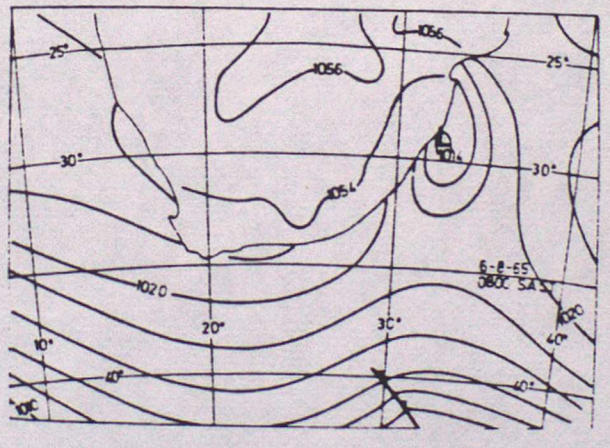

Fig. 1-6

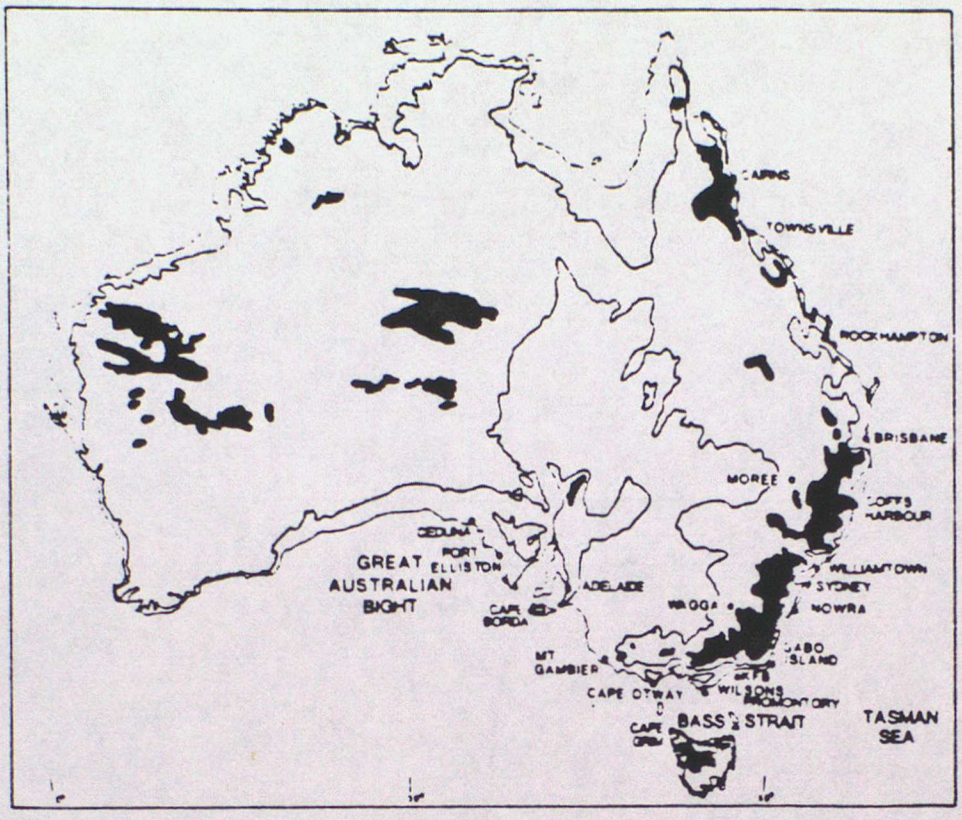
CAIRNS
TOWNSVILLE
ROCKHAMPTON
BRISBANE
MOREE
COFFS HARBOUR
WILLIAMTOWN
SYDNEY
NOWRA
GABO ISLAND
WILSONS PROMONTORY
CEDUNA
PORT ELLISTON
GREAT AUSTRALIAN BIGHT
ADELAIDE
CAPE BORDA
MT GAMBIER
CAPE OTWAY
BASS STRAIT
TASMAN SEA

(a)

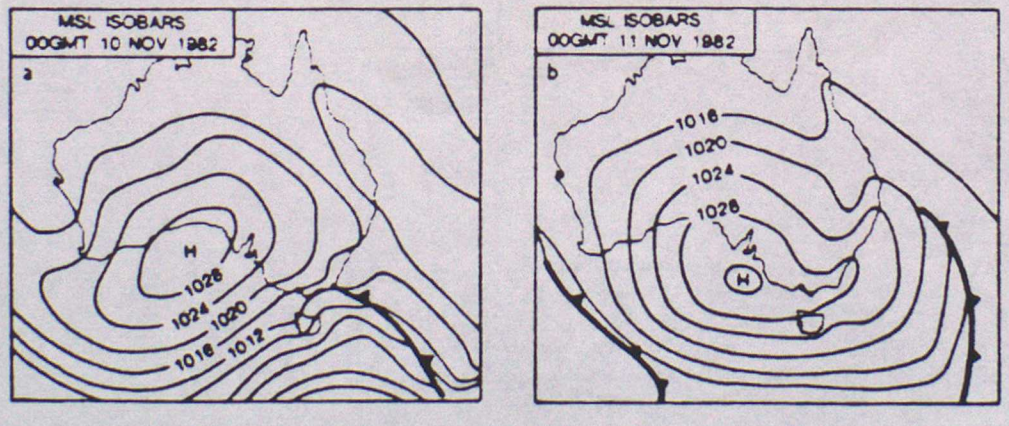
MSL ISOBARS
00GMT 10 NOV 1982
a
H
1028
1024
1020
1016
1012
MSL ISOBARS
00GMT 11 NOV 1982
b
1016
1020
1024
1028
H

(b)

Fig. 1-7

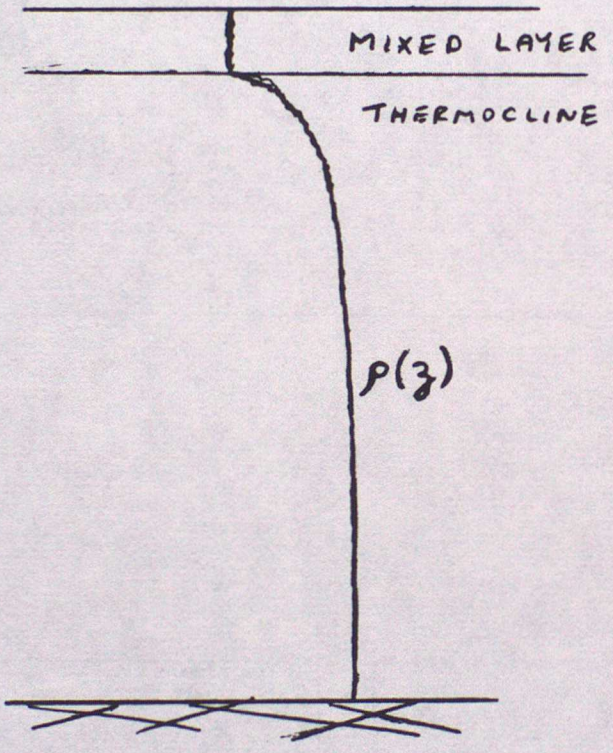

(a)

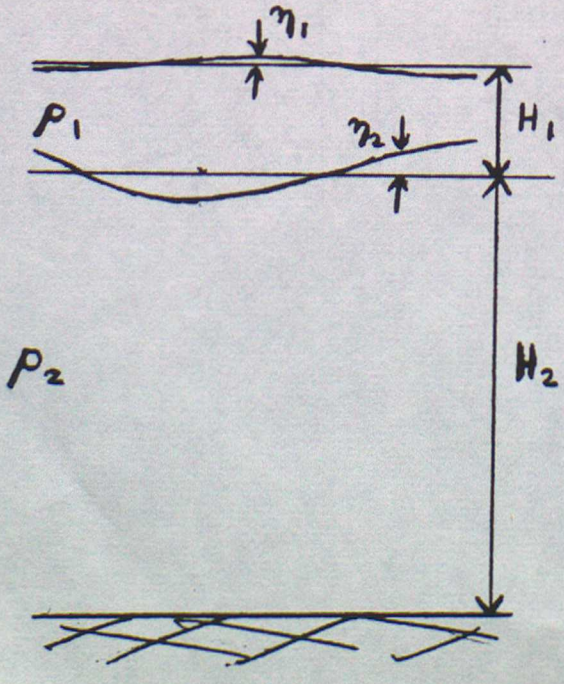

(b)

Fig. 1-8

Lecture 2 Equatorially trapped waves

The Somali Current is a major ocean current along the east equatorial coast of Africa, with a peak northward transport of about 60 Sv (1 Sverdrup = 10^6 m3 sec-1), mostly in the upper 200m. (This transport is comparable to the Gulf Stream.) The remarkable feature of this current is its seasonal variation: each year it switches from moderate southward flow in northern winter to large northward flow in northern summer, as seen in Fig. 2.1a. This change rapidly follows the onset of the southwest monsoon. In the Indian Ocean there are low-level south-easterly trade winds year round, but north of the equator there are north-easterlies in northern winter (as in the Pacific and Atlantic sectors) which change to south-westerlies in northern summer (see Fig. 2.1b).

Lighthill (1969) offered an explanation of this behaviour in terms of equatorially trapped waves 'rapidly' propagating westward from a region in the Indian Ocean forced by this change from northeast to southwest winds, modelled as a switch-on of a westerly wind anomaly. Lighthill used vertical modes as described in lecture 1, with sophisticated mathematical analysis to determine the evolution of each mode.

Since then there has been a flood of papers on equatorial dynamics. Equatorial waves in the atmosphere were already known (e.g. Matsuno 1966), but reflections from meridional boundaries make the oceans rather different. (The tropical oceans are a paradise for theoreticians! In addition, observations are sparse so dynamical processes are not well understood and there is scope for a wide range of models.) A fraction of the literature will be cited in these lectures: for more complete lists and general reviews see Cane & Sarachik (1983), Knox & Anderson (1985), McCreary (1985), and Gill's book.

2.1 The equatorial beta plane

The SWE in lecture 1 derived for an f-plane are equally valid if the Coriolis parameter $f=2\Omega \sin\phi$ is allowed to vary with latitude ϕ. Such variations make the equations more difficult to solve: for large-scale motion at mid-latitudes it is common to 'freeze' f and its derivative $\beta = df/fy$ at some central latitude ϕ_o. At low latitudes a similar procedure is to freeze β and allow f to vary linearly:

$$f = 2\Omega\phi \quad = \beta y \tag{2.1a}$$

where

$$\beta = 2\Omega / R \tag{2.1b}$$

and

$$y = R\phi \tag{2.1c}$$

is northward distance, R being the radius of the Earth. This approximation is best near the equator, but qualitatively it is reasonable to about $\pm 40^\circ$, more than half the earth's surface.

A crucial feature is that f changes sign across the equator at y=0. The SWE can have solutions with u and η symmetric and v antisymmetric about the equator. For such solutions a wall could be placed at the equator with no effect, and as for the coastally trapped waves seen in lecture 1, this 'wall' allows equatorially trapped waves. (The analogy is very loose: there are also trapped waves with the opposite symmetry.)

In lecture 1 we found the natural scale $a=c/f_o$. Here we replace f_o by an 'average' frequency-of-rotation $2\beta a$ to define

$$a = c/2\beta a \quad ,$$

i.e.

$$a = (c/2\beta)^{1/2} \qquad (2.2)$$

which is known as the equatorial Rossby radius. (The factor 2 is convenient in calculations to follow.) This scale will turn out to be the meridional trapping scale for equatorial waves. Typical values are

	atmosphere	ocean
barotropic	3000 Km	3000 Km
first baroclinic	1000 Km	200 Km

(Higher order vertical modes have smaller equatorial Rossby radii.)

The equatorial beta-plane is of marginal value for barotropic modes. However, the dominant modes in the tropical ocean and atmosphere are baroclinic, for which this approximation is very good.

2.2 Non-dimensional equatorial SWE

It is convenient at this stage to introduce some non-dimensional variables. Horizontal distance is scaled by the equatorial Rossby radius,

$$(x,y) = a\,(X,Y) \qquad (2.3a)$$

horizontal velocity is scaled by the gravity wave speed,

$$(u,v) = c\,(U,V) \qquad (2.3b)$$

vertical displacement is scaled by the equivalent depth,

$$\eta = He\ \eta^* \qquad (2.3c)$$

and time is scaled as

$$t = (a/c)\ T \qquad (2.3d)$$

From (2.1) and (2.2), the Coriolis parameter can be written

$$f = (c/a)\ f^* \qquad (2.4a)$$

where

$$f^* = \beta^*\ Y \quad , \qquad \beta^* = 1/2 \quad . \qquad (2.4b)$$

(Asterisks are used to denote some non-dimensional quantities.)

The SWE become

$$U_T - \tfrac{1}{2} Y\ V = -\ \eta^*_X \quad , \qquad (2.5a)$$

$$V_T + \tfrac{1}{2} Y\ U = -\ \eta^*_Y \quad , \qquad (2.5b)$$

$$\eta^*_T + U_X + V_Y = 0 \quad . \qquad (2.5c)$$

(For the 'shallow-water' ocean it is useful to think of $\underline{U}$ as upper layer current and η^* as changes in upper layer depth.)

Eliminating U and η^* leads to an equation for V alone:

$$V_{TTT} + \tfrac{1}{4} Y^2 V_T - (V_{XX} + V_{YY}) - \tfrac{1}{2} V_X = 0 \quad . \qquad (2.6)$$

The term $\frac{1}{4} Y^2$ should be thought of as f^2, and $\frac{1}{2}$ as β.

2.3 Waves

To look for wavelike solutions put

$$V = F(Y) \exp\{ i(kX-\omega T) \} \qquad (2.7)$$

into (2.6). Then

$$F_{YY} + (\omega^2 - k - \tfrac{1}{2} \frac{k}{\omega} - \tfrac{1}{4} Y^2) F = 0 \qquad (2.8)$$

The meridional structure F can be expressed in terms of standard mathematical functions: the parabolic cylinder functions

$$D_n(Y) = \exp\{-Y^2/4\} \text{ . Hermite polynomial of order n} \qquad (2.9)$$

which are solutions of

$$D_{nYY} + (n+\tfrac{1}{2} - \tfrac{1}{4} Y^2) D_n = 0 \qquad (2.10)$$

where n is an integer. These functions tend to zero as $Y \to \pm\infty$.

Clearly F can be identified with D_n when

$$\omega^2 - k^2 - \tfrac{1}{2} k/\omega = n + \tfrac{1}{2} \qquad (2.11)$$

This is the equatorial wave dispersion relation.

Solutions of (2.8) are wavelike for $|Y|<Y_c$ where

$$\frac{1}{4} Y_c^2 = \omega^2 - k^2 - \tfrac{1}{2} k/\omega \qquad (2.12)$$

$$\tfrac{1}{4} Y_c^{\,2} = n + \tfrac{1}{2} \quad ,$$

and exponential for $|Y| > Y_c$, so these waves are indeed equatorially trapped. As n increases, Y increases and the waves are less confined, but $F = D_n$ becomes more wiggly (see below).

Having obtained V, the properties

$$(d/dY + \tfrac{1}{2} Y)\, D_n = n\, D_{n-1} \tag{2.13a}$$

$$(d/dY - \tfrac{1}{2} Y)\, D_n = -D_{n+1} \tag{2.13b}$$

can be used to obtain

$$\left.\begin{aligned} V &= D_n(Y) \\ U &= U_n(Y) \\ \eta^* &= \eta_n^*(Y) \end{aligned}\right\} \exp\{\, i(kX - \omega T)\}$$

where

$$U_n = \frac{i}{2}\left[\frac{D_{n+1}}{\omega - k} + \frac{n\, D_{n-1}}{\omega + k}\right] \quad , \tag{2.14a}$$

$$\eta_n^* = \frac{i}{2}\left[\frac{D_{n+1}}{\omega - k} - \frac{n\, D_{n-1}}{\omega + k}\right] \quad . \tag{2.14b}$$

The first few functions D_n are

$$\left.\begin{aligned} D_0 &= 1 \\ D_1 &= Y \\ D_2 &= (Y^2 - 1) \\ D_3 &= (Y^3 - 3Y) \end{aligned}\right\} \exp\{-Y^2/4\} \tag{2.15a}$$

and it is convenient to define $D_{-1} = 0$. The recurrence relation is

$$D_n = Y D_{n-1} - (n-1) D_{n-2} \quad , \tag{2.15b}$$

These functions are orthogonal:

$$\int_{-\infty}^{\infty} D_m D_n \, dY = \begin{cases} (2\pi)^{1/2} \; n! & n = m \\ 0 & n \neq m \end{cases} \tag{2.16}$$

They are illustrated in Fig. 2.2 for n=0,2,16, each divided by $(n!)^{1/2}$ to ensure that each has the same square integral $(2\pi)^{1/2}$.

Analytic solutions of equatorial problems are often expressed in terms of these functions: Boyd & Moore (1986) describe techniques for efficiently evaluating such series.

2.4 The equatorial Kelvin wave

Before discussing these waves further, we must add another one that is not covered by the above analysis because it has V=0. For vanishing V the SWE (2.5) reduce to

$$U_T = - \eta^*_X \quad , \tag{2.17a}$$

$$\tfrac{1}{2} Y U = - \eta^*_Y \quad , \tag{2.17b}$$

$$\eta^*_T + U_X = 0 \quad , \tag{2.17c}$$

which has solutions of the form

$$\eta^* = U = G(X-T)\exp\{-Y^2/4\} \qquad (2.18)$$

where G is an arbitrary function. The dispersion relation is

$$\omega = k \qquad (2.19)$$

[n=-1 in (2.11)].

This is the counterpart of the coastal Kelvin wave found in lecture 1, and it is likewise known as the equatorial Kelvin wave. It has many similar properties:

- propagates at the gravity wave speed (non-dimensional speed is 1)
- only propagates eastward
- non-dispersive
- zonal flow in balance with the meridional pressure gradient (longequator geostrophy)

This wave is very important because it can rapidly and efficiently transmit information eastward along the equator. Examples of its spatial pattern are given in Fig. 2.3 .

These Kelvin waves have been observed in the atmosphere and the ocean. Typical scales for first baroclinic modes are

	atmosphere	ocean	
c	50	3	m sec-1
a	1000	250	Km
c/a	0.25	1	day

Thus a Kelvin wave in the ocean will cross the Pacific in about 50 days. By mid-oceanic standards this is like greased lightning --- the fastest low-frequency wave with the same equivalent depth (a long baroclinic Rossby wave) would take 10 years to travel westward across the Pacific Ocean at 30° N! Fig. 2.4 shows evidence for such a wave: a surge in transport was observed at widely separated locations with timing appropriate to a Kelvin wave (Knox & Halpern 1982).

An atmospheric Kelvin wave would take about 8 days to follow the equator around the world. (Puzzle: the 40-day oscillation looks like a first Kelvin wave! Why 40 days then? There are other processes to take into account such as interaction with rainfall --- see lecture 3.)

2.5 The dispersion diagram

Real solutions of (2.11) (i.e. propagating waves) are plotted in Fig. 2.5 for n=-1 to 5. (We restrict attention to $\omega > 0$ without loss of generality.) For n=-1 we have $\omega = k$, The Kelvin wave. For n=0

$$k = \omega - {}^{1}/_{2}\omega \qquad (2.20)$$

and this curve has k real for all frequencies .

When n>0 there are two branches, with

$$k = -\frac{1}{4\omega}\{\, 1 \pm [1-16\,\omega^2(n+\tfrac{1}{2}-\omega^2)]^{\frac{1}{2}} \,\} \quad . \qquad (2.21)$$

The branch with higher frequency has real solutions for

$$\omega > \omega_G = \tfrac{1}{2}[\,(n+1)^{\frac{1}{2}} + n^{\frac{1}{2}}\,] \quad , \qquad (2.22a)$$

For n=1 we find $\omega_G \approx 1.2$. For our typical ocean this corresponds to a maximum period of about 5 days, and about 1.5 days for our typical atmosphere.

The branch with lower frequency has real solutions for

$$\omega \quad < \omega_p \quad = \tfrac{1}{2}\left[(n+1)^{\frac{1}{2}} - n^{\frac{1}{2}} \right] \qquad (2.22b)$$

For n=1 , $\omega_p \approx 0.2$ so these waves have a minimum period of about 30 days (ocean), or 8 days (atmosphere). This branch can be seen more clearly in Fig. 2.6 .

Both these branches have zero group velocity $d\omega/dk$ for

$$k = k0 = -\frac{1}{4\omega} \qquad (2.23)$$

For $\omega_p < \omega < \omega_G$ solutions of (2.11) for n>0 have

$$\text{real } k = k0 \qquad (2.24a)$$

$$\text{imaginary } k = k0\,[-1+16\omega^2(n+\tfrac{1}{2}-\omega^2)]^{\frac{1}{2}} \qquad (2.24b)$$

These correspond to spatially decaying waves, decaying westward for im k > 0, and eastward for im k < 0. As n increases the waves decay more rapidly. These waves are important in wave reflection, as will be discussed below.

Away from the equator only waves that correspond to large n are found (remember the critical latitude Y_c) so there is a substantial spectral gap --- a range of frequency where little energy is observed. By contrast, waves of all frequencies occur near the equator (Eriksen 1980).

For future reference we note here a general property of symmetric waves (i.e. U and η^* symmetric about the equator). From (2.14) it can be shown that

$$\eta^* /U = \omega/k \qquad \text{at } Y=0 \quad . \tag{2.25}$$

2.6 Inertia-gravity waves

For the upper branch of the n>0 dispersion curves we have

$$\omega^2 \simeq n + \tfrac{1}{2} + k^2 \quad , \tag{2.26}$$

These are the equatorial equivalent of the inertia-gravity waves seen in lecture 1. For long waves (k<<1 , zonal wavelength >> a) $\omega^2 \simeq n + \frac{1}{2}$.

These waves can have eastward or westward phase and group velocity. They have been observed in sea-level fluctuations in the Pacific, and linear theory fits the observations very well (Wunsch & Gill 1976).

We will be more interested in low frequency phenomena, and will not consider these waves further.

2.7 Planetary waves

For the lower branch of n>0 waves,

$$\omega \simeq \frac{-\tfrac{1}{2} k}{n + \tfrac{1}{2} + k^2} \quad . \tag{2.27}$$

This relation bears obvious similarities to that for mid-latitude planetary (Rossby) waves, which is probably more familiar, and indeed these are equatorially trapped planetary waves. Basic properties are the same as for the mid-latitude waves:

- westward phase speed only
- eastward group velocity for short waves $k < k0$

  maximum eastward group velocity is

$$c_g = 1 / 8(2n+1) \qquad (2.28a)$$

for

$$k \leq -[3(n+\tfrac{1}{2})]^{\frac{1}{2}} \qquad (2.28b)$$

- westward group velocity for long waves $k0 < k < 0$

  maximum westward group velocity as $k \rightarrow 0$ is

$$c_g = -1 / (2n+1) \qquad (2.29)$$

- long waves are non-dispersive as k->0

The magnitude of the group velocity (the speed at which information is transmitted) is an important feature. For n=1 c_g for a long wave is one-third the gravity wave speed; far faster than its mid-latitude counterpart. In our typical ocean a long planetary wave would take about 150 days to travel west across the equatorial Pacific.

This relatively large wave speed means that linear theories are very useful: nonlinear effects tend to make quantitative rather than qualitative differences.

Because ω and k have opposite sign for Rossby waves, U and η^* have opposite sign at the equator from (2.25), in contrast to the Kelvin wave for which $U = \eta^*$. In lecture 5 we see that this may have important

implications for ocean-atmosphere coupling.

2.8 Structure of long Rossby waves

Long ($k \ll 1$) Rossby waves are non-dispersive, with

$$\omega / k = -1 / (2n+1) \tag{2.30}$$

and using (2.14) their structure can be expressed as

$$V = V_n \quad G'(kX - \omega T) \tag{2.31a}$$

$$U = U_n \quad G(kX - \omega T) \tag{2.31b}$$

$$\eta^* = \eta_n^* \quad G(kX - \omega T) \tag{2.31c}$$

where G is an arbitrary function, and

$$V_n = 4k \frac{(n+1)^{1/2} \, n^{1/2}}{(2n+1)^{3/2}} \hat{D}_n \tag{2.31d}$$

$$U_n = \frac{1}{(2n+1)^{1/2}} [\, n^{1/2} \hat{D}_{n+1} - (n+1)^{1/2} \hat{D}_{n-1} \,] \tag{2.31e}$$

$$\eta_n^* = \frac{1}{(2n+1)^{1/2}} [\, n^{1/2} \hat{D}_{n+1} + (n+1)^{1/2} \hat{D}_{n-1} \,] \tag{2.31f}$$

where

$$\hat{D}_n = \frac{1}{(n!)^{1/2}} D_n \tag{2.32}$$

In this form

$$\int_{-\infty}^{\infty} U_n^2 \, dY = \int_{-\infty}^{\infty} \eta_n^{*2} \, dY = \int_{-\infty}^{\infty} \hat{D}_n^2 \, dY = (2\pi)^{1/2} . \tag{2.33}$$

Thus U and η^* are O(1), while V is O(k) and hence much smaller. Fig. 2.7 shows U_n and η_n^* for n=1 and 15, and also for the Kelvin wave: note that η_n^* is largest near the critical latitude Y_c, whereas U_n is largest near the equator. There is longequator geostrophy in this long wave limit:

$$f^* U_n = -\eta_{nY}^* \quad . \tag{2.34a}$$

Note that differentiation gives

$$\beta^* U_n = -\eta_{nYY}^* \qquad \text{on } Y=0 \tag{2.34b}$$

so the variation of the Coriolis parameter still provides a geostrophic constraint at the equator, even though f vanishes there.

2.9 n=0: the Yanai wave

Also known as the mixed Rossby-gravity wave, this wave is unique to the equatorial region. Like the Kelvin wave it always has eastward group velocity. For k>>1 it behaves like a gravity wave with eastward phase velocity, but for k<<-1 it behaves like a short Rossby wave with westward phase velocity. The Yanai wave has U and η^* antisymmetric about the equator, while V is symmetric and is associated with cross-equatorial flow. Like the Kelvin wave, the Yanai wave has been detected in both the ocean and atmosphere.

2.10 Reflection from boundaries

All equatorial oceans have eastern and western land boundaries, and the different reflection properties at east and west coasts are very important to equatorial ocean dynamics. Only low frequency waves are considered

here: similar procedures apply to high frequency waves however. (See Moore & Philander 1978 for details.)

(a) west coast

As shown in Fig. 2.9 a vertical wall oriented north-south will represent the coast at X=0, so we require U=0 at all latitudes there. We consider one incident wave of frequency ω and meridional mode N. This wave must have westward group velocity, so it must be a long Rossby wave with $k0<k<0$. Any reflected wave must have the same frequency and must have eastward group velocity: from the dispersion diagram (2.6) it can be seen that short Rossby waves ($k<k0$) with $n \leq N$ have these properties, along with the Kelvin and Yanai waves.

Because these waves all have different meridional structure to the incident wave, no one wave can counter the incident wave to satisfy the boundary condition at X=0. However, a balance can always be achieved using the waves mentioned above that have the same symmetry as the incident wave. For example, an N=5 long Rossby wave reflects as n=5,3,1 short Rossby waves plus a Kelvin wave. An N=4 long Rossby wave reflects as n=4,2 short Rossby waves plus a Yanai wave.

To be more specific, consider the N=1 incident wave which has structure

$$U_{1I} = D_0(Y) + \frac{\omega + k_I}{\omega - k_I} D_2(Y) \quad . \qquad (2.35a)$$

The reflected waves are short Rossby with

$$U_{1R} = \alpha_1 \left[D_0 + \frac{\omega + k_R}{\omega - k_R} D_2 \right] \qquad (2.35b)$$

and Kelvin with

$$U_{-1R} = \alpha_{-1} D_0 \quad . \qquad (2.35c)$$

(Here k_I and k_R are different wavenumbers for the incident and reflected Rossby waves, and α_1 and α_{-1} are coefficients to be determined.) Matching coefficients of the parabolic cylinder functions in the boundary condition

$$U_{1I} + U_{1R} + U_{-1R} = 0 \qquad (2.36)$$

requires

$$\alpha_1 = -\left(\frac{\omega + k_I}{\omega - k_I}\right)\left(\frac{\omega - k_R}{\omega + k_R}\right) \qquad (2.37a)$$

and

$$\alpha_{-1} = -1 - \alpha_1 \qquad (2.37b)$$

For example, for $\omega << 1$ we have

$$k_I = -(2N+1)\omega \quad = -3\,\omega$$

and

$$k_R \approx -\tfrac{1}{2}\omega \quad >> \quad \omega$$

so

$$\alpha_1 = -1/2 = \alpha_{-1} \; .$$

General features of western boundary reflection are

- reflected pattern is trapped to the same latitude range as the incident wave, because $n \lesssim N$
- all wavenumbers are real, so all waves involved propagate along the equator
- incident symmetric waves generate the fast Kelvin wave and short Rossby waves which have much smaller group velocity
- incident antisymmetric waves generate the short Yanai and

(b) east coast

The incident wave must now have eastward group velocity (Kelvin, Yanai or short Rossby) and reflected waves must have westward group velocity (long Rossby). In contrast to the west coast, reflection now involves an infinite series of waves with $n \geq N$. Only a finite number of these may be propagating waves (see dispersion diagram); the rest decay westward as given by (2.24). The wave amplitudes can be obtained by matching coefficients as before. It can be shown that this infinite series adds up to the same effect as a coastal Kelvin wave propagating poleward. (Note that the coastal trapping scale c/f decreases poleward: the amplitude of this wave correspondingly increases poleward to conserve energy.)

Features of east coast reflection:

- energy escapes poleward as a coastal Kelvin wave
- reflected Rossby waves have $n \geq N$, so they are not trapped to within the same latitudes as the incident wave

Example: incident Kelvin wave

$$U_I = D_0(Y)$$

$$U_{1R} = \alpha_1 [D_0 + \frac{\omega + k_R}{\omega - k_R} D_2]$$

$$U_{3R} = \text{etc.}$$

Matching requires $\alpha_1 = -1$, so the reflected n=1 long Rossby wave will cancel the incident wave at the coast. For $\omega \ll 1$ the reflected n=1 wave will propagate westward (at speed -1/3), progressively cancelling the incident wave further from the coast and leaving a residual D_2 structure.

Fig. 2.10 from Anderson & Rowlands (1976a) illustrates the effect of an

incident Kelvin wave of step-function zonal profile reaching an eastern boundary. The events mentioned above can be clearly seen --- poleward propagation of a coastal Kelvin wave and cancellation of the incident wave. Also, turn the diagram upside-down to see a pure equatorial Kelvin wave being generated at an eastern boundary by just the right combination of a coastal Kelvin wave (travelling equatorward) plus incident long Rossby waves!

2.11 Somali Current again

This lecture began with a description of the Somali Current and its relation to monsoonal winds. Lighthill's (1969) explanation involves the generation of long Rossby waves by the wind that carry energy west to the African coast. Further investigation has shown that local winds at that coast also have an important effect (Anderson & Rowlands 1976b). Nevertheless, remote effects are important, and in following lectures further examples of the strong influence of equatorial waves will be described.

References (lecture 2)

Anderson, D.L.T. & P.B. Rowlands (1976a)
The role of inertia-gravity and planetary waves in the response of a tropical ocean to the incidence of an equatorial Kelvin wave on a meridional boundary
J. Mar. Res., 34, 295-312

Anderson, D.L.T. & P.B. Rowlands (1976b)
The Somali Current response to the southwest monsoon: the relative importance of local and remote forcing
J. Mar. Res., 34, 395-417

Boyd, J.P. & D.W. Moore (1986)
Summability methods for Hermite functions
Dyn. Atmos. Oceans, 10, 51-62

Cane, M.A. & E.S. Sarachik (1983)
Equatorial oceanography
Rev. Geophysics & Space Physics, 21, 1137-1148

Eriksen, C.C. (1980)
Evidence for a continuous spectrum of equatorial waves in the Indian Ocean
J. Geophys. Res., 85, 3285-3303

Knox, R.A. & D. Halpern (1982)
Long range Kelvin wave propagation of transport variations in Pacific Ocean equatorial currents
J. Mar. Res., 40 (supplement), 329-339

Knox, R.A. & D.L.T. Anderson (1985)
Recent advances in the study of low-latitude ocean circulation
Prog. Oceanog., 14, 259-317

Lighthill, M.J. (1969)
Dynamic response of the Indian Ocean to onset of the southwest monsoon
Phil. Trans. Roy. Soc. London, 265, 45-92

McCreary, J,P. (1985)
Modelling equatorial ocean circulation
Ann. Rev. Fluid Mech., 17, 359-409

Matsuno, T. (1966)
Quasigeostrophic motions in the equatorial area
J. Met. Soc. Japan, 44, 25-43

Moore, D.W. & S.G.H. Philander (1978)
Modelling of the tropical oceanic circulation
In: 'The Sea', Vol. 6, pp 319-361. John Wiley Interscience, N.Y.

Pickard, G.L. & W.J. Emery (1982)
Descriptive physical oceanography
Pergamon Press, 249pp

Wunsch, C. & A.E. Gill (1976)
Observations of equatorially trapped waves in Pacific sea-level variations
Deep-Sea Res., 23, 371-390

Yoshida, K. (1959)
A theory of the Cromwell Current (the equatorial undercurrent) and of the equatorial upwelling --- an interpretation in a similarity to a coastal circulation
J. Ocean. Soc. Japan, 15, 159-170

Fig. 2.1 (a) Sketch of indian Ocean surface currents. Note the seasonal reversal of the Somali Current.
(b) Sketch of surface winds over the Indian and Pacific oceans. Note the north-east and south-west monsoons.
(From Pickard & Emery 1982)

Fig. 2.2 The parabolic cylinder functions Dn for n=0,2,16, divided by $(n!)^{1/2}$ so each has the same square integral $(2\pi)^{1/2}$.

Fig. 2.3 Examples of equatorial Kelvin wave patterns.
For a 'shallow-water' ocean, (a) corresponds to eastward surface currents and increased upper layer depth, while (b) has westward surface current and decreased upper layer depth. For a baroclinic mode in the atmosphere, (a) shows westerly low-level winds and high surface pressure, (b) has easterly winds and low surface pressure. In each case the wave travels to the east at the speed of a gravity wave.

Fig. 2.4 Evidence of a baroclinic equatorial Kelvin wave travelling east across the Pacific ocean. (From Knox & Halpern 1982)

Fig. 2.5 The dispersion diagram for equatorial waves, for n=-1 (Kelvin wave), n=0 (Yanai wave), and n=1->5 (planetary and inertial-gravity waves).

Fig. 2.6 An enlargement of the dispersion diagram in Fig. 2.5 to emphasise the planetary waves for n=1->5.

Fig. 2.7 Meridional structure of (a) η_n^* (b) U_n for n=-1 (Kelvin) n=1 and 15 (long planetary) waves. In each case there is longequator geostrophic balance: $\frac{1}{2}YU_n = -\eta_n^* Y$.

Fig. 2.8 Spatial pattern of a long n=1 planetary wave with high surface pressure. This pattern propagates to the west at one-third the speed of a gravity wave.

Fig. 2.9 Geometry for (a) western boundary (b) eastern boundary

Fig. 2.10 The effect of a Kelvin wave of step-function zonal form arriving at an eastern boundary. (Adapted from Anderson & Rowlands 1976)

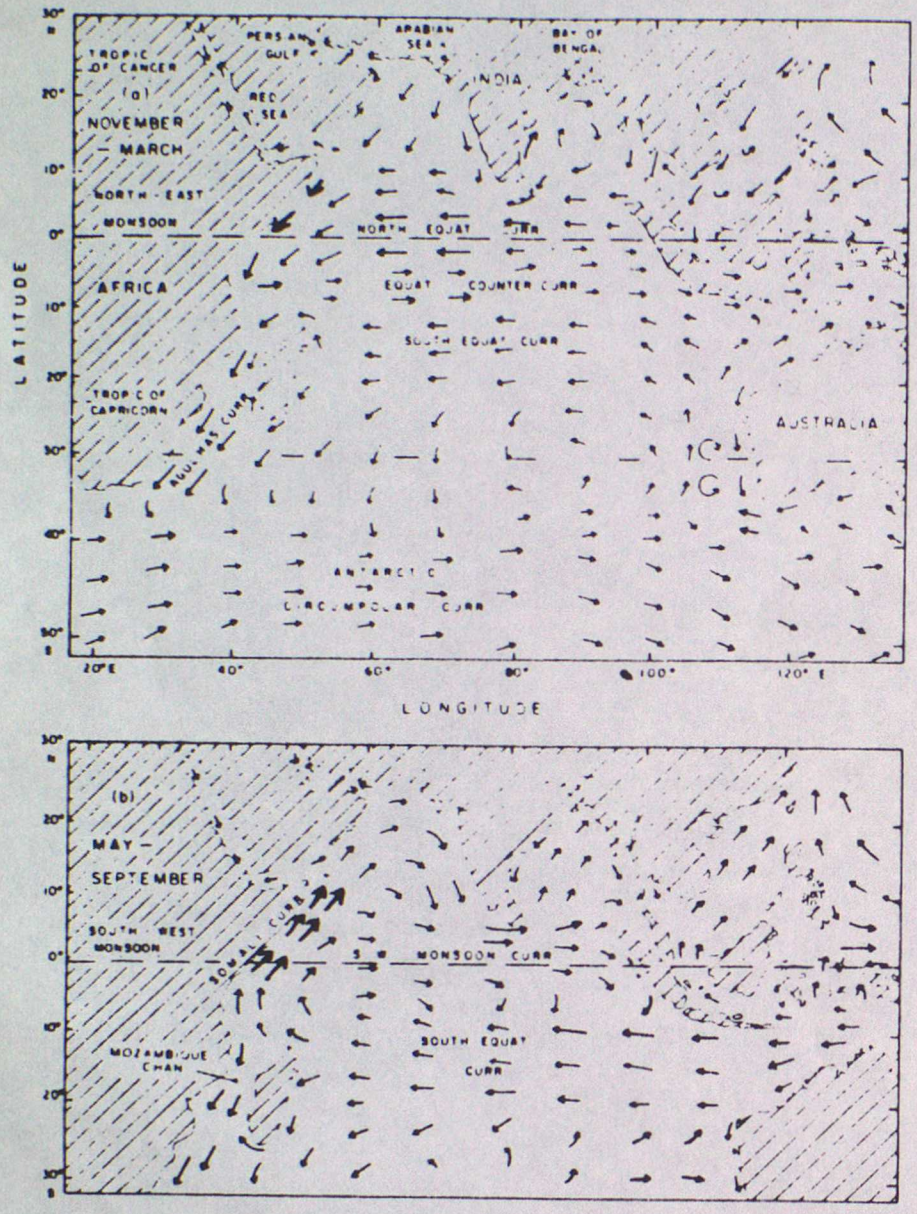
(a)
NOVEMBER – MARCH
TROPIC OF CANCER
PERSIAN GULF
ARABIAN SEA
BAY OF BENGAL
INDIA
RED SEA
NORTH - EAST MONSOON
NORTH EQUAT CURR
AFRICA
EQUAT COUNTER CURR
SOUTH EQUAT CURR
TROPIC OF CAPRICORN
AUSTRALIA
ANTARCTIC CIRCUMPOLAR CURR
LATITUDE
20°E
40°
60°
80°
100°
120° E
LONGITUDE

(b)
MAY – SEPTEMBER
SOUTH - WEST MONSOON
SOMALI CURR
MONSOON CURR
MOZAMBIQUE CHAN
SOUTH EQUAT CURR

Fig. 2.1a

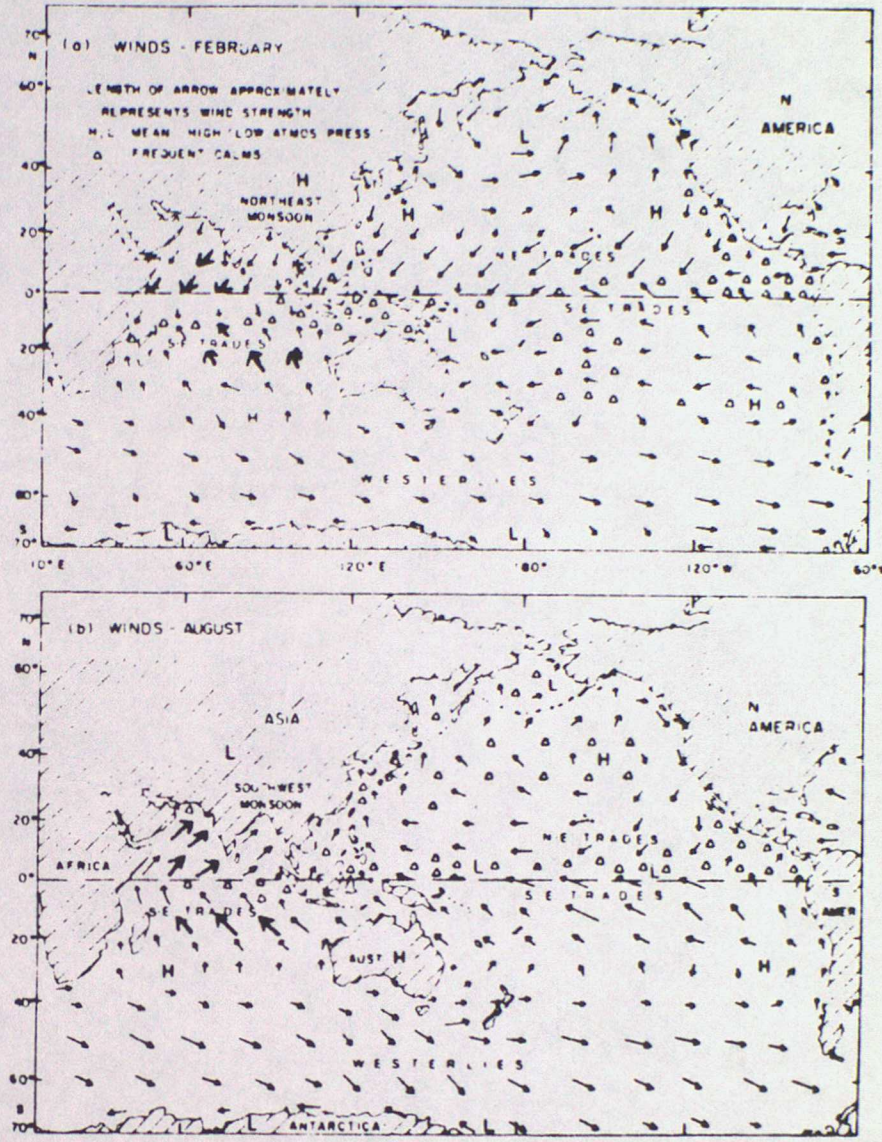
(a) WINDS - FEBRUARY
LENGTH OF ARROW APPROXIMATELY REPRESENTS WIND STRENGTH
H,L MEAN HIGH/LOW ATMOS PRESS
FREQUENT CALMS
N AMERICA
NORTHEAST MONSOON
NE TRADES
SE TRADES
ST TRADES
WESTERLIES
10°E
60°E
120°E
180°
120°W
60°W
(b) WINDS - AUGUST
ASIA
AFRICA
SOUTHWEST MONSOON
AUST
S AMER
ANTARCTICA

2.1b

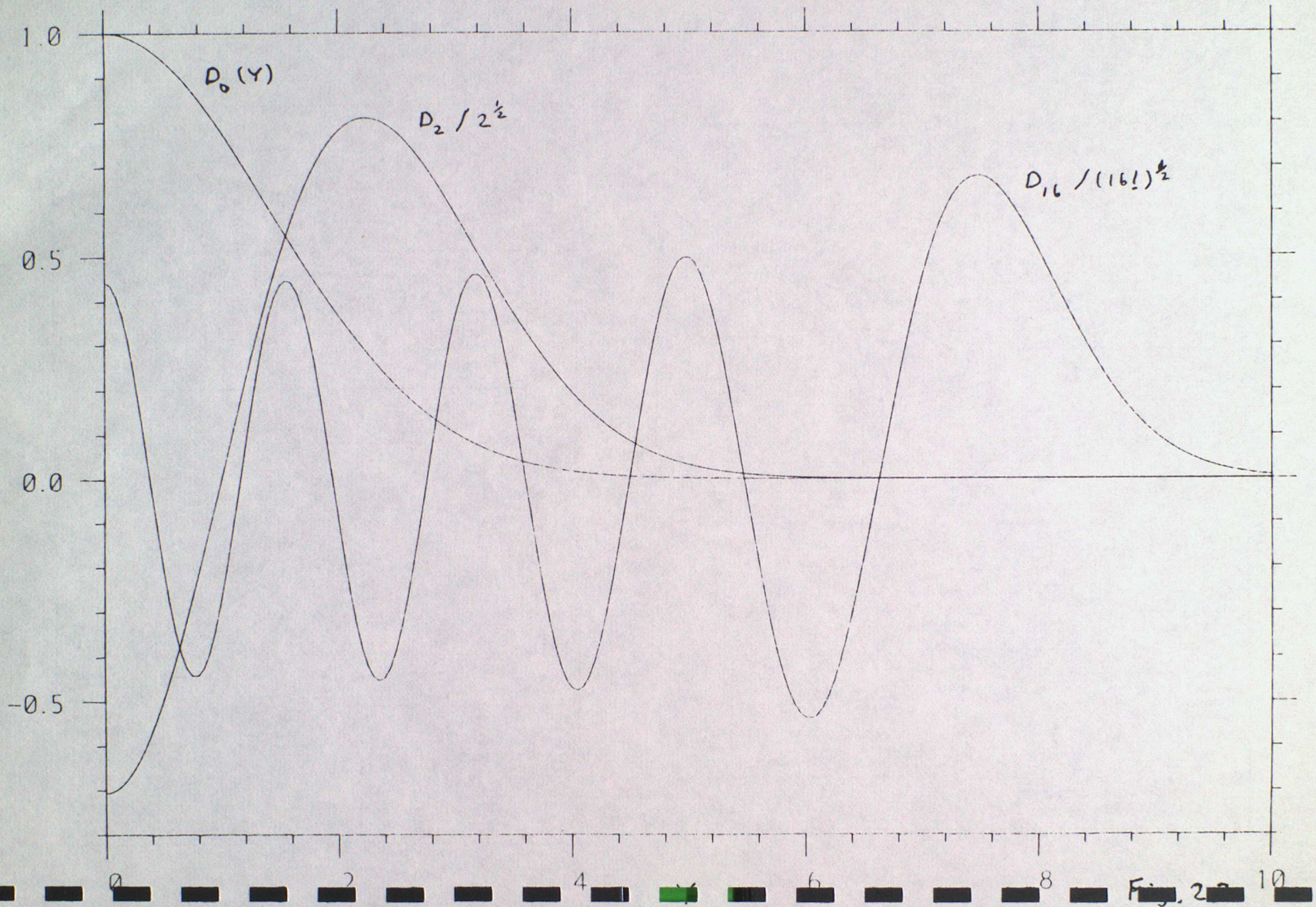

Fig. 2

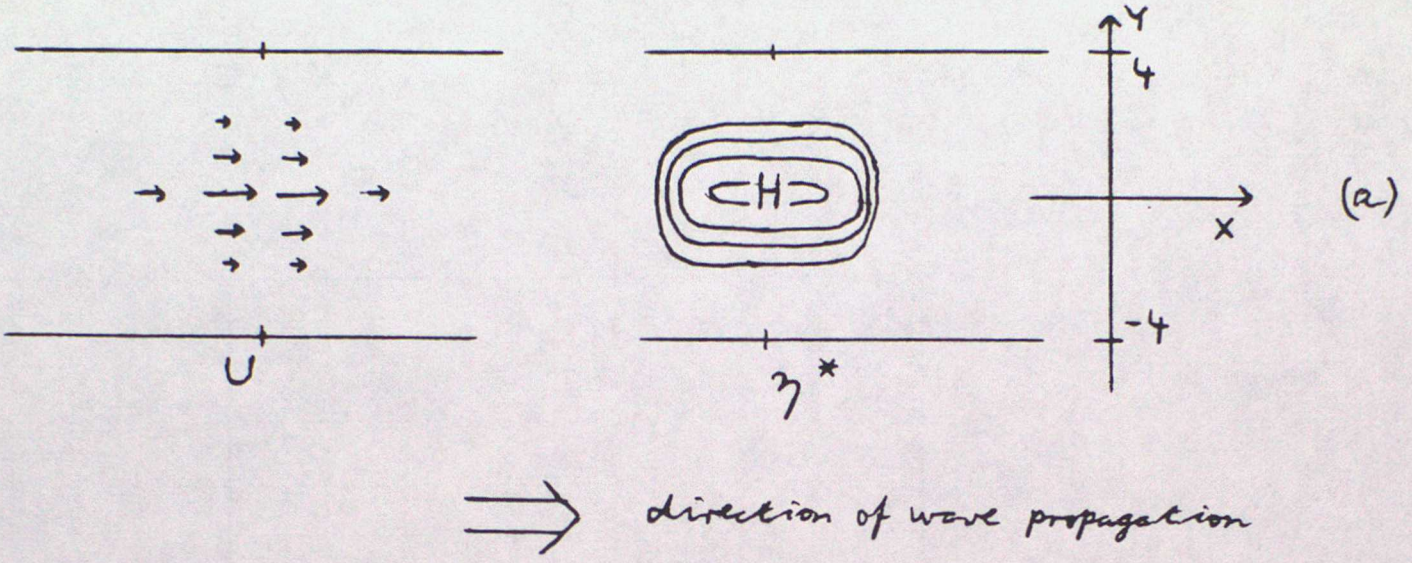
Y
4
X
-4
(a)
H
U
η*
direction of wave propagation

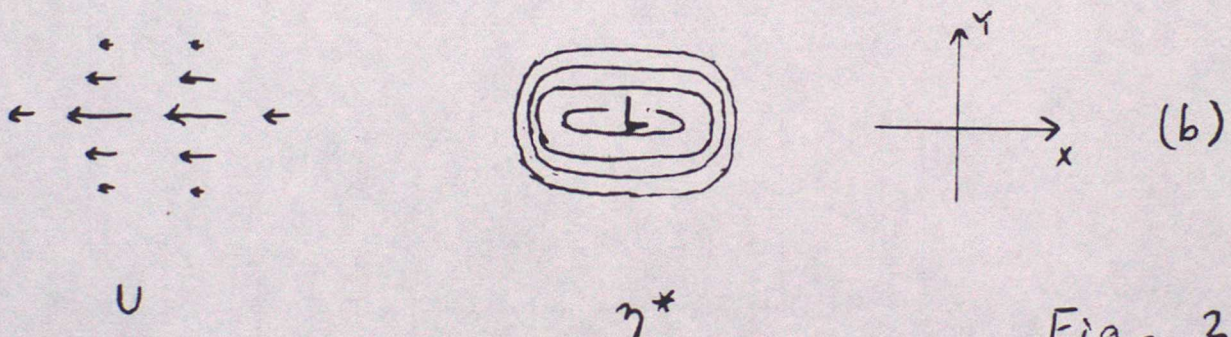
Y
X
(b)
U
η*

Fig. 2-3

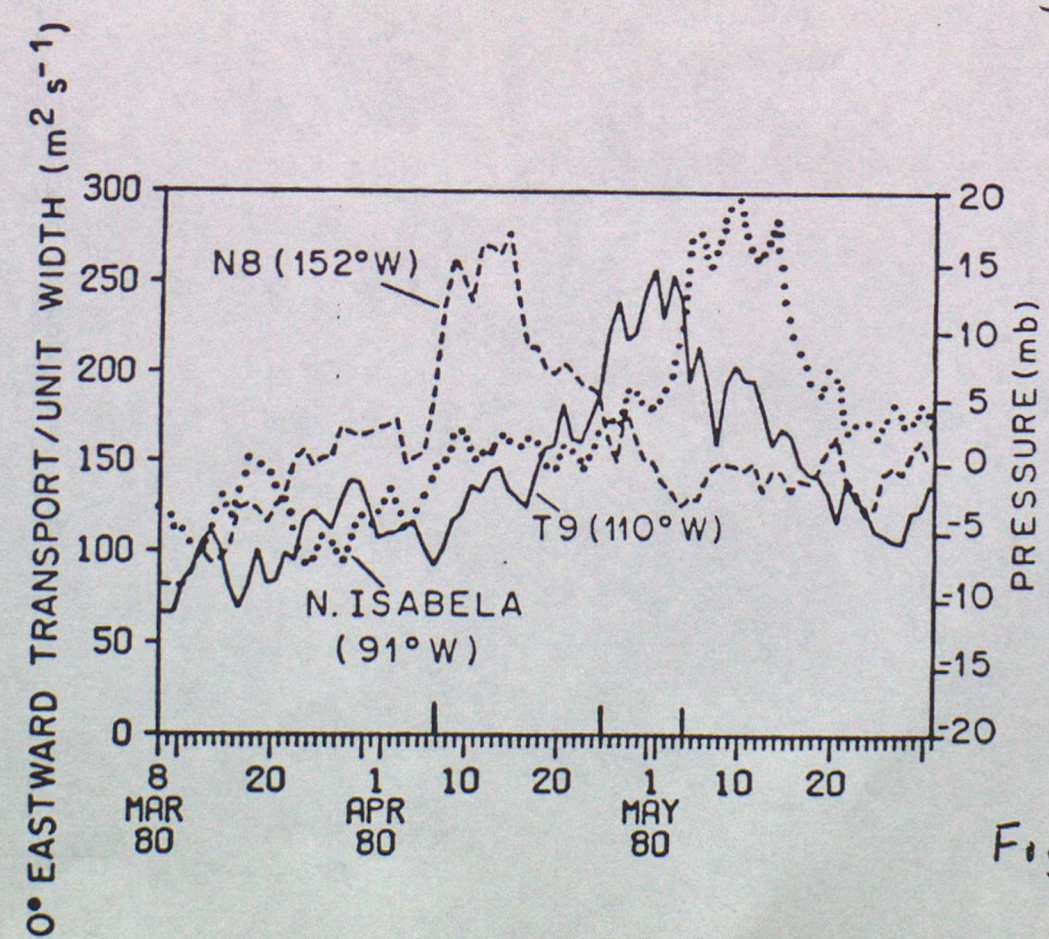
0° EASTWARD TRANSPORT/UNIT WIDTH (m² s⁻¹)
PRESSURE (mb)
N8 (152°W)
T9 (110°W)
N. ISABELA (91°W)
300
250
200
150
100
50
0
20
15
10
5
0
-5
-10
-15
-20
8 MAR 80
20
1 APR 80
10
20
1 MAY 80
10
20

Fig. 2-4

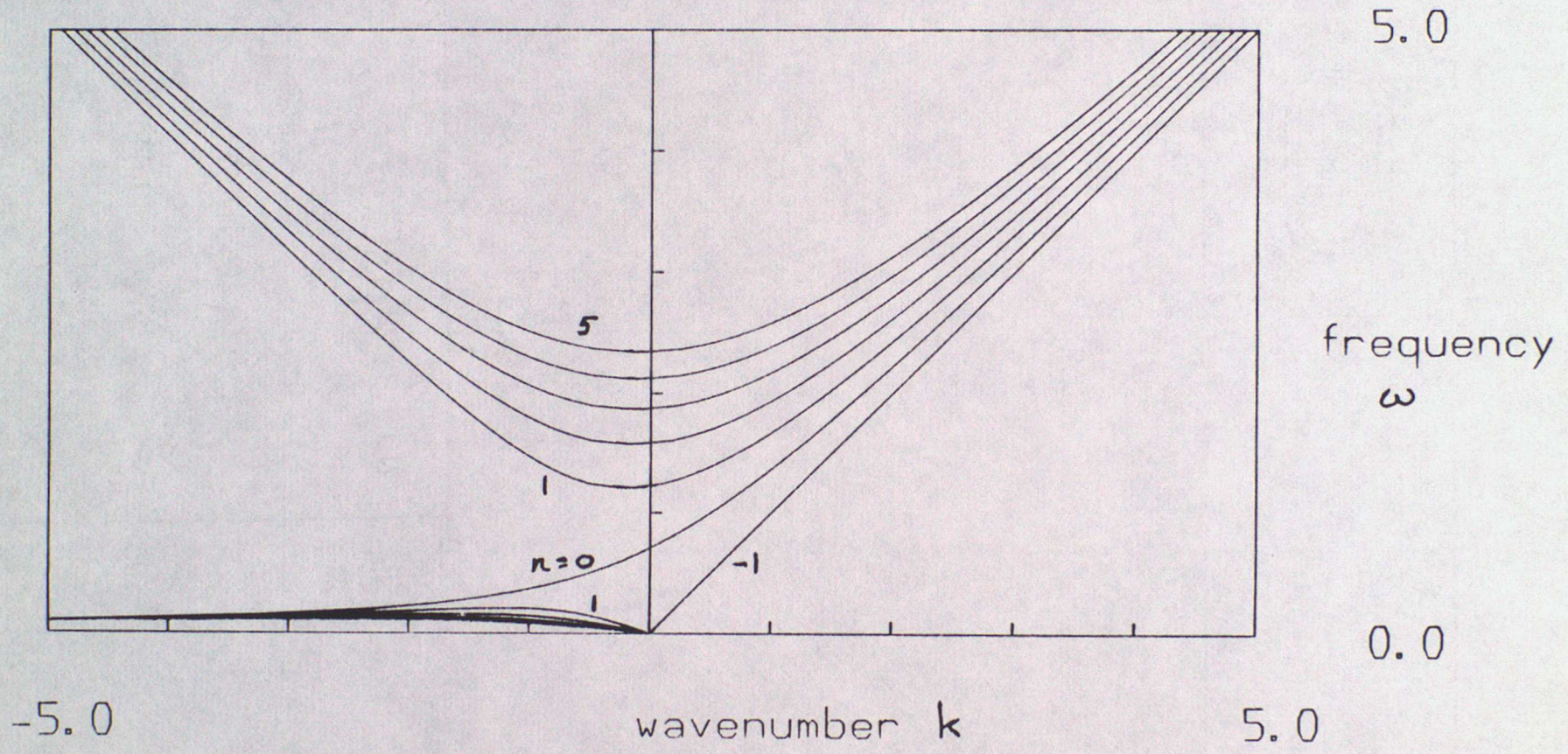

Fig. 2·5

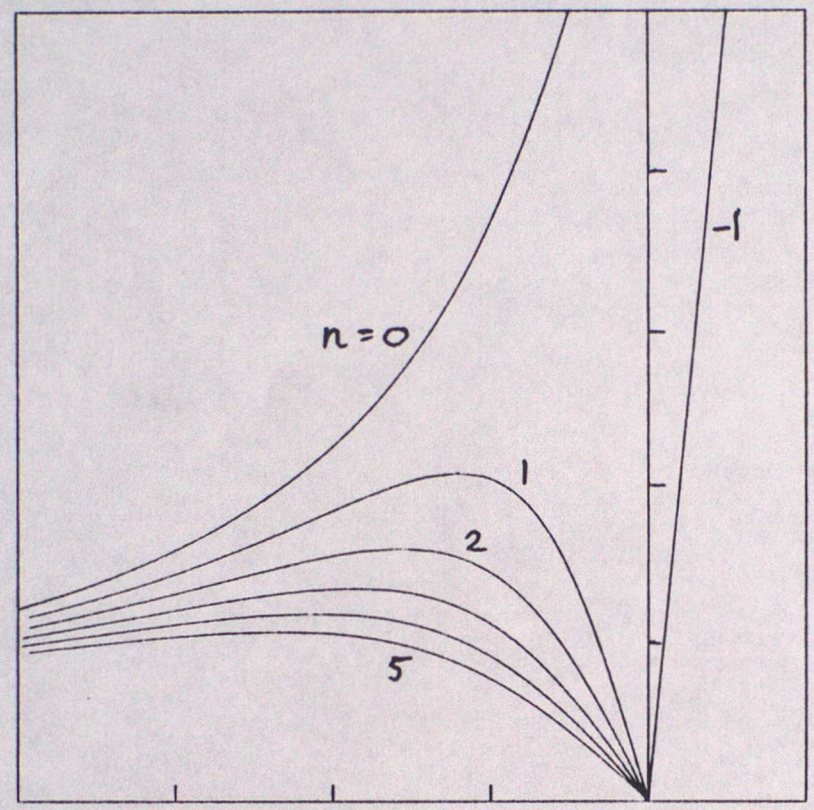

Fig. 2-6

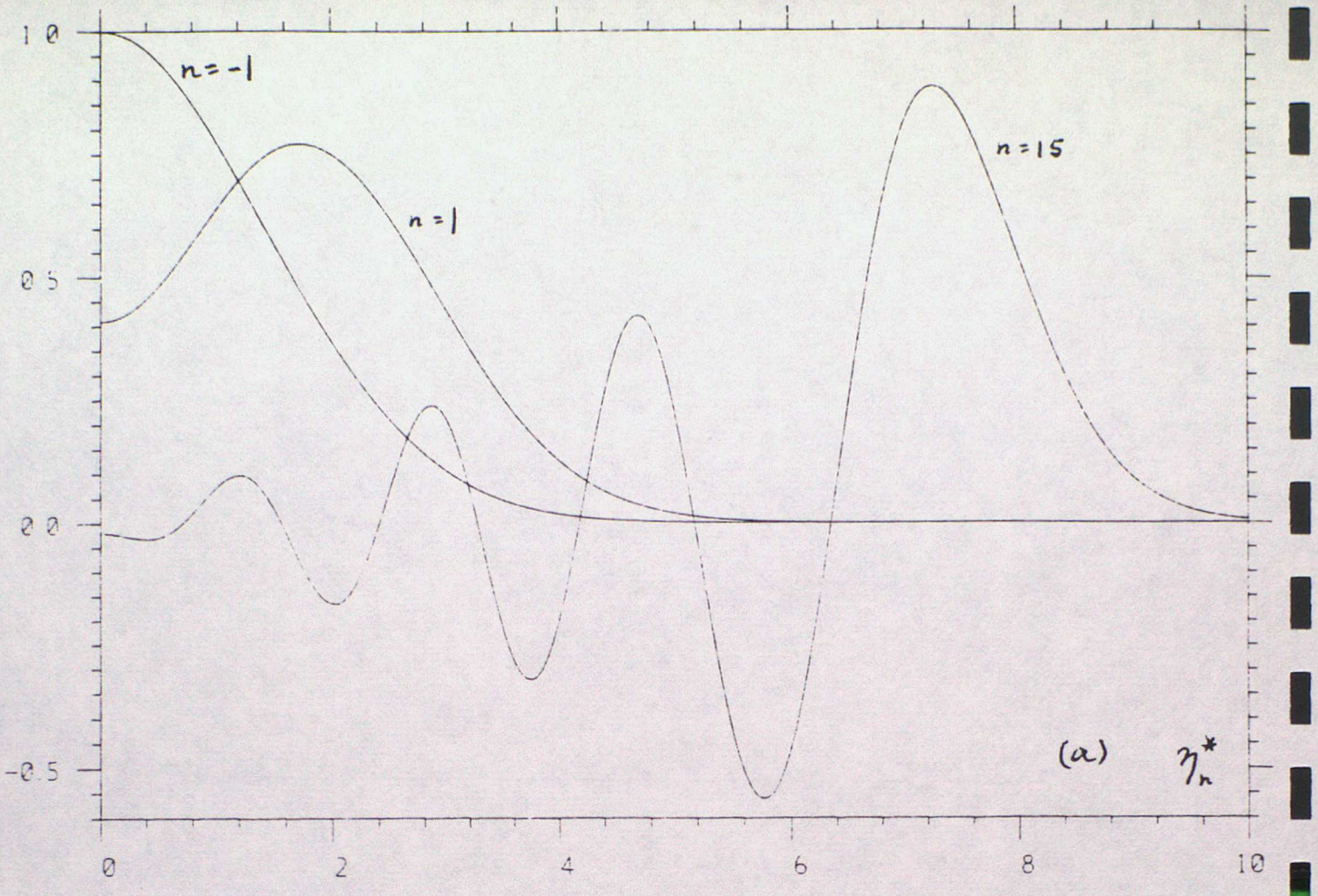
1.0
0.5
0.0
-0.5
0
2
4
6
8
10
n=-1
n=1
n=15
(a) η_n^*

Fig. 2-7

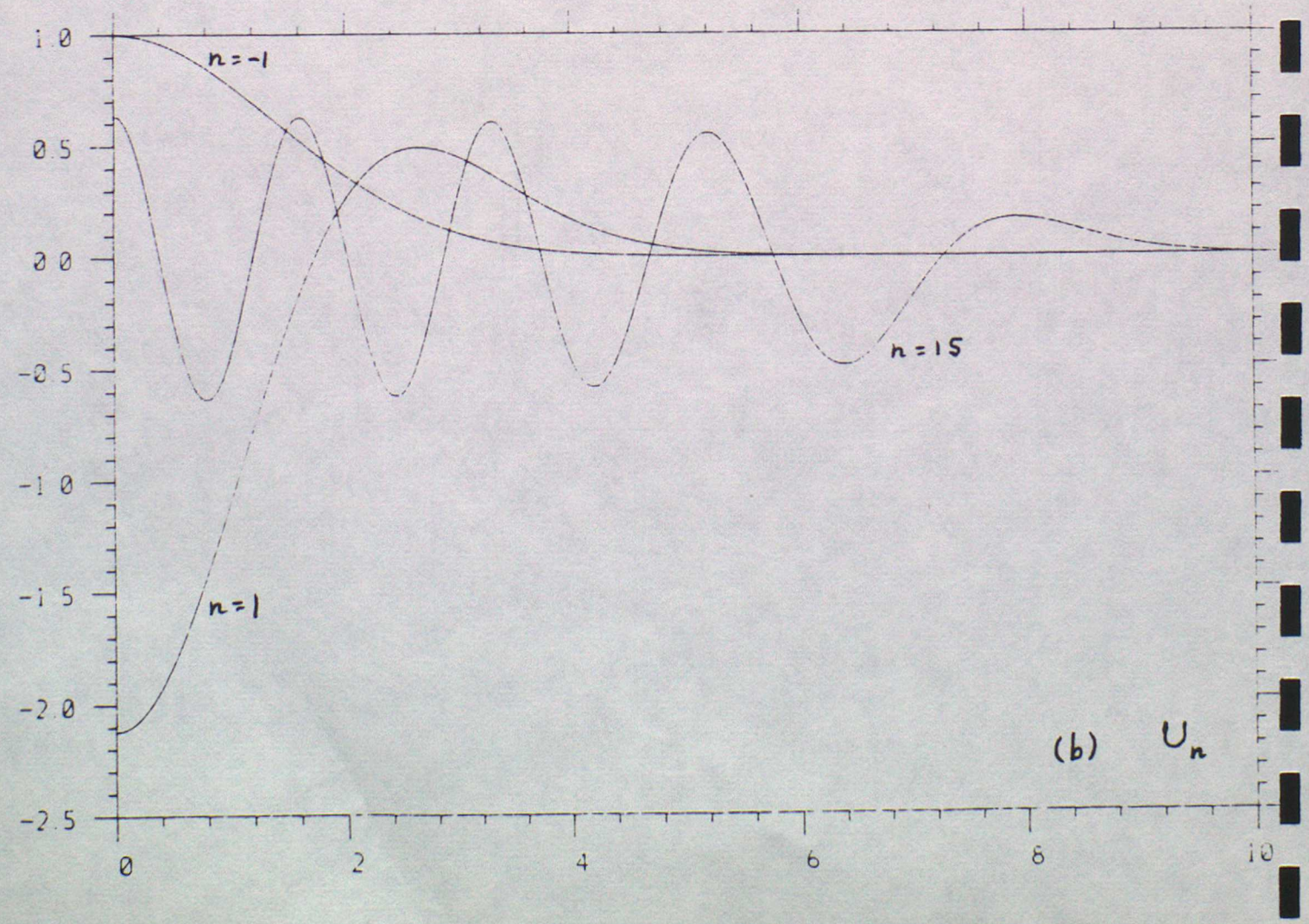
1.0
0.5
0.0
-0.5
-1.0
-1.5
-2.0
-2.5
0
2
4
6
8
10
n=-1
n=15
n=1
(b) U_n

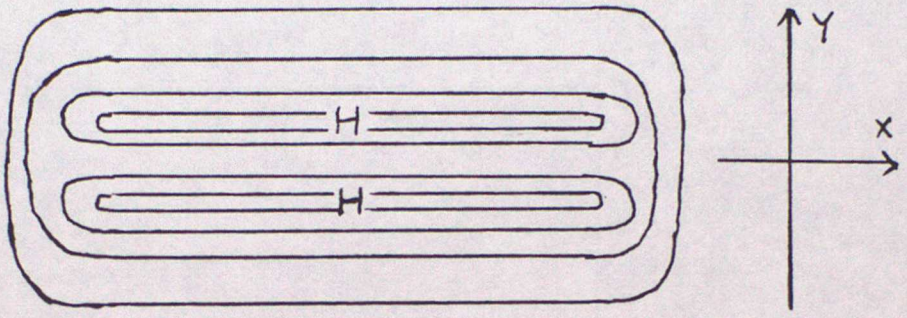

(a) ζ^*

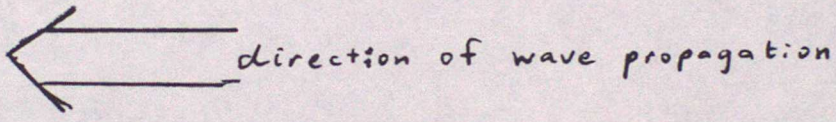

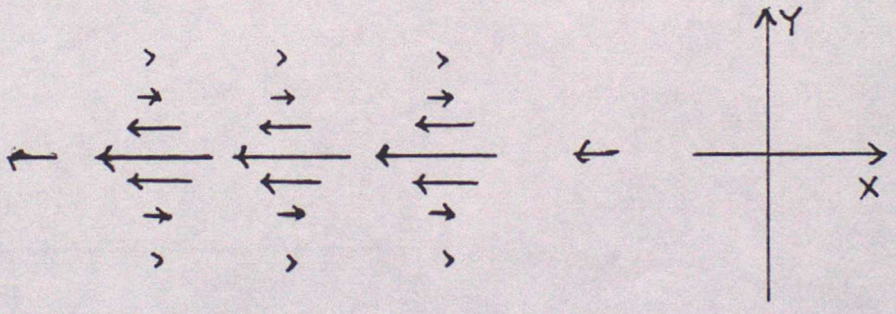

(b) U

Fig. 2.8

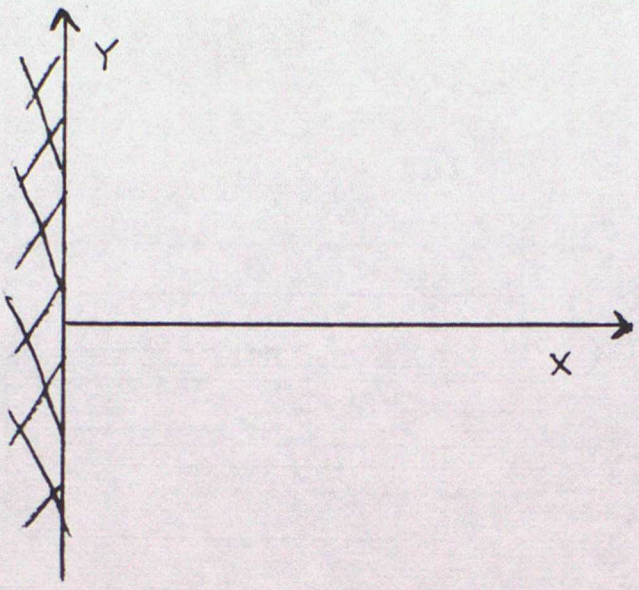

(a)

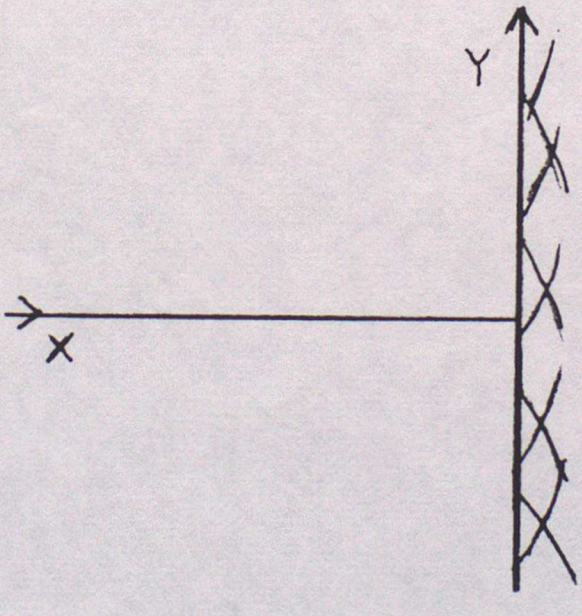

(b)

Fig. 2-9

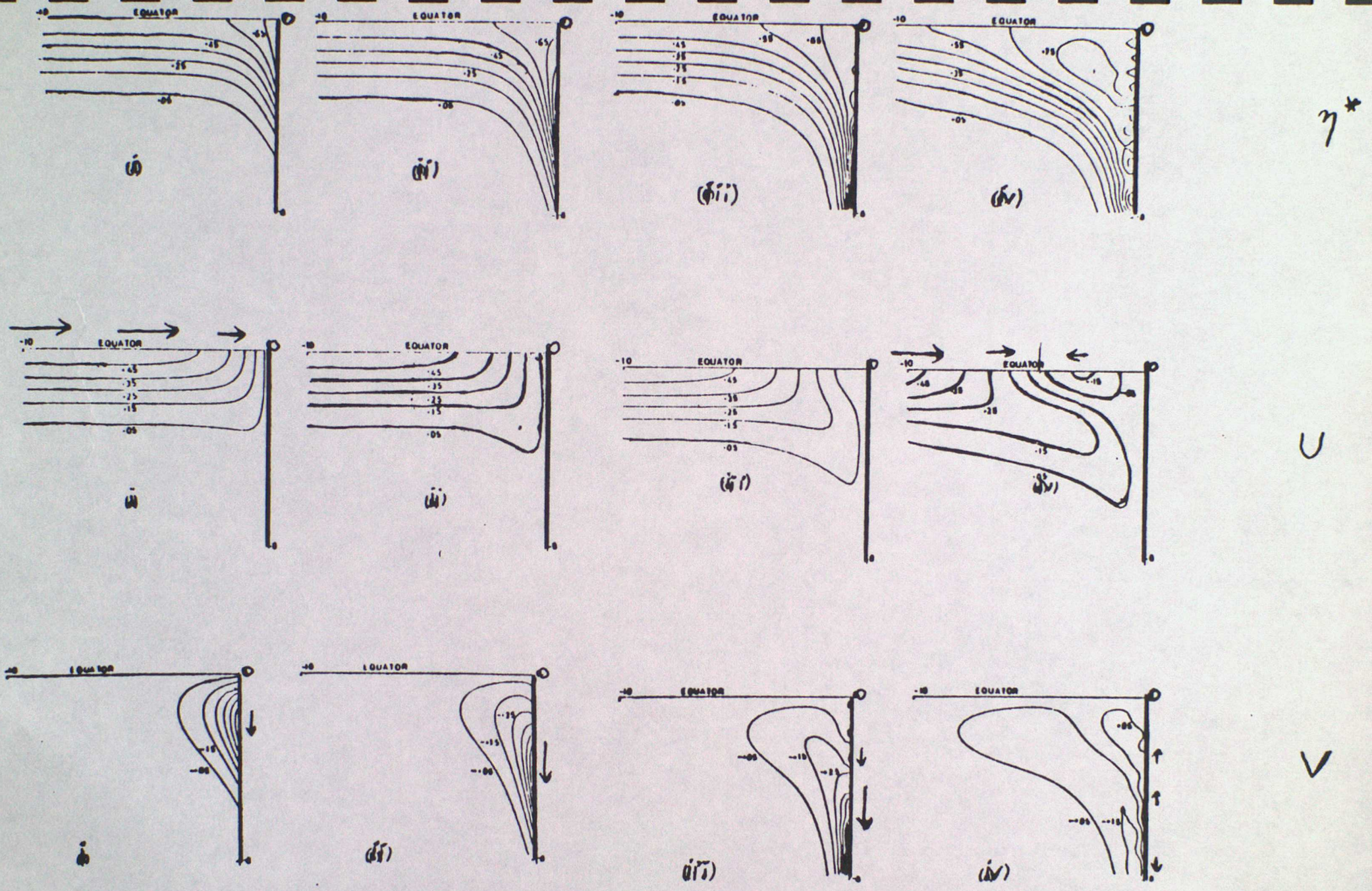

Fig. 2.10

Lecture 3 The ocean forced by wind stress

This lecture begins with a description of the Pacific Ocean. A range of models is then reviewed, followed by a more detailed look at some basic dynamics.

3.1 The observed Pacific

Fig. 3.1 shows a sketch of the main currents in the Pacific Ocean. Between 10°S and 4°N there is a westward surface flow known as the South Equatorial Current (SEC), which has speeds of about 0.5 m sec-1. To the north, between 4°N and 10° N, is the eastward flowing North Equatorial Countercurrent (NECC, with again speeds of 0.5 m sec-1), and further north again is the westward North Equatorial Current (NEC, speeds around 0.25 m sec-1). These currents are also shown in Fig. 3.2a along with the trade winds that drive them. Evidently the NECC flows in the opposite direction to the prevailing easterlies, in a region of lighter winds associated with the Intertropical Convergence Zone (ITCZ) --- one explanation for this opposition will be given below. These currents vary seasonally as winds change: detailed behaviour is not well known (except at particular places and times) due to the sparcity of observations.

Another important surface current is the Peru Current which flows north along the South American coast, south of the equator. Due to the southerly winds there is upwelling along the coast (c.f. the wind-driven rise in sea-level discussed in lecture 1), which brings cold water and nutrients to the surface promoting high biological productivity.

Returning to the equator, there is a remarkable subsurface current called the Equatorial Undercurrent (EUC), also known as the Cromwell Current. This is a narrow eastward subsurface flow with speeds of over 1 m sec-1 and a transport of around 40 Sv. It is about 100 m in vertical

extent, lies about 150 m below the sea surface, and is confined to $\pm 1^{\circ}$ from the equator (see Fig. 3.2b). The cause of this current will be explained later.

Fig. 3.2b also shows the meridional variation of sea-level and thermocline depth: the pressure gradients and zonal currents are in geostrophic balance.

Zonal variations of temperature in a section along the equator are shown in Fig. 3.3. (This particular figure is very common in equatorial oceanographic literature --- an indication of the paucity of data!) This can also be regarded as a density map, as density variations in the tropics are mostly due to temperature variations, being less sensitive to salinity. The figure shows a warm, deep mixed layer to the west that shallows and cools eastward. This distribution gives rise to a negative zonal pressure gradient that partly opposes the easterly surface wind stress.

Sea surface temperature (SST) is given in Fig. 3.4. There is a large area of very warm (>28°C) water in the west Pacific. Temperatures decrease to the east, and a tongue of relatively cool water can be seen along the equator in the east Pacific. The high temperatures are due to solar radiation of about 200 Watts m-2, partially offset by evaporative cooling of around 100 W m-2. (Longwave radiation transfers about 30 W m-2 from ocean to atmosphere, and sensible heat flux is about 10 W m-2 from atmosphere to ocean: these are minor effects for the ocean.) This influx of energy is balanced by mixing and by horizontal exchange. Fig. 3.5 shows a sketch of these processes. Upwelling is particularly strong near the equator (see below), and cool water is closest to the surface in the east (Fig. 3.3): this helps to maintain the cool tongue in the eastern

equatorial region. Water flowing westward along this tongue in the SEC is gradually warmed, to blend with the western warm pool.

Surface wind stress is shown in more detail in Fig. 3.6, for February and August. Generally the surface winds are easterly: two seasonal features to note are the monsoonal reversal over the far west Pacific, and the north-south movement of the ITCZ. The ITCZ is north of the equator in the eastern Pacific: winds over the equator there diminish when the ITCZ migrates equatorward in northern winter. Regional wind changes are important because equatorial waves can spread the effect rapidly along the equator.

3.2 The Yoshida Jet

We start the dynamics with a particularly simple case --- zonally symmetric flow in the 'shallow-water' ocean model driven by a uniform zonal wind. The non-dimensional SWE (2.5) reduce to

$$U_T - \tfrac{1}{2} Y V = F \quad , \tag{3.1a}$$

$$V_T + \tfrac{1}{2} Y U = - \eta^*_Y \quad , \tag{3.1b}$$

$$\eta^*_T + V_Y = 0 \quad , \tag{3.1c}$$

where F represents wind stress acting as a body force over the upper layer. From (3.1) we have

$$V_{YY} - \tfrac{1}{4} Y^2 V - V_{TT} = \tfrac{1}{2} Y F \quad , \tag{3.2}$$

which has a particular steady solution P(Y) satisfying

$$P_{YY} - \tfrac{1}{4} Y^2 P = \tfrac{1}{2} Y F \quad , \qquad (3.3)$$

For F=-1/2 (easterly trades) the standard solution is

$$P = \frac{\alpha Y}{2} \sum_0^\infty A_n (Y^4/4)^n - \frac{Y^3}{4} \sum_0^\infty B_n (Y^4/4)^n \quad , \qquad (3.4)$$

where

$$A_0 = 1 \quad , \quad A_n = A_{n-1} / (4n+1)4n \quad ,$$

$$B_0 = 1/6 \quad , \quad B_n = B_{n-1} / (4n+3)(4n+2) \quad ,$$

$$\alpha = 0.59907...$$

(Typically for an equatorial problem, our simple case has a rather inscrutable solution: see Gill (1975)for further details, or the original by Yoshida (1959).) Fig. 3.7 shows that this complicated function has a simple structure, with V=P representing poleward flow vanishing at the equator and as $Y \to \pm\infty$, with extrema at $Y \approx \pm 2$.

From (3.1), associated with this particular V we have

$$U = (\tfrac{1}{2} Y P - \tfrac{1}{2}) T \qquad (3.5a)$$

$$\eta^* = - P_Y T \quad . \qquad (3.5b)$$

In Fig. 3.7 the zonal flow is seen to be an accelerating westward jet centred on the equator (the Yoshida Jet), with weak eastward flow at higher latitudes. Upper layer depth is least at the equator ($\eta^* < 0$), and

slowly deepening at higher latitudes as required by mass conservation. From (3.1b), flow is longequator geostrophic. Away from the equator, U is negligible and V is just the steady Ekman drift (to the right of the wind in the northern hemisphere).

Divergence is strongest at the equator, and upward motion (upwelling) is strongest there to compensate. This effect can be seen near the equator in Fig. 3.3, with isotherms bowing upward near the surface (and sea-level correspondingly depressed).

When the wind is switched on other transient waves are also generated: see Moore & Philander (1978) for details and diagrams.

In practice U and η^* do not increase indefinitely but are limited by dissipation and, as will be shown, boundary effects.

3.3 Sverdrup balance

Another important simple case is that of steady, inviscid, wind-driven flow in an ocean with east and west boundaries. The SWE are now

$$-\tfrac{1}{2} Y V = -\eta^*_X + F \quad , \tag{3.6a}$$

$$\tfrac{1}{2} Y U = -\eta^*_Y + G \quad , \tag{3.6b}$$

$$U_X + V_Y = 0 \quad . \tag{3.6c}$$

From these equations we deduce

$$\tfrac{1}{2} V = G_X - F_Y \tag{3.7}$$

thus relating meridional flow to the wind stress curl. Following Sverdrup

(1947) we take U=0 at the east coast $X=X_E$ and use (3.6c) to obtain

$$\tfrac{1}{2} U = \int_X^{X_E} (G_x - F_Y)_Y \, dX \quad . \tag{3.8}$$

(In general $U \neq 0$ at the west coast according to this equation. Short planetary waves set up a boundary layer there --- c.f. western boundary currents like the Gulf Stream.) Hence

$$\eta^* = \int_{X_E}^{X} [F + Y(G_x - F_Y)] \, dX + \int_0^Y G(X_E, Y) \, dY + \tag{3.9}$$

$$+ \text{ some constant} \quad .$$

The main feature is that there is no flow if the wind stress curl vanishes. The wind stress is balanced by pressure gradients due to η^*, set up by waves and boundary effects. For example, with F=-1/2 and G=0 as for the Yoshida Jet case we find

$$\eta^* = -\tfrac{1}{2}[X - \tfrac{1}{2}(X_E + X_W)] \quad , \tag{3.10}$$

$$U = V = 0 \quad .$$

Pressure decreases eastward in this solution, as observed in the Pacific.

This theory offers one explanation of the NECC. In Fig. 3.2 we see that F>>G (winds are mainly zonal) and that $F_{YY} < 0$ in the NECC region, so (3.8) predicts an eastward current there, as observed. The theory as a whole is not entirely satisfactory however: e.g. observed currents are stronger than wind stress curl can explain, and no undercurrent is possible.

3.4 transient effects

The question arises as to how such a steady state could be established, and Cane & Sarachik (1976,1977,1979) investigated this as part of a series on forced inviscid shallow-water oceans.

When a constant wind stress is switched on at T=0 the initial response is a Yoshida jet, except at the east and west boundaries where zonal flow is blocked. At the west coast a Kelvin wave is generated along with (much slower) short planetary waves, while at the east coast long planetary waves are generated as described in lecture 2. In the interior the Yoshida jet continues to develop until a wave arrives from one of the boundaries. The Kelvin wave reaches the east coast at time $T_K = X_E - X_W$, and the fastest long Rossby wave reaches the west coast at time $T_R = 3(X_E - X_W)$. When these two waves meet at $X=(X_W + 3X_E)/4$ at time $T_Y = 3(X_E - X_W)/4$ the entire interior has been influenced by the boundary and the Yoshida Jet solution is no longer valid. Fig. 3.8 shows this sequence of exents diagrammatically.

The passage of these waves sets up a pressure gradient to oppose the wind stress. As slower waves (and reflections of faster waves) fill up the ocean the wind stress ans pressure gradient come into balance everywhere, more slowly further from the equator. Just along the equator the Kelvin and long Rossby waves slosh water to and fro, reflecting efficiently and delaying adjustment there. (See Cane & Sarachik 1977 for a detailed analysis and discussion of this adjustment.)

McCreary (1976) also describes solutions of the inviscid SWE for winds with assorted meridional structure, motivated by seeking the response to a

weakening of the trade winds (i.e. the onset of a westerly wind anomaly). Fig. 3.9 shows the effect near the eastern boundary for several zonal wind profiles: (a) uniform (c.f. Yoshide jet) (b) within 500 Km of equator (c) within 200 Km of equator (d) more than 500 Km from equator. Case (b) is very similar to case (a), case (c) shows a weaker response than (a), while (d) has very little equatorial signal. Clearly winds outside the equatorial band have little effect on the equator, but winds for 5°N to 5S need to be taken into account. Note in Fig. 3.9 the coastal Kelvin waves carrying equatorial disturbances poleward along the east coast. (Equivalently, higher mode waves with slower zonal propagation influence the higher latitudes, so the response is confined closer to the coast at higher latitudes.)

The westerly winds cause a deepening of the upper layer which is enhanced at the east coast (to create a positive zonal pressure gradient). Physically realistic parameters were chosen by McCreary for his examples: the 50m deepening after about 50 days is comparable to changes observed during El Nino events.

Another case selected from McCreary (1976) is the effect of northerly winds in a zonal band north of the equator. This is analogous to the longshore winds and storm surges described in lecture 1.: these winds drive a westward Ekman drift away from the coast. The result can be seen in Fig. 3.10. The upper layer deepens at the east coast and a coastal Kelvin wave carries this information poleward, as in lecture 1, but now Rossby waves also carry information westward away from the coast, more rapidly closer to the equator.

3.5 Dissipation effects and the Undercurrent

So far, dissipation has been ignored. In the ocean this effect is small

(typical decay scale is >100 days) so the fast waves (Kelvin and long Rossby) can cross even the Pacific virtually unaffected, as observed. Slower waves are affected more strongly, with important consequences.

In the context of the SWE with uniform forcing considered so far, Yamagata & Philander (1985) have considered the effect of mixing of 'heat' and momentum by adding Newtonian 'cooling' (damping of depth changes) and Rayleigh friction. For the long non-dispersive waves mixing of heat is far more effective than mixing of momentum as a damping mechanism.

Of more direct interest is McCreary (1981) who used a continuously stratified model with dissipation, separated into vertical modes governed by the SWE as described in lecture 1. The steady response to easterly wind stress is sought: there is a surface mixed layer and the wind acting on this layer as a body force is projected onto the vertical mode structure. In the absence of dissipation Sverdrup balance is realised for each mode: these sum together to give motion (due only to non-zero wind stress curl) only in the directly forced mixed layer, uniform with depth (no undercurrent).

With dissipation the higher mode (vertical and horizontal) waves are damped shorter distances from their region of generation by direct forcing or boundary reflection, so the process of adjustment toward Sverdrup balance is incomplete. Only for the fastest modes is a pressure gradient established across the ocean to balance the wind stress. In particular, the pressure gradient no longer matches the wind stress along the equator in the mixed layer, and no longer sums to zero below the mixed layer, so substantial zonal currents are driven there.

Fig. 3.11 shows the result: there is a westward surface current and, below the mixed layer, there is an eastward undercurrent of realistic

magnitude. (Note that the wind stress applied in this model is not zonally uniform, but strongest at mid-ocean.) Other features are the upwelling into the mixed layer, and the very weak flow at depths >200 m. Fig. 3.12 shows a mid-ocean meridional section: the undercurrent is realistically trapped to within 1° of the equator. Surface flow has a poleward component, while there is subsurface equatorward flow into the undercurrent to supply the equatorial upwelling.

3.6 SWE and simulation

A linear 'shallow-water' SWE ocean model has been constructed with the geometry of the Pacific Ocean from 18°N to 12° S, and forced with wind stress as observed over several years (subjectively analysed due to the paucity of data), as described by Busalacchi & O'Brien (1980,1981) and Busalacchi et. al. (1983). Despite its simplicity, this model produces variations in upper layer thickness that compare well with observed sea-level changes in the eastern, central and western Pacific. Strong El Nino events are reproduced, being associated with weakening of trade winds in the western Pacific. Currents are not realistic due to the limited vertical resolution and the absence of thermodynamics.

3.7 Other ocean models

We have concentrated on simple linear models to concentrate on the basic dynamical processes. There are of course many others of varying complexity. McCreary (1985) gives a good review of the range, so just a few are mentioned here. For the linear SWE, Cane & Patton (1984) describe an efficient procedure for numerical calculations, using the longwave approximation to eliminate all but the long non-dispersive waves (Kelvin and long Rossby). Cane (1979a,b) presents a model which is essentially a 'shallow-water' ocean with a directly wind-driven sub-layer of constant

depth —— this structure allows an undercurrent; linear and nonlinear effects are described. A variation of the 'shallow-water' ocean that includes simple thermodynamics and allows varying sea-surface temperature can be found in Anderson & McCreary (1985).

Ocean general circulation models have been applied to the tropics. An example illustrating the response to the switch-on of a zonal wind stress can be seen in Philander & Pacanowski (1980). Such models often use non-uniform grid spacing, concentrated near the equator to better represent the major equatorial waves: e.g. Philander & Seigel (1985). A related ocean GCM is being used in Met. O. 20 to simulate the tropical ocean, and this has been coupled to the Met. O. atmospheric global GCM (as has a global ocean GCM of lower resolution).

References for lecture 3

Anderson, D.L.T. & J.P. McCreary (1985)
Slowly propagating disturbances in a coupled ocean-atmosphere model
J. Atmos. Sci., 42, 615-629

Busalacchi, A.J. & J.J. O'Brien (1980)
The seasonal variability in a model of the tropical Pacific
J. Phys. Oceanog., 10, 1929-1951

Busalacchi, A.J. & J.J. O'Brien (1981)
Interannual variability of the equatorial Pacific in the 1960's
J. Geophys. Res., 86, 10901-10907

Busalacchi, A.J., K. Takeuchi & J.J. O'Brien (1983)
Interannual variability of the equatorial Pacific --- revisited
J. Geophys. Res., 88, 7551-7562

Cane, M.A. (1979)
The response of an equatorial ocean to simple wind stress patterns
I Model formulation and analytic results
II Numerical results
J. Mar. Res., 37, 233-252, 355-398

Cane, M.A. & E.S. Sarachik (1976)
Forced baroclinic ocean motions
I The linear equatorial unbounded case
J. Mar. Res., 34, 629-665

Cane, M.A. & E.S. Sarachik (1977)
Forced baroclinic ocean motions
II The linear equatorial bounded case
J. Mar. Res., 35, 395-432

Cane, M.A. & E.S. Sarachik (1979)
Forced baroclinic ocean motions
III The linear equatorial basin case
J. Mar. Res., 37, 355-398

Cane, M.A. & R.J. Patton (1984)
A numerical model for low-frequency equatorial dynamics
J. Phys. Oceanog., 14, 1853-1863

Gill, A.E. (1975)
Models of equatorial currents
In: 'Numerical models of ocean circulation', pp181-203
National Acad. Sci., Washington D.C.

Gill, A.E. (1982)
Atmosphere-Ocean Dynamics
Academic Press, 666pp

McCreary, J.P. (1976)
Eastern tropical ocean response to changing wind systems --- with appliation to El Nino
J. Phys. Oceanog., 6, 632-645

McCreary, J.P. (1981)
A linear stratified ocean model of the Equatorial Undercurrent
Phil. Trans. Roy. Soc. London, 298, 603-635

McCreary, J.P. (1985)
Modelling equatorial ocean circulation
Ann. Rev. Fluid Mech., 17, 359-409

Moore, D.W. & S.G.H. Philander (1978)
Modelling of the tropical oceanic circulation
In: 'The Sea', Vol. 6, pp319-362
Wiley (Interscience), New York

Philander, S.G.H. & R.C. Pacanowski (1980)
The generation of equatorial currents
J. Geophys. Res., 85, 1123-1136

Philander, S.G.H. & A.D. Seigel (1985)
Simulation of El Nino of 1982-83
In: 'Coupled Ocean-Atmosphere Models' (J.C.J. Nihoul ed.)
Elsevier Oceanography Series Vol. 40, pp517-541

Pickard, G.L. & W.J. Emery (1982)
Descriptive physical oceanography
Pergamon Press, 249pp

Sverdrup, H.V. (1947)
Wind-driven currents in a baroclinic ocean: with application to the equatorial currents of the Eastern Pacific
Proc. National Acad. Sci., 33, 318-326

Toole, J.M. (1984)
Sea surface temperature in the equatorial Pacific
Oceanus, 27, 29-34

Yamagata, T. & S.G.H. Philander (1985)
The role of damped equatorial waves in the oceanic response to winds
J. Ocean. Soc. Japan, 41, 345-357

Yoshida, K. (1959)
A theory of the Cromwell current (the equatorial undercurrent) and of the equatorial upwelling --- an interpretation in a similarity to a coastal circulation
J. Ocean. Soc. Japan, 15, 159-170

Fig. 3.1 Major currents in the Pacific Ocean (from Pickard & Emery 1982)

Fig. 3.2 A typical meridional section across the equatorial Pacific.
(a) surface currents and trade winds
(b) vertical structure of the upper ocean
(from Pickard & Emery 1982)

Fig. 3.3 A vertical section of temperature along the Pacific equator (from Toole 1984)

Fig. 3.4 Climatological sea-surface temperature in the tropical Pacific (from Toole 1984)

Fig. 3.5 Structure of the upper ocean in the eastern equatorial Pacific (from Toole 1984)

Fig. 3.6 Climatological surface wind stress over the tropical Pacific
(a) February (b) August (from Gill 1982)

Fig. 3.7 The Yoshida Jet: zonally symmetric response to a uniform easterly wind. Poleward flow V is steady, while U and η^* increase linearly with time.

Fig. 3.8 The principal effect of boundaries when a uniform wind stress is switched on: a Kelvin wave travels at speed 1 from the west coast and a long Rossby wave travels at speed -1/3 from the east coast. They meet at time $T_Y = 3(X_E - X_W)/4$, opposing the Yoshida jet.

Fig. 3.9 The change in upper-layer depth in response to the onset of westerly wind stress in a zonal strip, with latitudinal dependence shown to the left of each case. Horizontal distances are in Km (from McCreary 1976)

Fig. 3.10 The change in upper-layer depth in response to the onset of northerly winds in a zonal strip north of the equator. Horizontal distances are in Km (from McCreary 1976)

Fig. 3.11 The response along the equator to easterly wind stress in a continuously stratified model with dissipation.
(1) contours of zonal velocity in cm sec-1
(2) circulation in the zonal plane: calibration arrows show 100 cm sec-1 horizontally and 0.005 cm sec-1 vertically.
Note the strong eastward undercurrent (from McCreary 1981)

Fig. 3.12 As Fig. 3.11, but showing a meridional mid-ocean section. Calibration arrows are 10 cm sec-1 (horizontal) and 0.005 cm sec-1 (vertical) (from McCreary 1981)

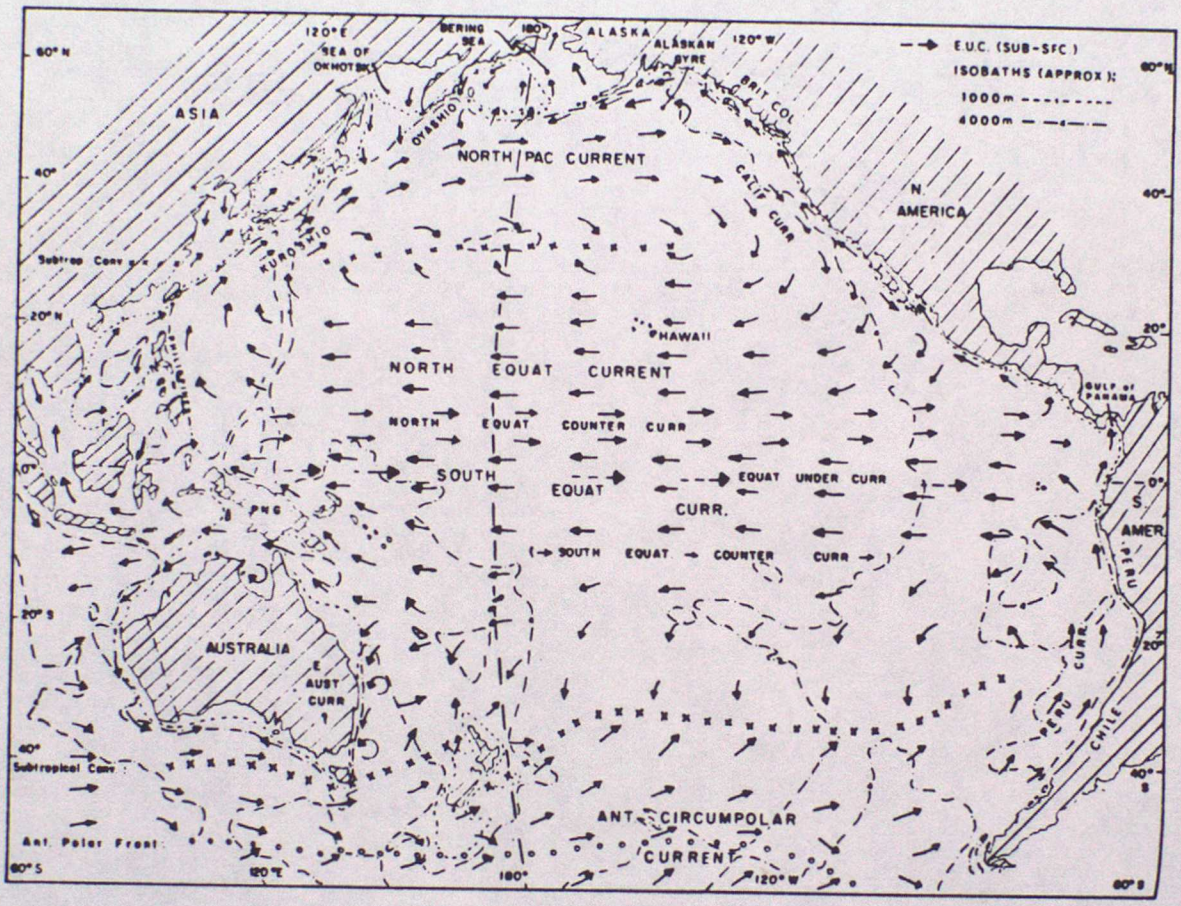
E.U.C. (SUB-SFC.)
ISOBATHS (APPROX.):
1000m
4000m
ASIA
N. AMERICA
AUSTRALIA
S. AMER.
HAWAII
NORTH PAC CURRENT
NORTH EQUAT CURRENT
NORTH EQUAT COUNTER CURR
SOUTH EQUAT CURR.
EQUAT UNDER CURR
SOUTH EQUAT COUNTER CURR
ANT. CIRCUMPOLAR CURRENT
Ant. Polar Front
Subtrop Conv
Subtropical Conv
KUROSHIO
OYASHIO
CALIF CURR
PERU CURR
CHILE
AUST CURR
GULF of PANAMA
BERING SEA
ALASKAN GYRE
SEA OF OKHOTSK
PNG
120°E
180°
120°W
60°N
40°
20°N
0°
20°S
40°S
60°S

Fig. 3-1

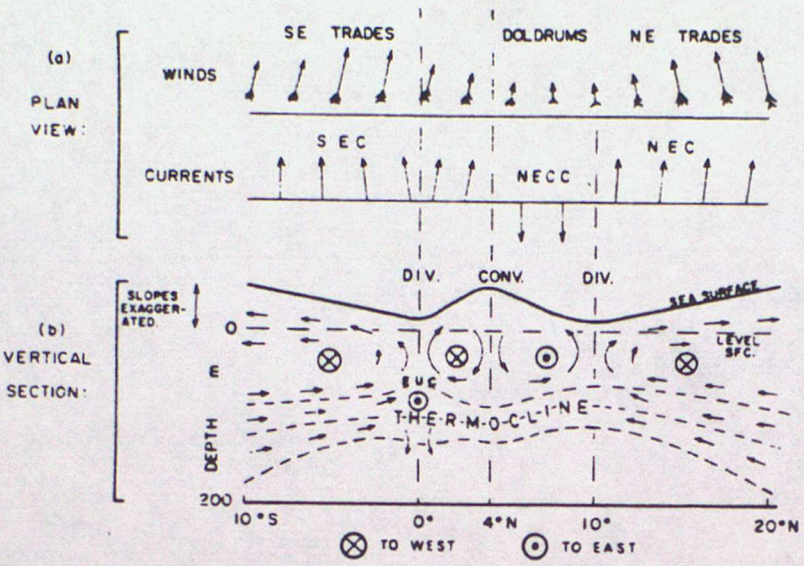
(a)
PLAN VIEW:
WINDS
SE TRADES
DOLDRUMS
NE TRADES
CURRENTS
SEC
NECC
NEC
(b)
VERTICAL SECTION:
SLOPES EXAGGERATED.
DIV.
CONV.
DIV.
SEA SURFACE
LEVEL SFC.
0
E
EUC
THERMOCLINE
DEPTH
200
10°S
0°
4°N
10°
20°N
TO WEST
TO EAST

Fig. 3-2

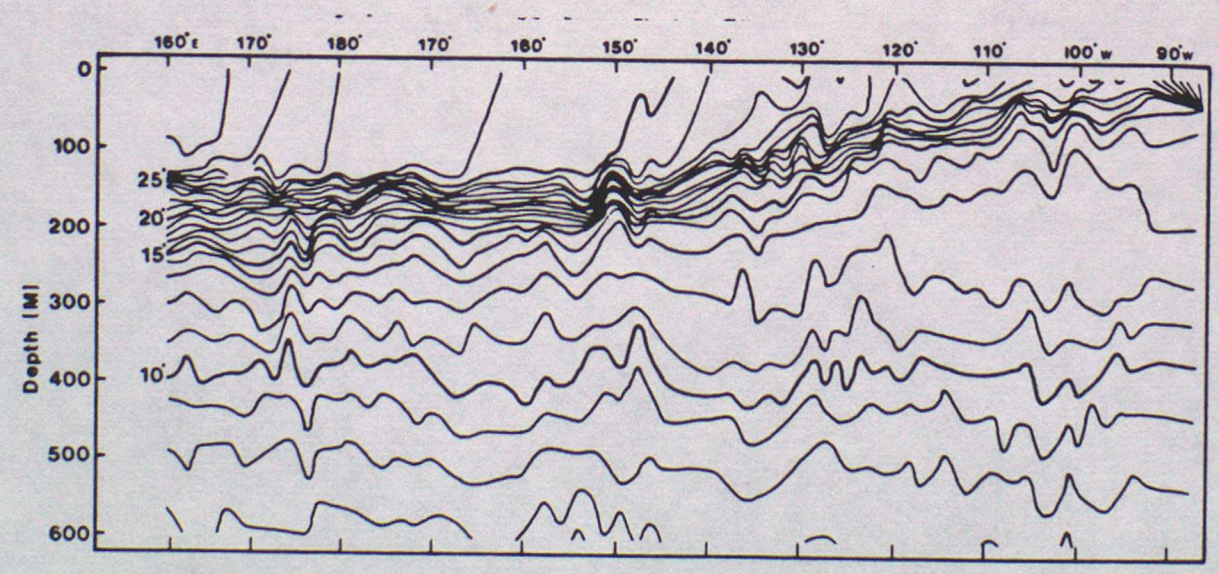
160°E
170°
180°
170°
160°
150°
140°
130°
120°
110°
100°W
90°W
0
100
200
300
400
500
600
Depth (M)
25°
20°
15°
10°

Fig. 3-3

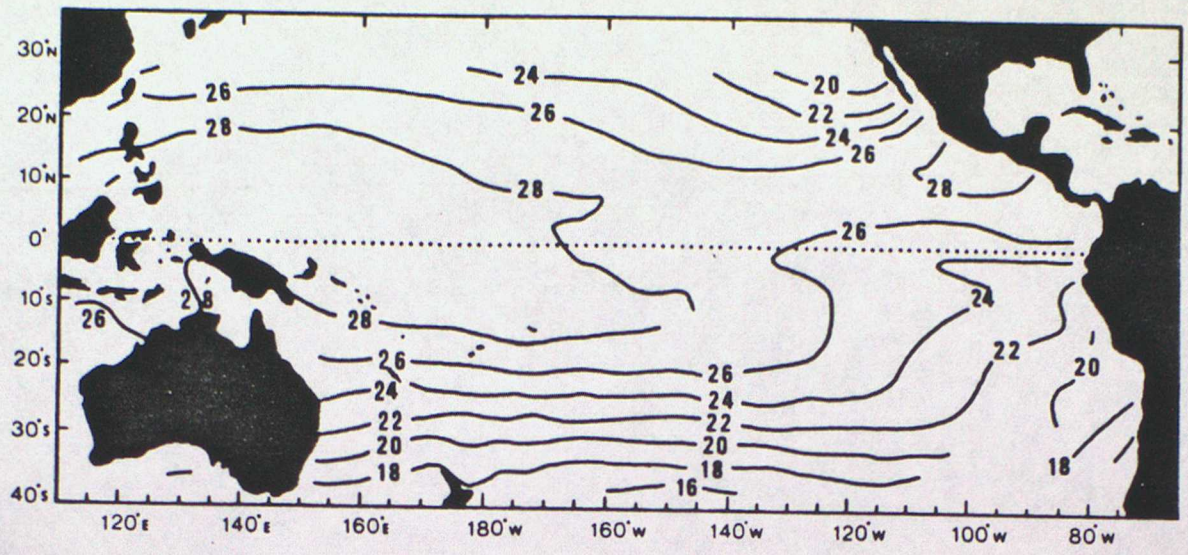
30°N
20°N
10°N
0°
10°S
20°S
30°S
40°S
120°E
140°E
160°E
180°W
160°W
140°W
120°W
100°W
80°W
26
28
24
20
22
18
16

Fig. 3-4

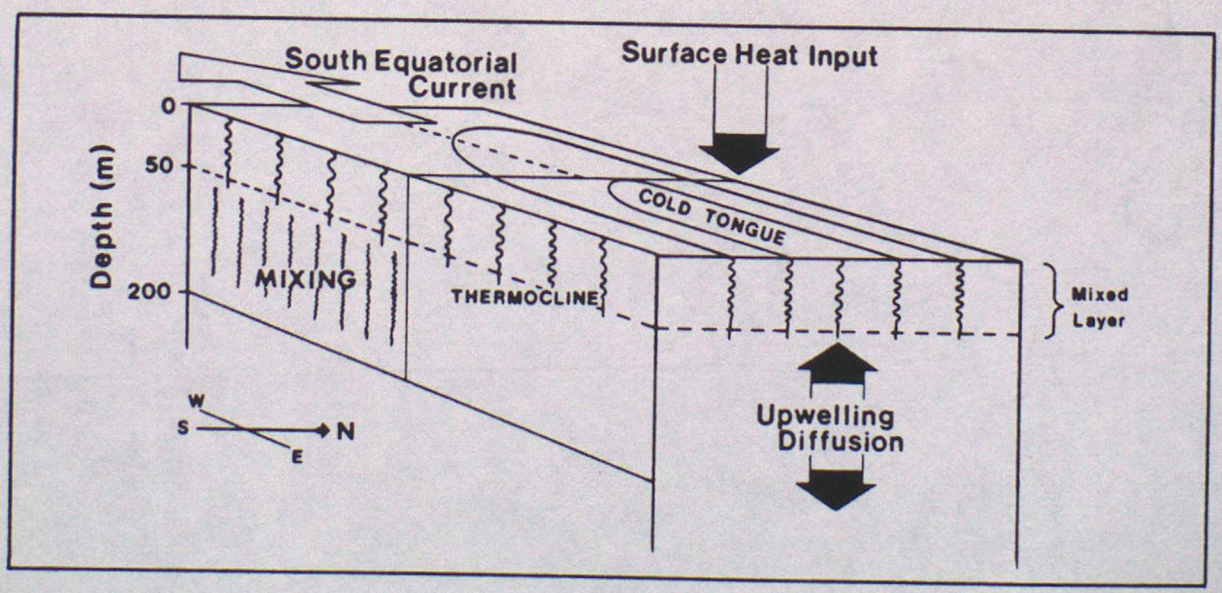
South Equatorial Current
Surface Heat Input
Depth (m)
0
50
200
COLD TONGUE
MIXING
THERMOCLINE
Mixed Layer
Upwelling
Diffusion
W
S
N
E

Fig. 3.5

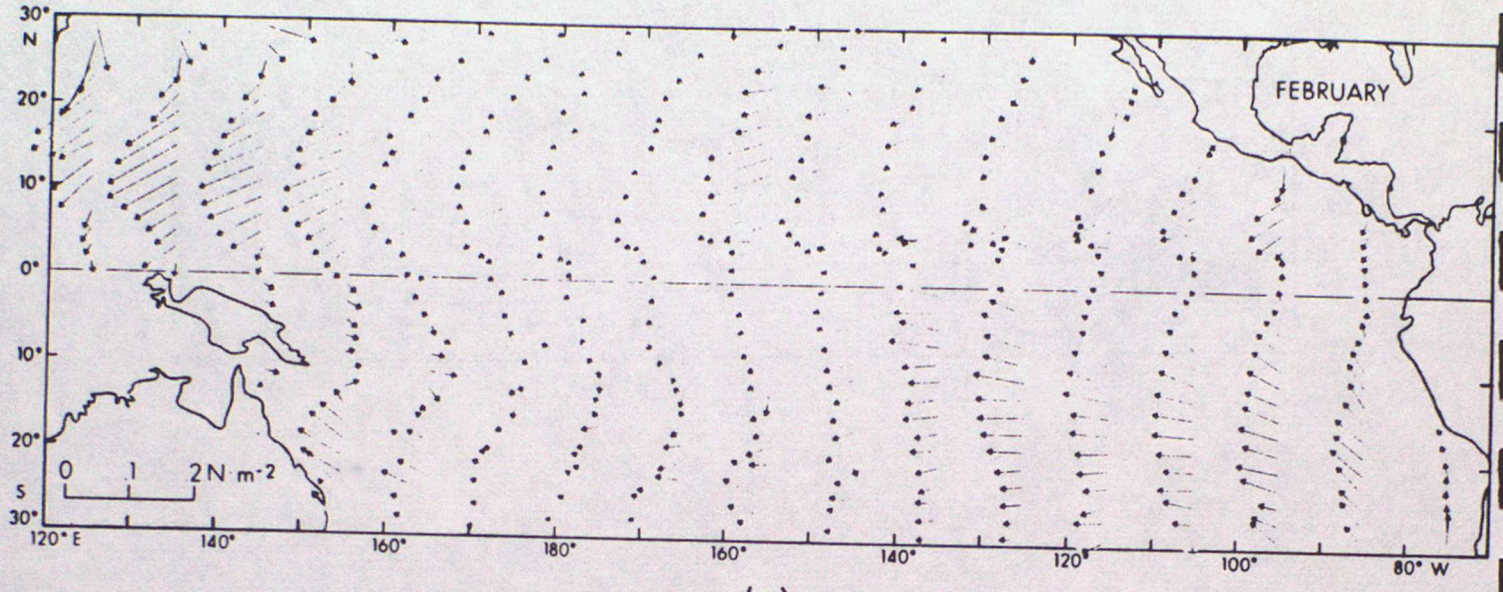
30° N
20°
10°
0°
10°
20°
S 30°
FEBRUARY
0 .1 2N·m-2
120° E
140°
160°
180°
160°
140°
120°
100°
80° W

(a)

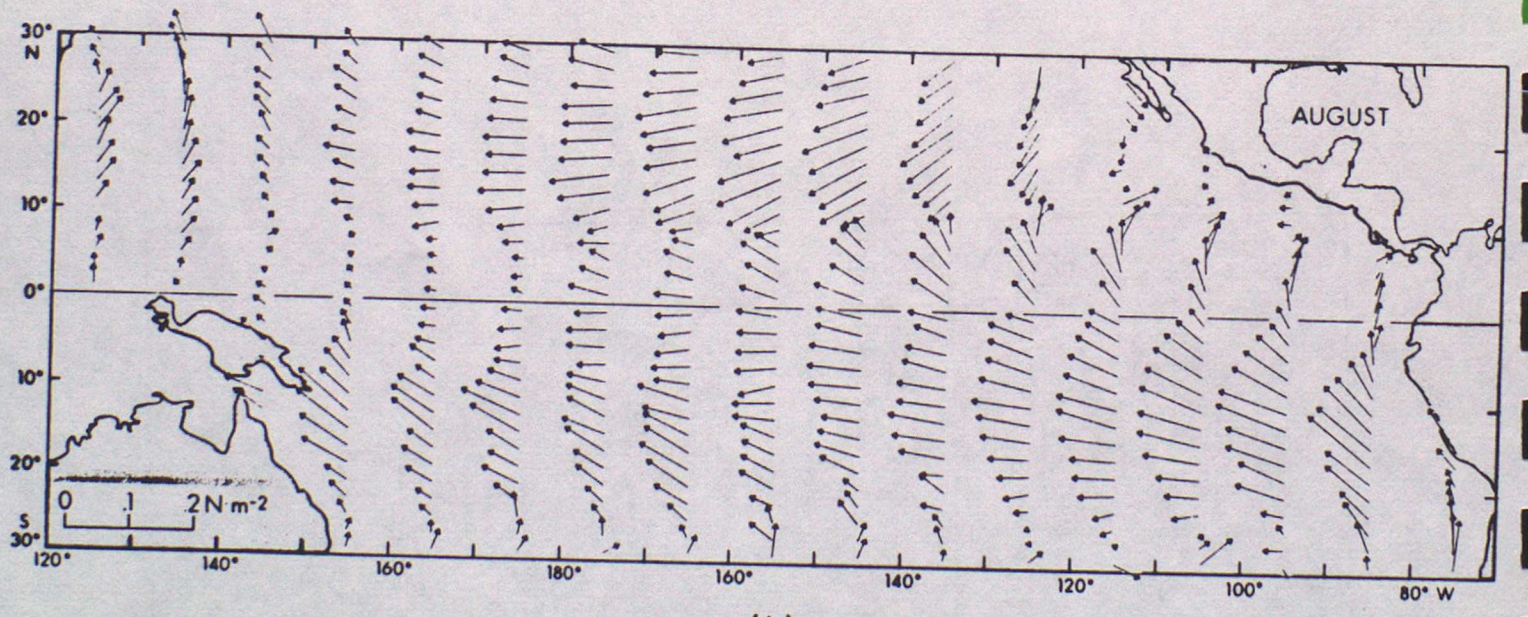
30° N
20°
10°
0°
10°
20°
S 30°
AUGUST
0 .1 2N·m-2
120°
140°
160°
180°
160°
140°
120°
100°
80° W

(b)

Fig. 3-6

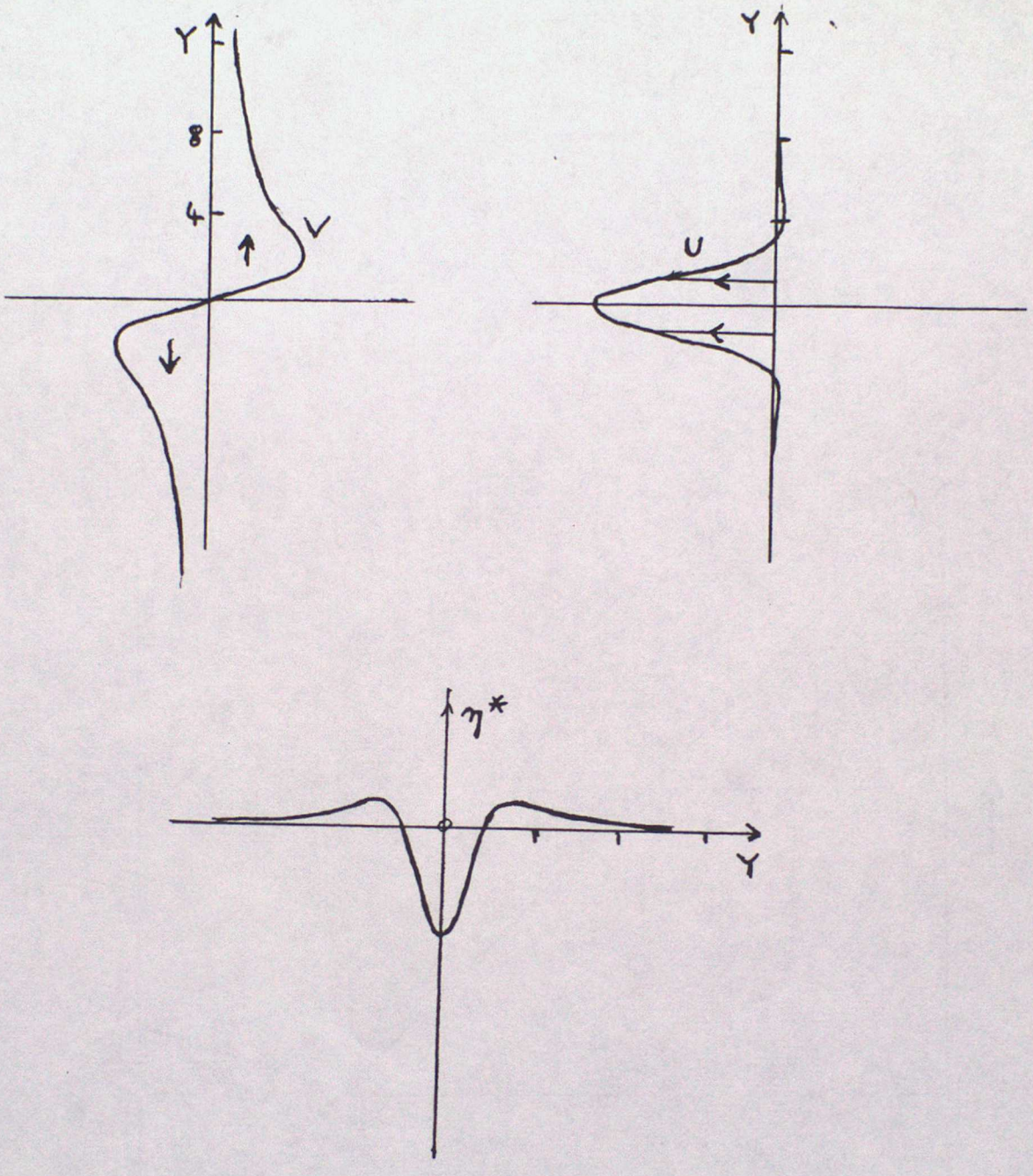

Fig. 3.7

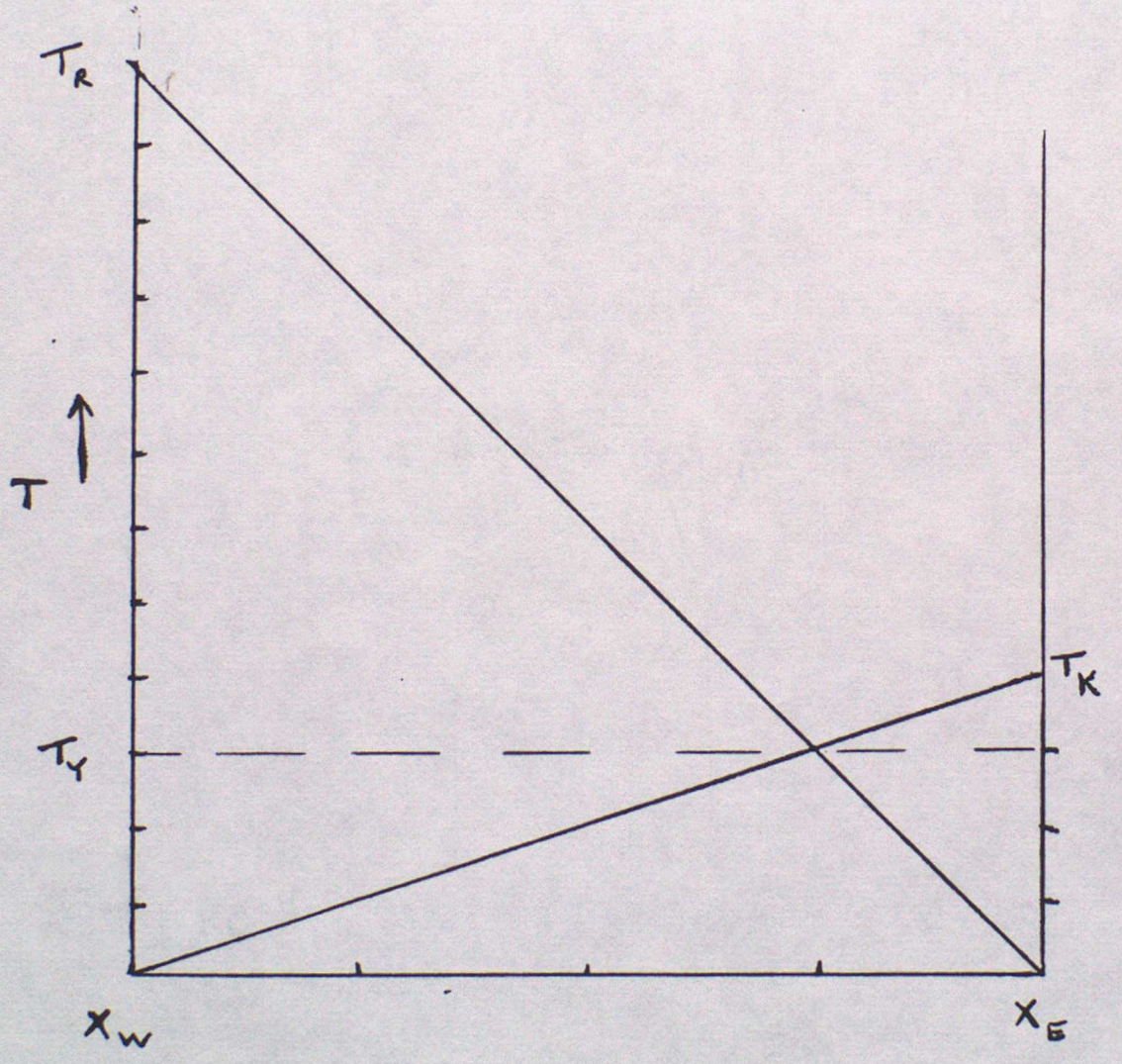

Fig. 3.8

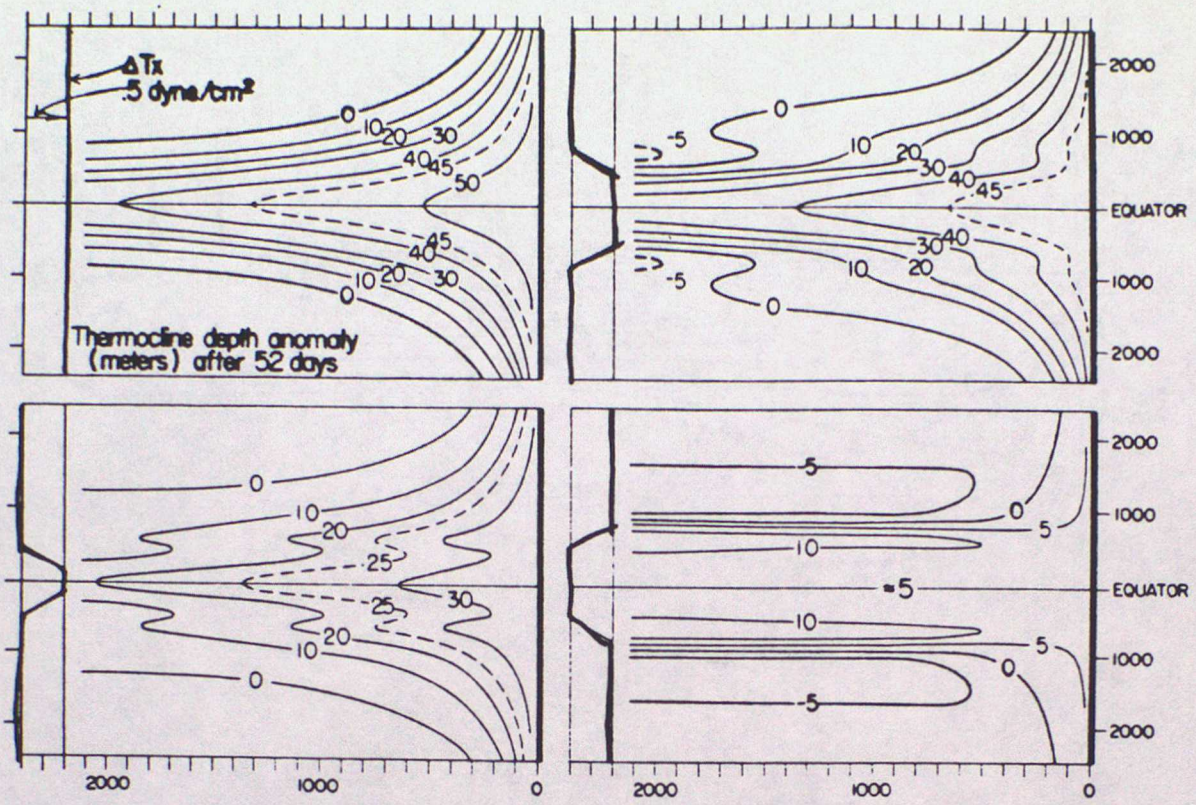

Fig. 3-9

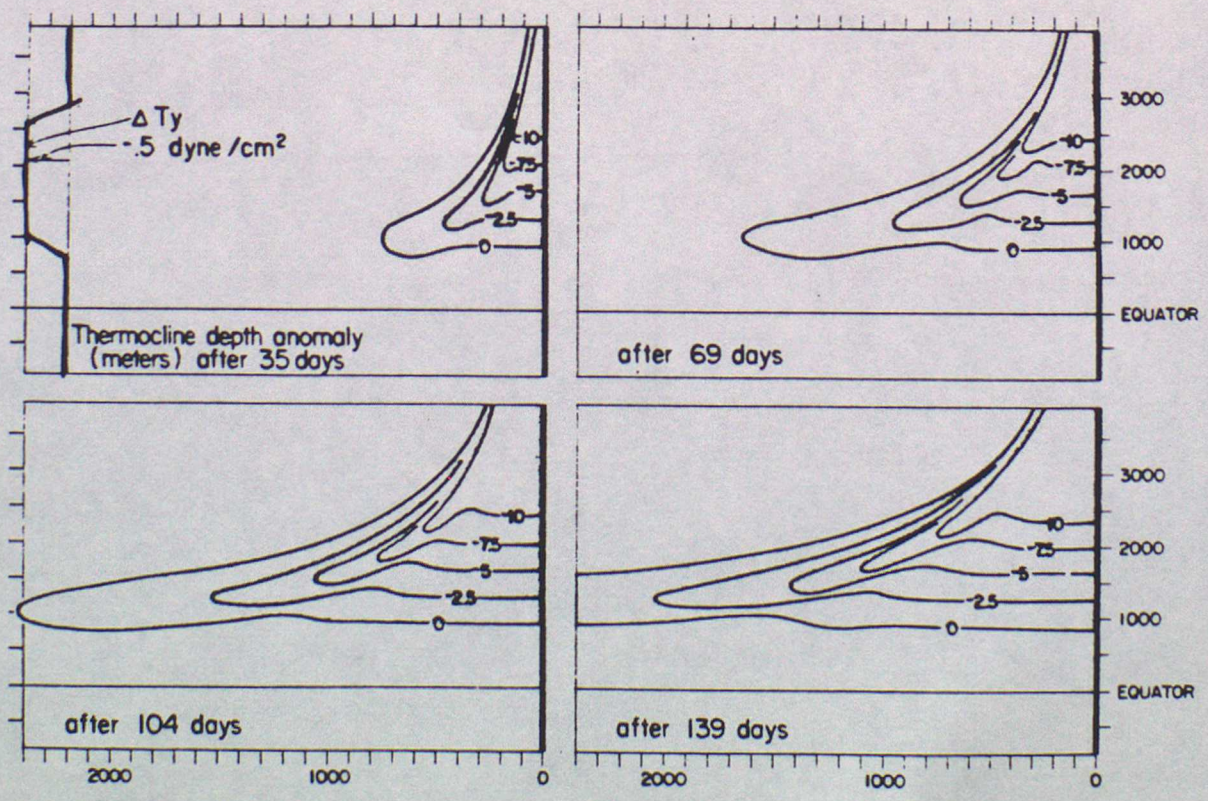

Fig. 3-10

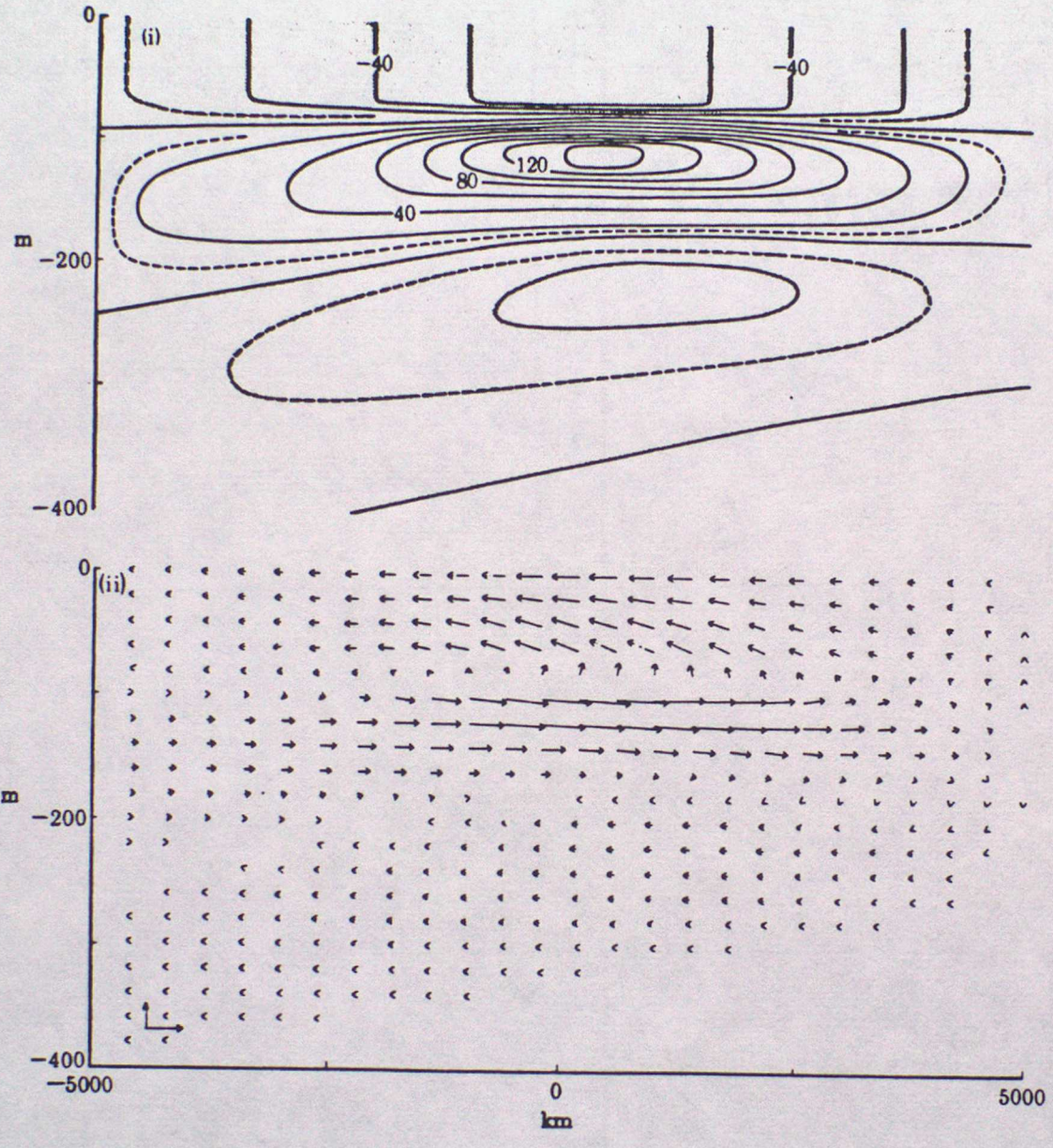

Fig. 3-11

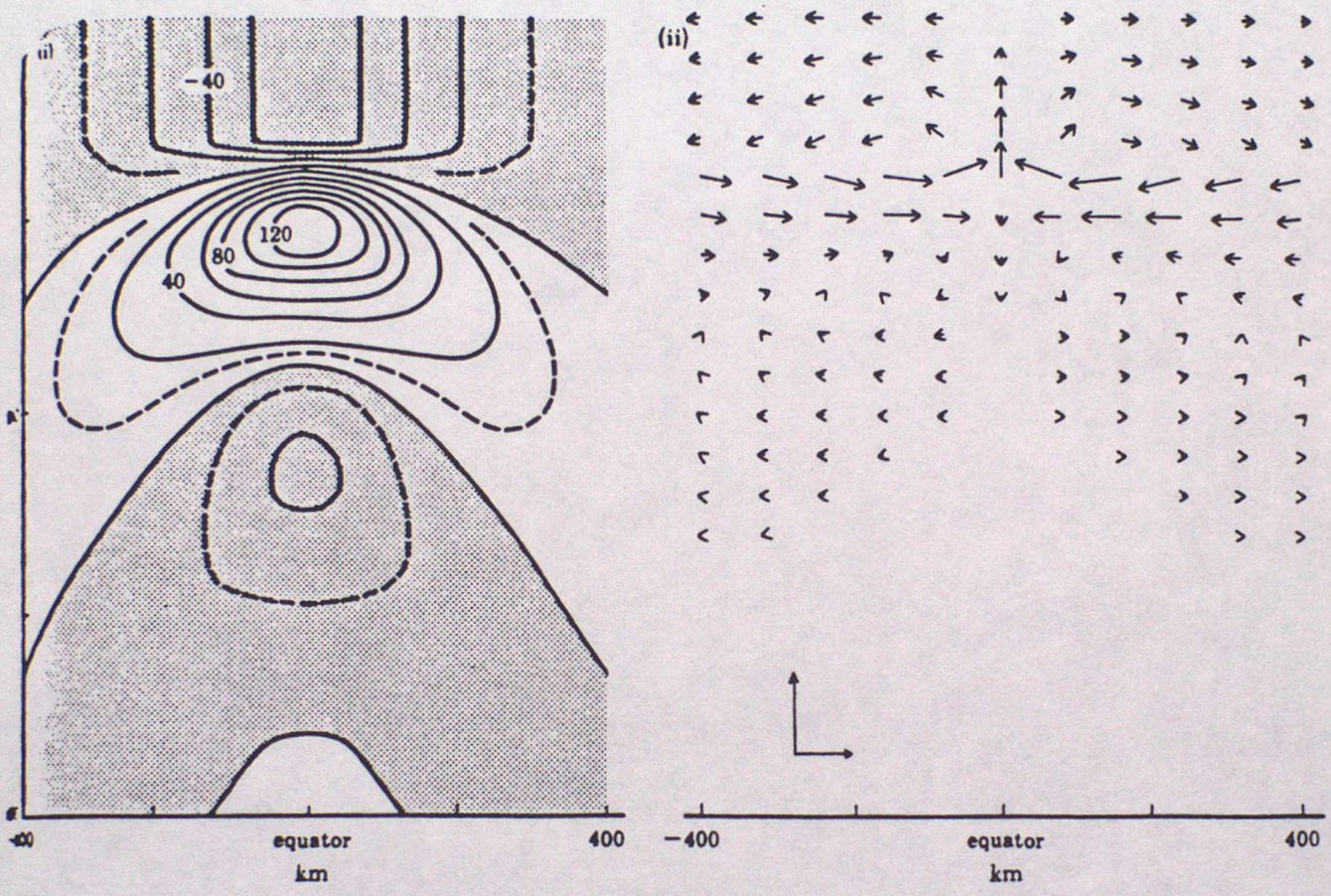

Fig. 3·12

LECTURE 4 The atmospheric response to heat sources

Over the tropical Pacific, rainfall can be in excess of 5 m/year (>0.5"/day) in the Intertropical and South Pacific Convergence Zones, with about 4 m/year in the Indonesian region. This corresponds to a latent heating rate of several degrees/day, with a vertical distribution which is strongest in the mid-troposphere (see Fig. 4.1). The response of the tropical atmosphere to this diabatic heating has a strongly 'first-baroclinic' structure: that is, oppositely directed horizontal flow at upper (e.g. 200mb) and lower (e.g. 850mb) levels, high pressure aloft over low surface pressure and vice-versa, largest vertical motion at mid-levels. In this lecture the SWE will be applied to determine the horizontal evolution of this baroclinic structure, in simple models of the tropical atmosphere.

Prescribed heating will first be considered, producing the basic Hadley and Walker circulations. The latent heating depends on the circulation however, so a model that allows self-determination of the heating pattern will also be presented.

4.1 Basic equations

In previous lectures the basic equations were presented in terms of density and vertical displacement. It is here more convenient to use potential temperature θ.

Consider perturbations from a background state $\rho_o(z)$, $p_o(z)$, $\theta_o(z)$, governed by

$$u_t - fv = -(p'/\rho_o)_x \quad , \qquad (4.1a)$$

$$v_t + fu = -(p'/\rho_o)_y \quad , \qquad (4.1b)$$

$$(p'/\rho_0)_z = g\,(\theta'/\theta_0) \quad , \tag{4.1c}$$

$$(\theta'/\theta_0)_t + w\,N^2/g = 0 \quad , \tag{4.1d}$$

$$u_x + v_y + w_z = 0 \quad , \tag{4.1e}$$

where

$$N^2(z) = \frac{g}{\theta_0}\,\frac{d\theta_0}{dz} \quad .$$

p' and θ' are perturbations from p_0 and θ_0, and (4.1c) is a convenient approximate form of the hydrostatic equation for perturbations.

For vertical modes we put (c.f. lecture 1)

$$(u,v) = \psi(z)\,(\hat{u},\hat{v}) \quad , \tag{4.2a}$$

$$p'/\rho_0 = \psi(z)\,\hat{p}'/\rho_{00} \quad , \tag{4.2b}$$

$$w = \phi(z)\,\hat{w} \quad , \tag{4.2c}$$

where ρ_{00} is a constant reference density. The hydrostatic equation requires

$$(\theta'/\theta_0) = \frac{1}{g}\,\psi_z\,(\hat{p}'/\rho_{00}) \quad , \tag{4.3}$$

and we put

$$-(\hat{p}'/\rho_{00}) = gHe\,(\hat{\theta}'/\theta_{00}) \tag{4.4}$$

to rewrite (4.3) as

$$(\theta'/\theta_{oo}) = -He\ \psi_z\ (\hat{\theta}'/\theta_{oo}) \qquad (4.5)$$

$$= He^2 (N^2/c^2)\ \phi\ (\hat{\theta}'/\theta_{oo})\ . \text{ (see below)}$$

Separation of vertical structure requires

$$\psi = He\ \phi_z\ , \qquad (4.6a)$$

$$\psi_z = -(N^2/g)\ \phi\ , \qquad (4.6b)$$

which combine to give

$$\phi_{zz} + (N^2/c^2)\ \phi = 0\ . \qquad (4.7)$$

As before, $c = (gHe)^{1/2}$ will be the gravity wave speed of a mode with equivalent depth He.

For example, assuming a rigid lid at the tropopause at height π H, the boundary conditions for (4.7) are

$$\phi = 0 \qquad \text{at } z=0\ ,\ \pi H\ , \qquad (4.8)$$

With constant N^2 for simplicity, we find that the first baroclinic mode has

$$\phi = \sin (z/H) \quad , \tag{4.9a}$$

$$\psi = (He/H) \cos (z/H) \quad , \tag{4.9b}$$

$$c^2 = gHe = N^2 H^2 \quad . \tag{4.9c}$$

This structure is illustrated in Fig. 4.2: note that positive θ' at mid-level is associated with low surface pressure and high upper-level pressure.

Equations (4.1) reduce to

$$\hat{u}_t - f\hat{v} = -(\hat{p}'/\rho_{oo})_x = gHe\,(\hat{\theta}'/\theta_{oo})_x \quad , \tag{4.10a}$$

$$\hat{v}_t + f\hat{u} = -(\hat{p}'/\rho_{oo})_y = gHe\,(\hat{\theta}'/\theta_{oo})_y \quad , \tag{4.10b}$$

$$(\hat{\theta}'/\theta_{oo})_t = -\hat{w}/He = \hat{u}_x + \hat{v}_y \quad . \tag{4.10c}$$

These SWE equations are made non-dimensional in the usual way, with

$$\begin{gathered} (u,v) = c\,(U,V) \quad , \quad w = (He/a)\,c\,W \quad , \\ (x,y) = a\,(X,Y) \quad , \quad z = H\,Z \quad , \\ t = (a/c)\,T \quad , \end{gathered} \tag{4.11}$$

$$\hat{\theta}'/\theta_{oo} = \theta^* \quad , \quad \hat{p}'/\rho_{oo} = g\,He\,p^* \quad ,$$

where

$$a = (c/2\beta)^{1/2}$$

to obtain

$$U_\tau - \tfrac{1}{2} Y V = \Theta^*_X \quad , \tag{4.12a}$$

$$V_\tau + \tfrac{1}{2} Y U = \Theta^*_Y \quad , \tag{4.12b}$$

$$\Theta^*_\tau = -W = U_X + V_Y \quad . \tag{4.12c}$$

(Note: $p^* = -\Theta^*$)

The atmosphere rapidly comes into equilibrium with low-frequency forcing, as effects like radiative cooling and cumulus friction act to damp out perturbations on a timesale of a few days. Here we add Newtonian cooling and Rayleigh friction to (crudely) represent these processes, and will only consider the steady state governed by

$$-\tfrac{1}{2} Y V = \Theta^*_X - \varepsilon U \tag{4.13a}$$

$$\tfrac{1}{2} Y U = \Theta^*_Y - \varepsilon V \tag{4.13b}$$

$$W = -\varepsilon \Theta^* + Q \tag{4.13c}$$

where Q is a prescribed heating rate. A reminder of typical atmospheric scales: a = 1000 Km , c = 50 m sec-1 , timescale = 0.25 days. Typically $\varepsilon \lesssim 0.1$ which corresponds to a damping timescale of $\gtrsim$ 2.5 days: in this time a Kelvin wave with speed c would travel $\gtrsim$ 10000 Km (the width of the Pacific).

4.2 Zonally symmetric

When forcing is independent of X we obtain from (4.13)

$$V_{YY} - (\tfrac{1}{4}Y^2 + \varepsilon^2)\, V = -Q \quad . \tag{4.14}$$

For $\varepsilon \tilde{<} 0.1$ the term ε^2 can be neglected, leaving

$$V_{YY} - \tfrac{1}{4}Y^2 V = -Q \quad . \tag{4.15}$$

Consider broad heating centred on the equator of the form

$$Q = \varepsilon [\, 1 - (Y/B)^2 \,] \quad , \tag{4.16}$$

then (4.15) is the same as the Yoshida Jet equation seen in lecture 3! This heating (4.16) is not reasonable at high latitudes, so 'sidewalls' are placed at $Y = \pm B$, and, as an example, solutions for B=4 are given in Fig. 4.3. Low-level meridional flow is everywhere equatorward (poleward at high level). There are low-level easterly jets either side of the equator, with weak flow (doldrums) at the equator. Vertical motion is upward in a broad region around the equator, with compensating sinking at higher latitudes. In the absence of motion the mid-level perturbation potential temperature would be $\Theta_s^* = Q/\varepsilon$. The adiabatic cooling due to upward motion reduces Θ^* below Θ_s^* around the equator; vice-versa at higher latitudes. This atmospheric version of the Yoshida Jet is a thermally direct circulation: a Hadley cell.

Thermal forcing is generally more concentrated than in the example

above, but the general features of the response are robust. An example from the other extreme is the infinitely narrow delta-function heating concentrated along $Y=Y_0$:

$$Q = \delta(Y-Y_0) \quad , \tag{4.17}$$

The solution in this case is

$$V = \begin{cases} -\varepsilon H_Y(-Y_0)\, H(Y) / A & Y_0 < Y \leqslant B \\ \varepsilon\, H_Y(Y_0)\, H(-Y) / A & -B \leqslant Y < Y_0 \end{cases} \tag{4.18}$$

where

$$A = H_Y(Y_0)\, H(-Y_0) + H(Y_0)\, H_Y(-Y_0)$$

$$= -2\, Ve(B)\, Vo(B)$$

and

$$H(Y) = Ve(Y) - Vo(Y)\, Ve(B) / Vo(B) \quad ,$$

Here Ve and Vo are even and odd free solutions of (4.15):

$$Vo(Y) = Y \sum_0^\infty A_n\, (Y^4/4)^n \tag{4.19a}$$

$$Ve(Y) = \sum_0^\infty B_n\, (Y^4/4)^n \tag{4.19b}$$

where

$$A_0 = B_0 = 1$$

$$A_n = A_{n-1} / 4n(4n+1)$$

$$B_n = B_{n-1} / 4n(4n-1) \quad .$$

Correspondingly,

$$\theta^* = \begin{cases} -H_1(-Y_0)\, H_1(Y) / A & Y_0 \leqslant Y \leqslant B \\ -H_1(Y_0)\, H_1(-Y) / A & -B \leqslant Y \leqslant Y \end{cases} \quad . \qquad (4.20)$$

The shape of these functions is far from obvious! (Typical.) The response is not complicated however, and is ilustrated in Fig. 4.4 for $Y_0=0$ and $Y_0=1$. Low-level wind is toward the latitude of heating: for $Y_0=1$ this means substantial cross-equatorial flow. For $Y_0=0$ the zonal easterly double jet appears as in the previous case; for $Y_0=1$ however westerlies appear between the equator and the latitude of heating, with easterlies elsewhere —— the flow across the equator switches from easterly to westerly as the Coriolis parameter changes sign. Vertical motion (not shown) is concentrated in an upward spike at Y_0, with weak descent elsewhere. Again circulation is Hadley-like —— the case $Y_0=1$ may be regarded as the the ITCZ situated north of the equator, and $Y_0=0$ as the ITCZ moved south over the equator.

4.3 A patch of heating

Heating in practice is not zonally uniform. Normally heating is strongest over the Indonesian region where sea-surface temperatures are high and surface air can hold a lot of water vapour. During strong El Nino events there is anomalously strong heating over the central Pacific when SST rises there.

Gill (1980) presented an SWE model of the response to such heating, and some of his results will be described here. Matsuno (1966) also considered such effects in an SWE model forced by zonally-distributed mass sources and sinks. Other more complex models will be mentioned later.

Gill used the longwave approximation (valid for long zonal wavelength and small dissipation $\varepsilon \ll 1$) to replace (4.13b) by the longequator geostrophic form

$$\tfrac{1}{2} Y U = \Theta^*_Y \quad . \tag{4.21}$$

He first considered heating centred on the equator of the form

$$Q(X,Y) = F(X) \exp\{-Y^2/4\} = \exp\{-Y^2/4\} \begin{cases} \cos(kX) & -L<X<L \\ 0 & \text{otherwise} \end{cases} \tag{4.22}$$

where

$$k = 2\pi/L \quad .$$

The transient response is described in Heckley & Gill (1984). A Kelvin wave propagating eastward at unit non-dimensional speed affects the region $X>-L$, and only this wave influences $X>L$. This contributes

$$V_K = 0 \tag{4.23a}$$

$$U_K = -\Theta^*_K = \tfrac{1}{2} q_0(X) \exp\{-Y^2/4\} \tag{4.23b}$$

where

$$q_0(X) = \frac{1}{\varepsilon^2+k^2} \begin{cases} 0 & X<-L \\ -\varepsilon\cos(kX) - k\,[\,\sin(kX) + \exp\{-\varepsilon(X+L)\,]\,\} & -L<X<L \\ -k\,[\,1+\exp\{-2\varepsilon L\}\,]\exp\{\varepsilon(L-X)\} & L<X \end{cases}$$

This Kelvin response decays eastward on a length scale $1/\varepsilon$ east of the forced region, and sets up easterly low-level flow toward the region of heating.

Likewise a long Rossby wave propagating west at speed -1/3 affects the region X<L, and only this wave affects X<-L. It contributes

$$U_R = \tfrac{1}{2}\, q_2(X)\,(Y^2-3)\exp\{-Y^2/4\}\,, \qquad (4.24a)$$

$$V_R = [F(X) + 4\varepsilon\, q_2(X)]\, Y \exp\{-Y^2/4\}\,, \qquad (4.24b)$$

$$\Theta_R^* = -\tfrac{1}{2} q_2(X)\,(1+Y^2)\exp\{-Y^2/4\}\,, \qquad (4.24c)$$

where

$$q_2(X) = \frac{1}{9\varepsilon^2+k^2} \begin{cases} -k\,[\,1+\exp\{-6\varepsilon L\}\,]\exp\{3\varepsilon(X+L)\} & X<-L \\ -3\varepsilon\cos(kX) + k\,[\,\sin(kX) - \exp\{3\varepsilon(X-L)\}\,] & -L<X<L \\ 0 & L<X \end{cases}$$

This decays westward on a length scale $1/3\varepsilon$. Near the equator there are westerly low-level winds toward the region of heating, with cyclonic

low-level flow to the north-west and south-west of the heated region.

The net response is the sum of these two forced waves, and is shown in Fig. 4.5. In the forced region the sum gives low-level poleward flow, away from the heating. To understand this effect: from (4.13a,b)

$$\tfrac{1}{2} Y (U_x + V_y) + \tfrac{1}{2} V = - \varepsilon (V_x - U_y) \qquad (4.25)$$

which combined with (4.13c) for $\varepsilon << 1$ leads to

$$\tfrac{1}{2} V = \tfrac{1}{2} Y Q \quad , \qquad (4.26)$$

i.e. poleward motion where $Q>0$. Thus rotational effects induce this counter-intuitive meridional low-level flow away from a region of rising motion. (Net upward motion is fed by the larger zonal flow into the region of heating.)

The zonally-integrated flow in Fig. 4.5d shows a thermally direct Hadley circulation. Average low-level meridional flow (due to V_R alone) is equatorward, despite the poleward component noted above. There is no net zonal flow along the equator: in fact the whole structure is very similar to Fig. 4.3. (This is a linear model, so the zonally-integrated flow is simply that driven by the zonally-integrated heating.)

The meridionally integrated flow in Fig. 4.5c shows a Walker cell —— a thermally direct circulation oriented zonally along the equator, as observed in the Pacific.

Further examples for antisymmetric heating, and superposition with symmetric heating, can be seen in Gill (1980).

Similar effects in somewhat more complex models have been described by

Webster (1972) and Geisler (1980). Transient effects in a shallow-water model have also been investigated by Lau & Lim (1982). Zebiak (1982) has used the Gill model with heating related to sea-surface temperature.

4.4 Moisture effects

The forcing in the above examples represents latent heating. The distribution of this heating is not really independent of the circulation, as assumed above, but rather occurs where there is low-level convergence and a supply of moisture. Gill (1982) introduced an extension of the simple baroclinic model to include a moisture budget, and applied it to equatorial dynamics as in Gill (1985). A detailed description appears in DCTN 41 (Davey & Gill 1986), so only an outline will be given here.

The basic idea is to add a new variable q which represents moisture content in a vertical column. Moisture is concentrated at low levels, so q is advected by the low-level wind $\underline{U}$. It is increased by surface evaporation up to some saturation value qsat, and at a given location it tends to increase when there is low-level convergence (and vice-versa). If q=qsat and there is a net tendency to further increase q then excess moisture is precipitated out (falling straight into the ocean and out of the model), releasing latent heat to the atmosphere.

Latent heating occurs where motion is upward, and it affects the static stability (which in our simple model so far had a fixed, stable background value) by counteracting the adiabatic cooling associated with the upward motion. In a suitable non-dimensional form, qsat=1 implies neutral conditions where adiabatic cooling and latent heating balance each other, and qsat<1 means conditions are moist stable.

The tropical atmosphere is generally moist unstable, but as deep convection takes place on scales too small to be properly represented by our large-scale model we take qsat<1 to represent average conditions over a large area: qsat=8/9 is used in the example to follow. Constant qsat is chosen for simplicity; in practice it is related to sea-surface temperature via the Clausius-Clapeyron equation to increase qsat over warmer water.

The non-dimensional rate of latent heating is qsat.W, and in the simple steady zonally-symmetric model it always rains where W>0. Thus (4.13c) is modified by moisture effects to

$$W = \begin{cases} -\varepsilon\Theta^* + Q & W<0, \text{ dry} \\ -\varepsilon\Theta^* + Q + qsat\ W & W>0, \text{ wet} \end{cases} \qquad (4.27)$$

Where W>0 we can write

$$(1-qsat)\ W = -\varepsilon\Theta^* + Q \qquad (4.28)$$

to emphasise the effective change in static stability discussed above.

The response with $Q= \varepsilon\,[1-(Y/4)^2]$ is shown in Fig. 4.6, and should be compared with Fig. 4.3 (the same example with no interactive heating). The main effect is that upward motion is enhanced and takes place over a smaller latitude band. Meridional circulation is intensified, and there is precipitation for $|Y|<1$. As qsat is increased toward 1 the precipitation band narrows and intensifies further, with an effect like Fig. 4.4 in the limit qsat→1.

A similar version of this model has been used to produce qualitatively realistic circulation and precipitation patterns over the Pacific, and it is presently being adapted for use in simple coupled ocean-atmosphere experiments.

Other simple models have been developed to take into account the interactive nature of latent heating, based on diagnosing the heating pattern and the circulation by iterative methods (Webster 1981, Weare 1986, Zebiak 1984).

4.5 Extratropical effects

As well as the baroclinic response analysed above, which is trapped near the equator, there can be a substantial larger-scale barotropic response which is dominant at higher latitudes. This barotropic response can be directly forced by heating (a weak effect because the vertical heating profile is largely baroclinic), or indirectly through modification of the baroclinic component by e.g.non-linearities or surface friction. There is observational evidence (Horel & Wallace 1981) that equatorial SST affects the global atmosphere, with distinctive correlation patterns (teleconnections, Fig. 4.7 shows a typical Pacific pattern), and a large modelling effort has been made to understand and simulate such patterns.

Amongst simple models, Webster (1981) has used a linear two-level model to demonstrate the barotropic extra-tropical influence of tropical SST. Lim & Chang (1983) used an equatorial beta-plane model including barotropic and baroclinic components (at high latitudes the response is distorted by the beta-plane, but the results remain qualitatively significant).

Most effort has gone into using atmospheric general circulation models

however, to analyse the response to prescribed SST changes. An early example is Rowntree (1972), using a hemispheric model to look at the effect of tropical East Pacific SST. Other notable tropical Pacific cases are Shukla & Wallace (1983), Julian & Chervin (1978), and more recently Palmer & Mansfield (1986) using the Met. O. atmospheric GCM. A collection of examples of the response to the prescribed SST change during the 1982-83 El Nino is included in the proceedings of the meeting on Coupled Ocean-Atmosphere Models held at Liege in 1984 (published 1985).

References (lecture 4)

(1985) Coupled Ocean-Atmosphere Models (J.C.J. Nihoul ed.)
Elsevier Oceanography Series, Vol. 40, 767pp

Davey, M.K. & A.E. Gill (1986)
Experiments on tropical circulation with a simple moist model
Submitted to Q.J.Roy.Met.Soc.

Geisler, J.E. (1981)
A linear model of the Walker circulation.
J. Atmos. Sci., 38, 1390-1400

Gill, A.E. (1980)
Some simple solutions for heat-induced tropical circulation.
Q. J. Roy. Met. Soc., 106, 447-462

Gill, A.E. (1982)
Studies of moisture effects in simple atmospheric models:
the stable case.
Geophys. Astrophys. Fluid Dyn., 19, 119-152

Gill, A.E. (1985)
Elements of coupled ocean-atmosphere models for the tropics.
In: 'Coupled Ocean-Atmosphere Models' (J.C.J. Nihoul ed.)
Elsevier Oceanography Series Vol. 40, pp 303-327

Heckley, W.A. & A.E. Gill (1984)
Some simple analytic solutions to the problem of forced equatorial long waves.
Q. J. Roy. Met. Soc., 110, 203-217

Horel, J.D. & J.M. Wallace (1981)
Planetary scale atmospheric phenomena associated with the Southern Oscillation
Mon. Weath. Rev., 109, 813-829

Julian, P.R. & R.M. Chervin (1978)
A study of the Southern Oscillation and Walker circulation phenomenon
Mon. Weath. Rev., 106, 1433-1451

Lau, K-M, & H. Lim (1982)
Thermally-driven motions in an equatorial beta-plane: Hadley and Walker circulations during the winter monsoon.
Mon. Weath. Rev., 110, 336-353

Matsuno, T. (1966)
Quasigeostrophic motions in the equatorial area.
J. Met. Soc. Japan, 44, 25-43

Palmer, T.N. & P.A. Mansfield (1986)
A study of wintertime circulation anomalies during past El Nino events using a high resolution general circulation model
I: Influence of model climatology
II: Variability of the seasonal mean response
Q. J. Roy. Met. Soc., 112, 613-638, 639-660

Rowntree, P.R. (1972)
The influence of tropical East Pacific Ocean temperatures on the atmosphere
Q. J. Roy. Met. Soc., 98, 290-321

Shukla, J. & J.M. Wallace (1983)
Numerical simulation of the atmospheric response to equatorial Pacific sea surface temperature anomalies
J. Atmos. Sci., 40, 1613-1630

Weare, B.C. (1986)
A simple model of the tropical atmosphere driven by a circulation-dependent forcing.
Q. J. Roy. Met. Soc., 112, 409-429

Webster, P.J. (1971)
Mechanisms determining the atmospheric response to sea surface temperature anomalies.
J. Atmos. Sci., 38, 554-571

Webster, P.J. (1972)
Response of the tropical atmosphere to local, steady forcing.
Mon. Weath. Rev., 100, 518-541

Zebiak, S.E. (1982)
A simple atmospheric model of relevance to El Nino
J. Atmos. Sci., 39, 2017-2027

Zebiak, S.E. (1984)
Tropical atmosphere-ocean interaction and the El Nino/Southern Oscillation phenomenon
Ph.D. Thesis, M.I.T., 261pp

Fig. 4.1 A representative distribution of latent heating, corresponding to a precipitation rate of 1 cm/day (adapted from Geisler 1980)

Fig. 4.2 Idealised first baroclinic structure for an atmosphere with constant N^2.

Fig. 4.3 The response to zonally-symmetric heating $Q = \varepsilon [1-(Y/4)^2]$
(a) low-level flow (U,V), mid-level vertical velocity W, mid-level potential temperature perturbation θ^*, and $\theta_s^* = Q/\varepsilon$.
(b) vertical cross-section showing zonal flow on the left, meridional circulation on the right.

Fig. 4.4 The response to zonally symmetric heating $Q = \delta(Y-Y_0)$ for $Y_0=0$ (solid curves) and $Y_0=1$ (dashed).

Fig. 4.5 The response to a patch of heating in the region $-2 < X < 2$, centred on the equator, with $\varepsilon = 0.1$
(a) low-level velocity vectors, plus contours of vertical motion (solid for W=0, 0.3, 0.6 and dashed for W=-0.1)
(b) low-level velocity vectors, plus contours of the mid-level potential temperature perturbation θ^* ($\theta^*>0$ everywhere)
(c) meridionally-integrated flow in a vertical section showing the Walker cell
(d) zonally-integrated flow in a vertical section showing the Hadley circulation (c.f. Fig. 4.3)
(from Gill 1980)

Fig. 4.6 The response to heating $Q = \varepsilon[1-(Y/4)^2]$ when latent heating dependent on the circulation is included. Latent heating qsat.W occurs where W>0.

Fig. 4.7 (a) an impression of the upper troposphere geopotential height anomaly and
(b) surface pressure and wind anomalies due to
(c) the sea-surface temperature anomaly during a typical El Nino event.

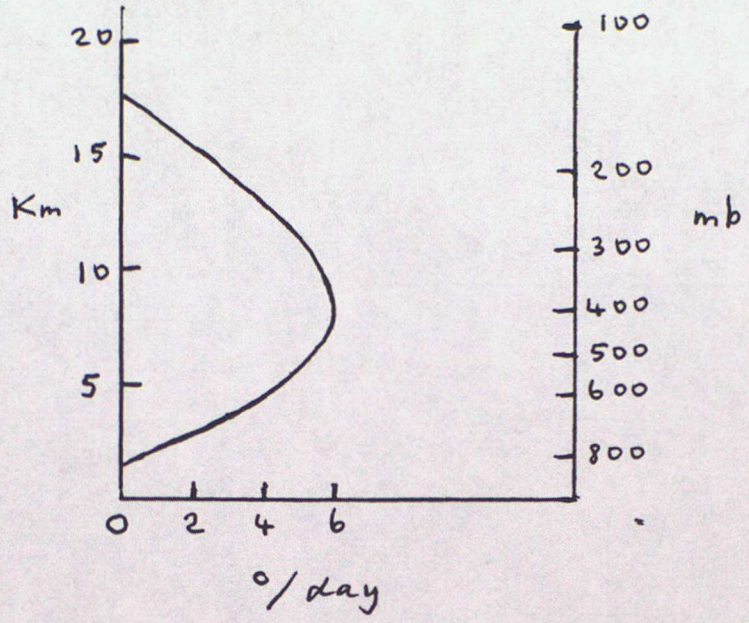

Fig. 4.1

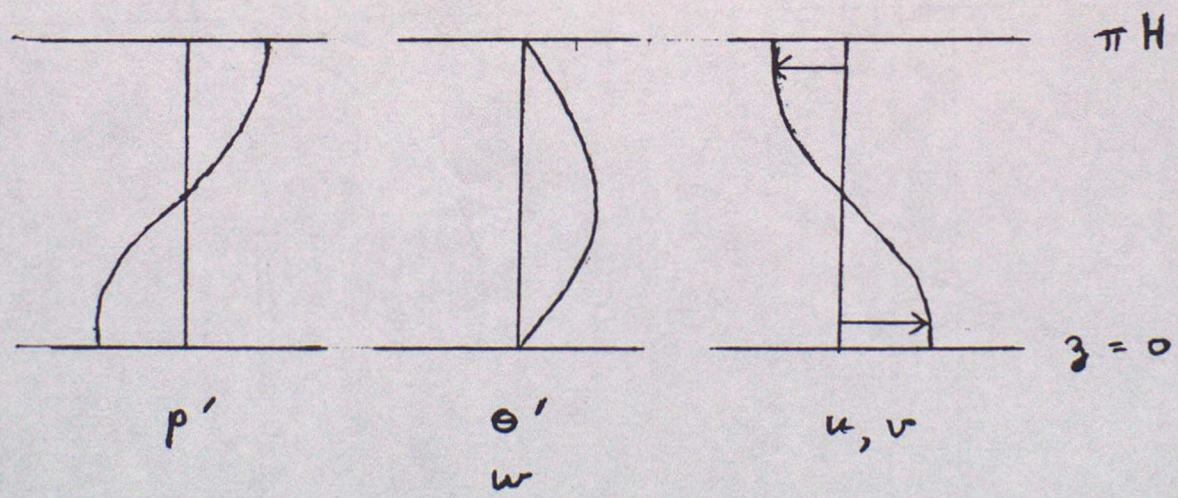

Fig. 4.2

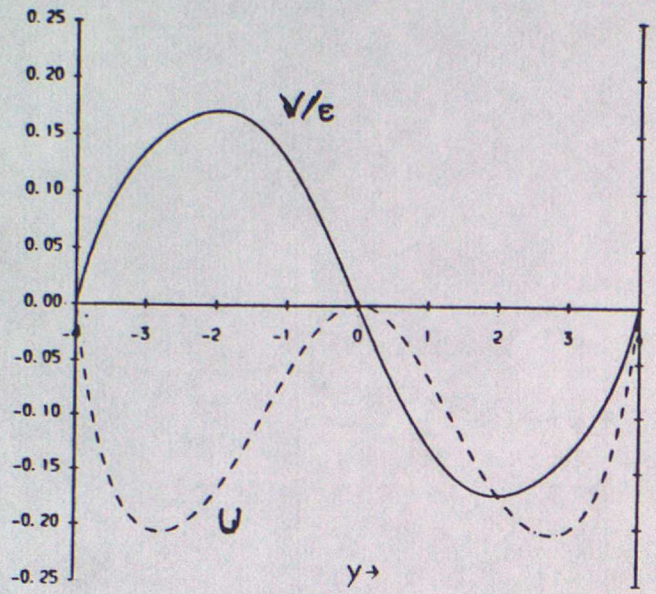

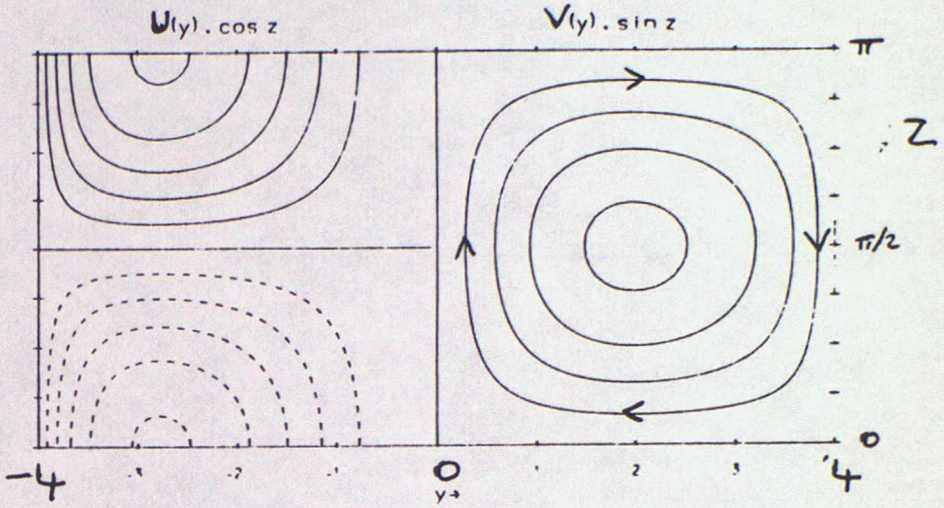

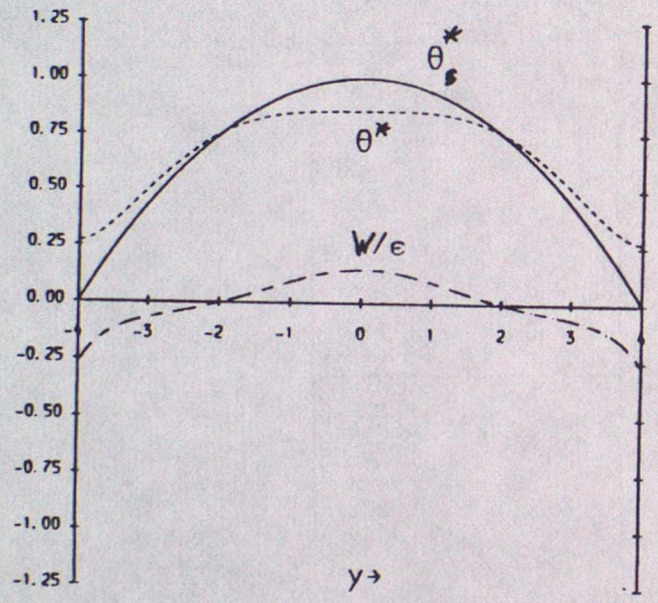

Fig 4-3

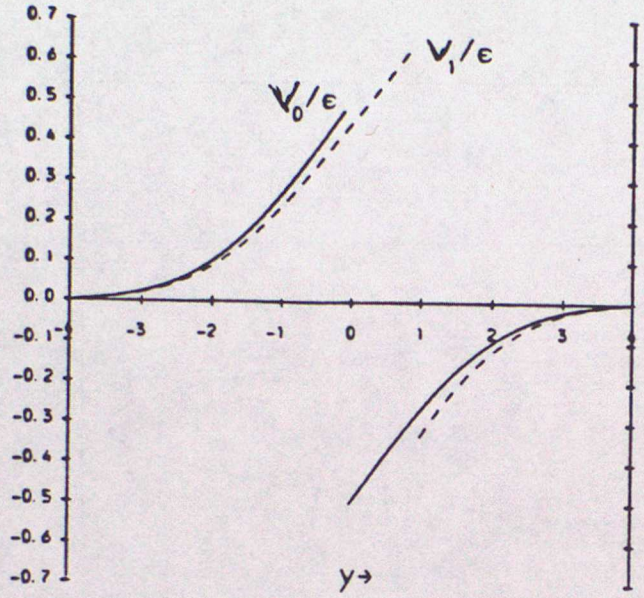
0.7
0.6
0.5
0.4
0.3
0.2
0.1
0.0
-0.1
-0.2
-0.3
-0.4
-0.5
-0.6
-0.7
-3
-2
-1
0
1
2
3
V_0/ϵ
V_1/ϵ
y→

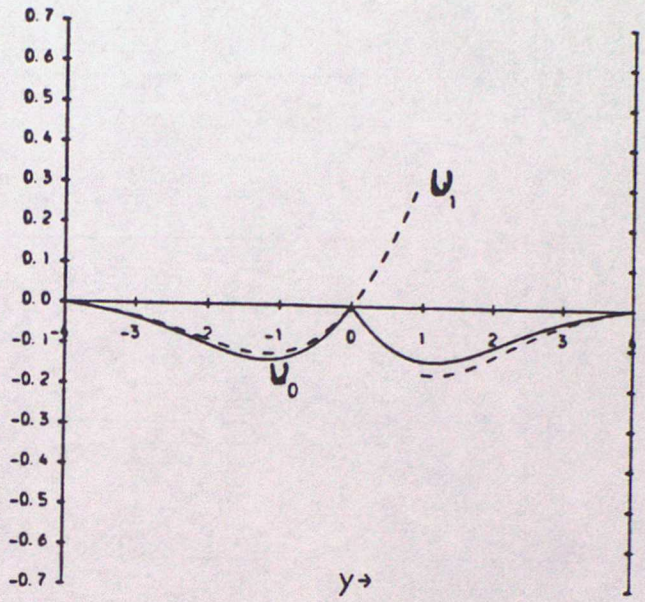
0.7
0.6
0.5
0.4
0.3
0.2
0.1
0.0
-0.1
-0.2
-0.3
-0.4
-0.5
-0.6
-0.7
-3
-2
-1
0
1
2
3
U_1
U_0
y→

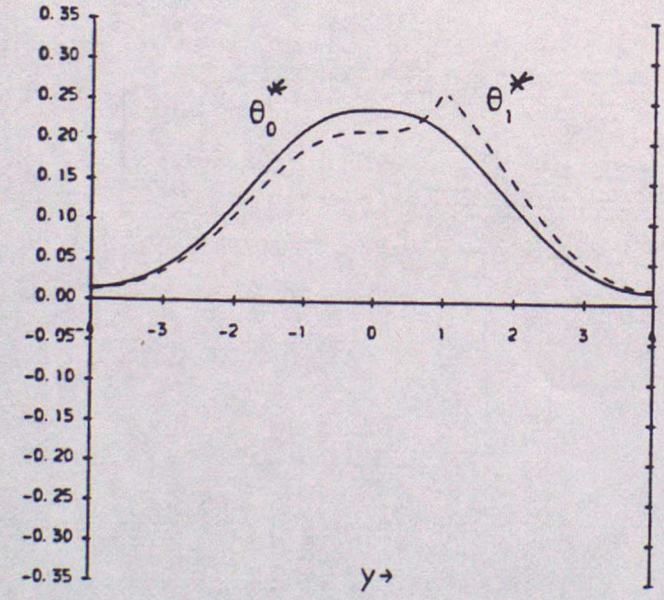
0.35
0.30
0.25
0.20
0.15
0.10
0.05
0.00
-0.05
-0.10
-0.15
-0.20
-0.25
-0.30
-0.35
-3
-2
-1
0
1
2
3
θ_0^*
θ_1^*
y→

Fig. 4.4

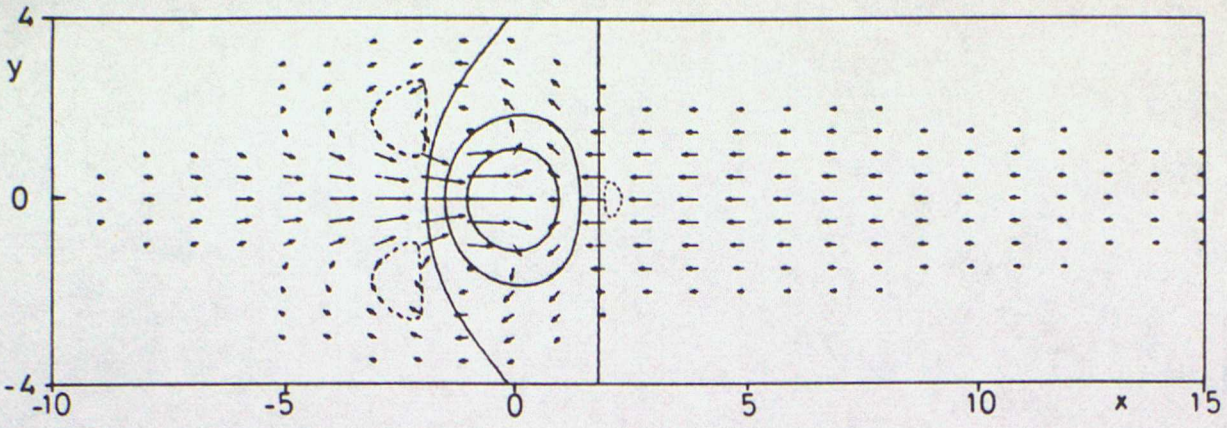

(a)

(U, V)

W

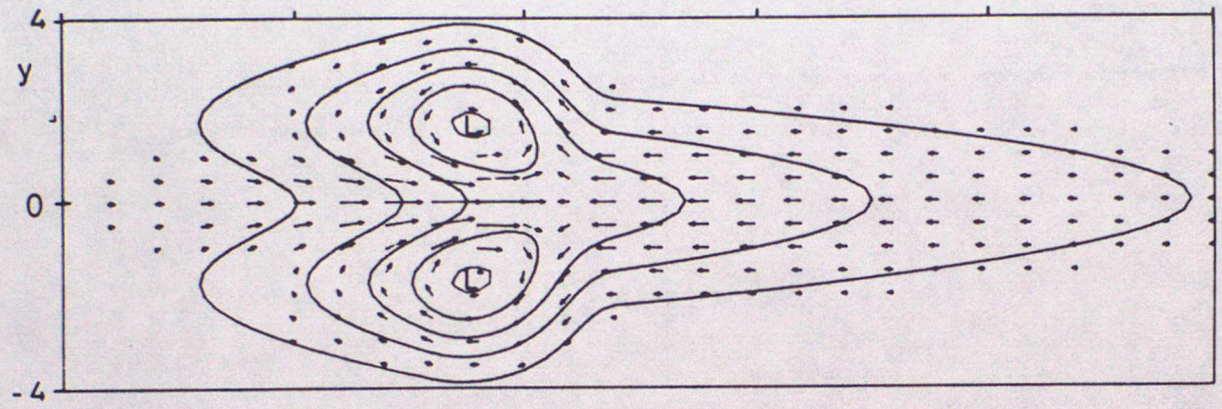

(b)

(U, V)

θ^*

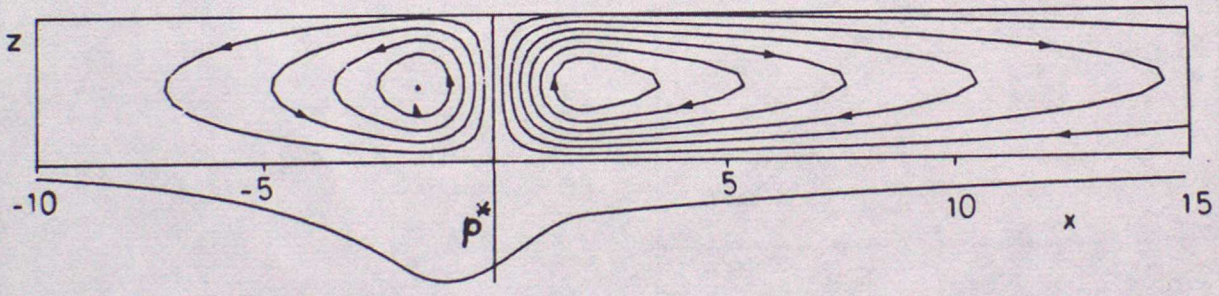

(c)

Walker

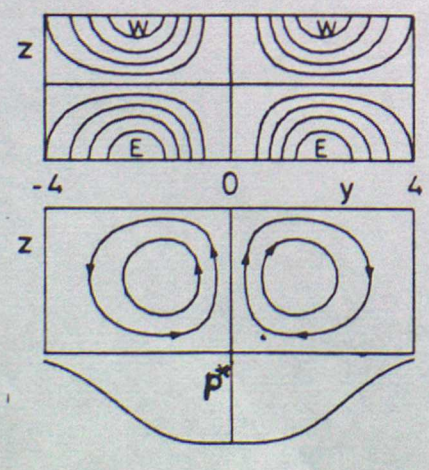

(d)

Hadley

Fig. 4-5

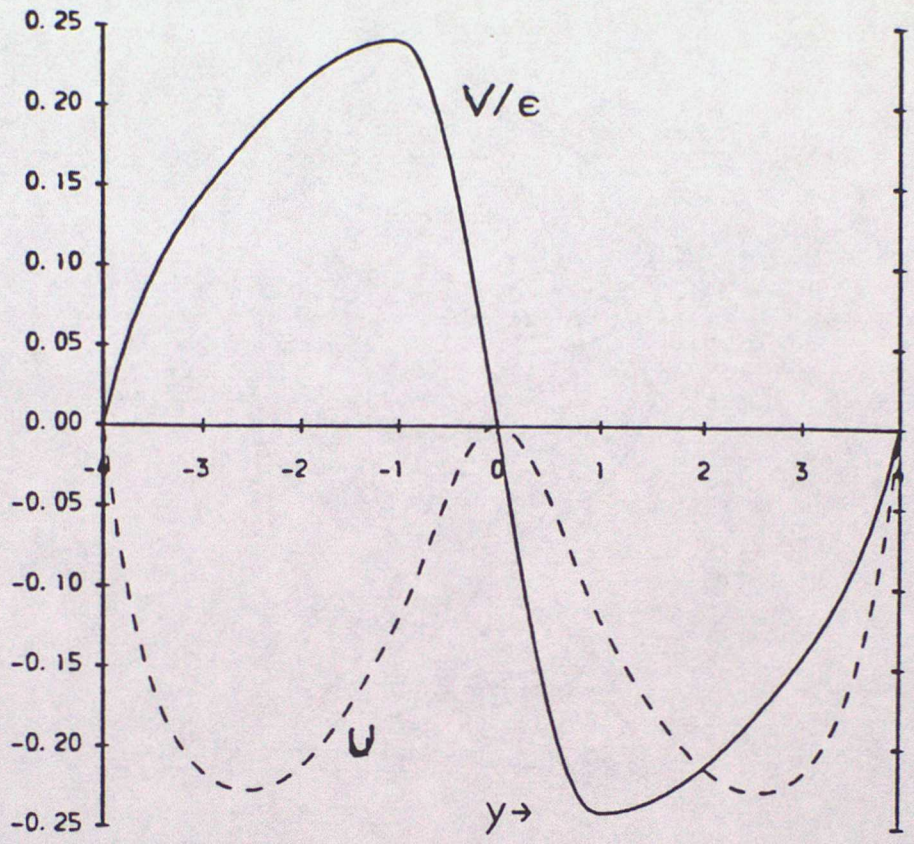
0.25
0.20
0.15
0.10
0.05
0.00
-0.05
-0.10
-0.15
-0.20
-0.25
-4
-3
-2
-1
0
1
2
3
4
V/ε
U
y→

Fig. 4-6

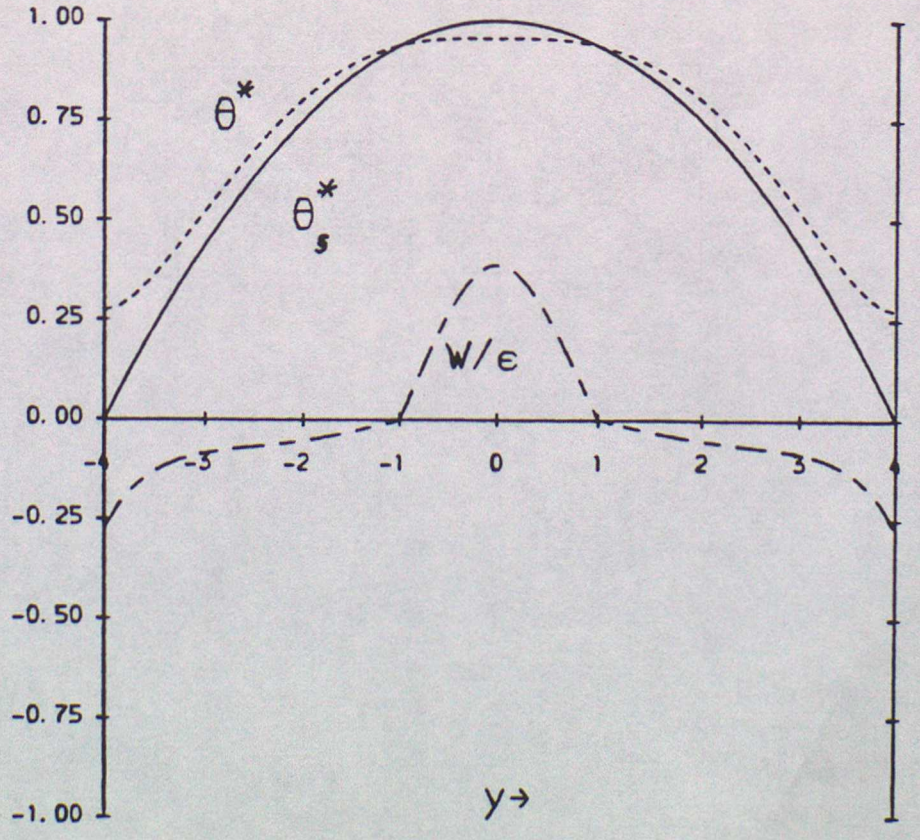
1.00
0.75
0.50
0.25
0.00
-0.25
-0.50
-0.75
-1.00
-4
-3
-2
-1
0
1
2
3
4
θ*
θ*s
W/ε
y→

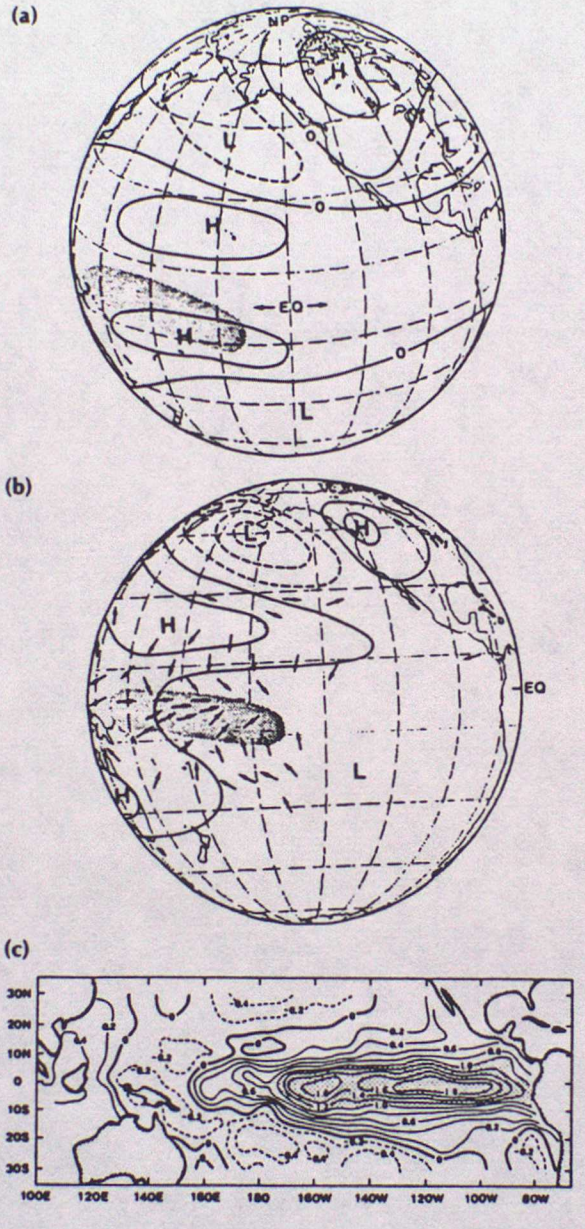
(a)
NP
H
L
H
EQ
H
L
(b)
L
H
H
EQ
L
(c)
30N
20N
10N
0
10S
20S
30S
100E
120E
140E
160E
180
160W
140W
120W
100W
80W

Fig. 4-7

Lecture 5 Ocean-atmosphere coupling

This lecture begins with a reminder of Pacific climatology, followed by a description of composite El Nino and of the strong 1982-83 El Nino event. A simple model is then used to show how coupled instabilities may occur, then a predictive simple model is described.

A large international programme of observation and modelling is underway, called Tropical Ocean Global Atmosphere (TOGA). It began in 1985, will run for ten years, and the aim is to understand and predict events such as El Nino. Useful collections of papers can be found in the proceedings of the International Conference on the TOGA Scientific Programme (Paris 1984), in the proceedings of a meeting on Coupled Ocean-Atmosphere Models (Liege 1984), and Vol. 27 of Oceanus (1984) (see reference list).

5.1 Pacific climatology

The mean wind stress over the Pacific ocean for February and August is shown in Fig. 5.1, sea surface temperature for January and July appears in Fig. 5.2a, and the usual annual cycle of SST along the equator is in Fig. 5.2b. The western warm pool where SST>28^{o} C shows very little seasonal variability: changes there are mostly interannual ones due to changes in the extent and intensity of the warm pool. Between 140^{o}W and South America seasonal variability is much more pronounced, with warmer SST appearing each year in northern winter. This variability is not due to changes in surface heat flux (unlike the extratropical oceans), but is probably related to changes in the surface winds. In northern winter the ITCZ moves south, closer to the equator, with consequent weakening of the south-easterly trades in the east Pacific (see Fig. 5.1). This weakening

(a) causes deepening of the thermocline as the zonal pressure

gradient opposing the wind stress relaxes, so water upwelled to the surface is warmer

(b) decreases westward advection of cold water by the South Equatorial Current and decreases the rate of upwelling, so surface heating is more effective

(c) decreases coastal upwelling south of the equator so the Peru Current is warmer and weaker

Fig. 5.3 shows mean outgoing longwave radiation (OLR). [Low OLR (<240 W m-2) corresponds to high, cold clouds and is a measure of convective rainfall.] Convection areas over Africa and the Americas can be seen in the summer hemisphere. The main convective area is over the pool of warm west Pacific water and adjacent land (principally the 'maritime continent' of Indonesia). Convection associated with the ITCZ and SPCZ is evident, again overlying relatively warm SST.

5.2 Composite El Nino

The annual cycle is occasionally (every few years) interrupted by an El Nino event when sea surface temperature becomes anomously warm over a large area of the eastern and central Pacific, accompanied by anomalously high rainfall.

A phenomenon closely related to El Nino is the anomaly in the Tahiti-Darwin surface pressure difference. Normally surface pressure is relatively low over Darwin and high over Tahiti (these locations are representative of conditions over a wide surrounding area), as required for the normal Walker circulation with low-level easterlies over the Pacific. This pressure difference is an index for the Southern Oscillation —— negative values are associated with weaker easterly winds and an eastward shift of the Walker circulation. It fluctuates as seen in Fig.

5.4, and provides an indicator of ENSO events.

Rasmusson & Carpenter (1982) compiled a cohesive picture of such events by combining data from the 1951, 1953, 1957, 1965, 1969 and 1972 episodes. (This composite was needed due to the lack of data for any one event.) Fig. 5.5 provides a summary of related global climate anomalies —— note in particular the eastward shift of rainfall over the tropical Pacific. Fig. 5.6 shows the evolution of composite sea surface temperature anomalies during an event, and Fig. 5.7a shows SST anomalies along the equator.

Preceding an event (year -1) Pacific SST is slightly cooler then normal in the east, warmer than normal in the west. There are stronger than average easterlies in the west Pacific, sea level is correspondingly high in the west and low in the east. Near the end of year -1 westerly wind anomalies occur west of the dateline, and sea level slope along the equator begins to relax. SST begins to rise off the South American coast, as in the normal seasonal cycle. During year 0 SST at the east coast then continues to increase until about June; the peak SST anomaly then moves offshore as the positive SST anomaly spreads westward along the equator, merging with a smaller central Pacific anomaly. A rise in sea-level propagates polewards along the American coast, as coastally trapped waves. Westerly wind anomalies are found along the equator, sea-level generally falls in the west and rises in the east Pacific, and the strength of the Equatorial Undercurrent is reduced. The ITCZ is south of its usual position and the SPCZ is displaced northeastward; accordingly rainfall is enhanced in the tropical eastern and central Pacific, and is below normal over Indonesia. Effectively the upward branch of the Walker circulation moves to the central Pacific from the west Pacific.

Conditions return to normal in the following year, with a decrease in SST spreading west along the equator.

The timing and nature of the changes in sea-level are consistent with an oceanic Kelvin and Rossby wave response to weakening tradewinds near the equator. The SST changes along the equator can be related to a weaker South Equatorial Current and reduced upwelling. Gill (1983) used a shallow-water model to deduce the evolution of oceanic anomalies during the 1972 El Nino from sea-level observations at the east coast.

5.3 The 1982-83 El Nino

The indicators in Fig. 5.4 show that the 1982-1983 El Nino was an extreme event. It was relatively well observed (but not well enough to unambiguously trace its cause) —— see Gill & Rasmusson (1983), Cane (1983), Rasmusson & Wallace (1983), Barber & Chavez (1983), Philander (1983), Quiroz (1983) for example.

This event differed from the usual pattern in many ways. The usual precursors were absent, so its occurrence was unexpected. As can be seen in Fig. 5.7b, anomalous SST increases occurred simultaneously across the central and eastern Pacific, rather than spreading from the east coast. Warming at the east coast began around June, rather than the usual January start. Fig. 5.8 shows an eastward surge of warm SST (actual value, rather than the anomaly) bringing 28° water right up to the east coast, accompanied by anomalous rainfall and westerly winds. The change is shown schematically in Fig. 5.9. Fig. 5.10 shows the large area of the central and eastern Pacific affected by this SST change. Accompanying changes in sea-level are shown in Fig. 5.11 (Wyrtki 1984), reflecting the large movement of warm water to the east and changes in thermocline depth. The usual zonal pressure gradient disappears entirely in this extreme event,

as does the Equatorial Undercurrent (Firing et al. 1983).

How did such a strong event take place? It may have been self-amplified, given a start, in the following way. Anomalous latent heat release induces anomalous westerly winds to the west of the heated region (as seen in lecture 4); these westerly winds drive anomalous eastward surface currents in the ocean which advect warm water eastward, tending to move the region of latent heat release eastward, etc. Fig. 5.12 summarises the mechanisms involved. The process is terminated by oceanic Rossby waves reflecting from the east coast which oppose the eastward current anomaly (Gill & Rasmusson 1983).

5.4 Unstable modes in simple coupled models

Mechanisms such as the one outlined above have been investigated using simple coupled models. The simplest such models involve the linear SWE ocean and atmosphere with no boundaries, and these demonstrate the existence of amplifying coupled disturbances (Lau 1981, Philander et. al. 1984, Hirst 1986, Yamagata 1986). We briefly describe here some results from Hirst (1986).

His atmospheric component is essentially the same as the SWE model presented in lecture 4 (without moisture). The heating Q is not prescribed however, but is linearly related to sea surface temperature perturbations T' by

$$Q = K_Q T' \qquad (5.1)$$

where K_Q is a coupling coefficient with a value observationally based on an excess rainfall of 11 cm/month for each °C of SST increase. A damping time of 2.5 days and a gravity wave speed c=30 m sec-1 were used for the

atmosphere. (With this rapid damping the atmosphere is effectively in equilibrium with the underlying ocean, which changes on a much longer time scale.)

The ocean component is a shallow-water ocean with Rayleigh friction and Newtonian 'cooling'. The damping time is about 100 days, and the gravity wave speed is 1.4 m sec-1. (A range of values was actually used with qualitatively similar results.) Low-level winds $\underline{u}_a$ from the atmosphere model provide the surface stress to force the ocean, as a body force

$$(F,G) = K_S \, \underline{u}_a \qquad (5.2)$$

where K_S is about 140 day-1.

Thermodynamics is included in the linearised form

$$T'_t + u \, \overline{T}_x = K_T \, h' - \varepsilon \, T' \qquad (5.3)$$

where T' represents a perturbation in the upper layer (hence surface) temperature, h' is the upper layer depth perturbation, and u is the zonal ocean current. The upper layer has a mean temperature $\overline{T}$ which can have a zonal gradient (as in the normal Pacific Ocean), so T' can change due to zonal advection. . The term K_T h' represents the warming that can occur when the thermocline deepens, as observed, due to the upwelling of (relatively) warmer water within the upper layer (rather than cooler water upwelling from below the thermocline). Typical values are $\overline{T}_x \approx -0.5$ °C /1000 Km , and $K_T \approx 3.5 \times 10^{-9}$ °C m-1 sec-1 (obtained by linearising a standard mixed-layer model). Linear damping again has a timescale of about 100 days.

Temperature variations are ignored in the calculation of pressure gradient in the momentum equations however, as depth change effects dominate. Thus the ocean circulation is controlled by the usual 'shallow-water' equations

$$\underline{u}_t + f\underline{k} \times \underline{u} = -g' \nabla h' - \varepsilon \underline{u} + K_s \underline{u}_a \ , \qquad (5.3a)$$

$$h'_t + H(u_x + v_y) = -\varepsilon h' \ . \qquad (5.3b)$$

An energy analysis shows that the atmosphere gains energy if the heating Q (proportional to T') is positively correlated with warmer air, and this is the energy source for growing coupled disturbances. The ocean also gains energy if wind stress and upper layer currents are positively correlated (i.e. are oriented in roughly the same direction).

We will look at two cases representing different mechanisms for ocean temperature change.

I Local thermal equilibrium

When the terms on the right of (5.2) balance we have

$$T' = (K_T / \varepsilon)\, h' \qquad (5.4)$$

which can be regarded as a diagnostic equation for T'. This balance is most likely to occur where mixed-layer depth is small.

Typically, atmospheric waves are virtually unaffected by the addition of an ocean —— timescales for these waves are too short for the ocean to respond significantly and feed back to the atmosphere. Oceanic Kelvin, Yanai and Rossby waves are affected by the addition of an atmosphere

however. In this case, as $K_Q K_S$ is increased a Kelvin-like mode becomes unstable, Yanai waves are less damped, and Rossby waves are more damped. This behaviour can be explained by looking at the structure of these waves for a section along the equator —— see Fig. 5.13a.

For the Kelvin wave, h' and u have the same sign, as seen in lecture 2. Hence (from eq. (5.4)) warm SST is associated with eastward current, and vice-versa. This warm SST causes latent heating of the atmosphere such that low-level westerlies largely overly the eastward currents. Thus the ocean disturbance is amplified, which increases h' and hence T' and hence Q and hence...etc. The pattern as a whole moves eastward at a speed somewhat slower than a free oceanic Kelvin wave.

For the Rossby wave (mode n=1 symmetric about the equator) h' and u have opposite sign, so warm SST is associated with westward currents. This westward current is opposed by the surface westerlies generated in the atmosphere, and the coupled mode decays.

Horizontal structure of these waves is shown in Fig. 5.14; as one would expect, the atmospheric component has a much larger meridional scale than the oceanic component.

II Thermal advection limit

For a deep mixed-layer situated in a region of mean surface temperature gradient, temperature perturbations are mainly due to advection. Ignoring upwelling effects in (5.3) leaves

$$T'_t + u \overline{T}_x = - \varepsilon T' \qquad (5.5)$$

Again ocean waves are influenced by the coupling, but now the effect is very different. The Kelvin wave decays while the Rossby wave is unstable (the more so for increasing wavelength). Vertical structure can be seen in Fig. 5.13b. Effectively the $u\overline{T}_x$ dependence of T' shifts SST perturbations (and hence atmospheric heating Q) by a quarter wavelength compared to case I. Surface currents and low-level winds now have a negative correlation for the Kelvin wave, positive for the Rossby mode. The net effect is an unstable pattern that propagates westward.

Thus different physical mechanisms for generating SST anomalies can have very different stability properties.

5.5 More simple coupled models, with boundaries

The above model is useful for exploring the type of situations that allow a disturbance to amplify. Other coupled models have been developed with the aim of explaining the quasiperiodic nature of El Nino. Effects such as oscillations of a sloping thermocline, the time for waves to cross the Pacific and reflections from coasts are important in these models, so east and west coasts for the oceanic component are included. Continental effects are also sometimes included in the atmospheric component. McCreary (1983), McCreary & Anderson (1984) and Anderson & McCreary (1985) is a series of such models with simple SWE ocean dynamics and increasingly sophisticated (well, less crude) thermodynamics. These models are nonlinear, and disturbances grow to a finite amplitude and decay again, rather than growing indefinitely as in the previous section. The 1985 paper contains an equilibrium SWE atmosphere (atmospheric winds were parameterised in the 1983 and 1984 articles) and in that case disturbances could develop in the western or central 'Pacific', propagate slowly eastward, and vanish at the eastern boundary while a new disturbance grew

to the west (see Fig. 5.15). Such features are typical of ENSO, however other details do not agree with observations (e.g. onset is too slow, oscillations are too regular). Interestingly, disturbances do not amplify in narrower oceans, e.g. model 'Indian' or 'Atlantic'.

For other varieties of simple coupled models see for example Gill (1985), Schopf & Suarez (1986). Another model that has received considerable attention is that by Cane & Zebiak (1985). Only an outline is given in this reference; details are in a series of papers soon to appear.

In the Cane & Zebiak model the mean seasonal cycle is prescribed and the aim is to simulate and predict perturbations from that state. The atmosphere is an equilibrium SWE model with iteration to take into account the interdependence of latent heating and circulation. The heating pattern is influenced by the prescribed mean convergence field. The ocean model has circulation dynamics and thermodynamics separated. Circulation is controlled by an SWE model with an embedded wind-drived mixed layer of constant depth. The thermodynamics includes upwelling, advection, and surface heat flux. Upwelling is parameterised in a way that takes into account mean thermocline depth and temperatures. Irregular oscillations occur in this coupled model with features similar to observed El Nino events.

This model has been used to successfully hindcast El Nino events. The method is to force the ocean with the observed winds (thus building up a realistic thermocline anomaly), then to let the model run freely in coupled mode (subject to the prescribed mean annual cycle). By this means the past few ENSO events have been successfully hindcast several months (and even years) in advance. Evidently the state of the ocean thermocline (a measure of heat storage) contains enough information for such a

prediction.

Such results encourage the belief that El Nino events can be successfully predicted, and hopefully coupled general circulation models (such as that developed in Met. O. 20) will enable quantitatively useful long-range forecasts to be made.

References (lecture 5)

Anderson, D.L.T. & J.P.McCreary (1985)
Slowly propagating disturbances in a coupled ocean-atmosphere model.
J. Atmos. Sci., 42, 615-629

Barber, R.T. & F.B.Chavez (1983)
Biological consequences of El Nino.
Science, 222, 1203-1210

Cane,M.A. (1983)
Oceanographic events during El Nino.
Science, 222, 1189-1195

Cane, M.A. & S.E. Zebiak (1985)
A theory for El Nino and the Southern Oscillation.
Science, 228, 1085-1087

Firing, E., R.Lukas, J.Sadler & K.Wyrtki (1983)
Equatorial Undercurrent disappears during 1982-1983 El Nino.
Science, 222, 1121-1123

Gill, A.E. & E.M.Rasmusson (1983)
The 1982-83 climate anomaly in the equatorial Pacific.
Nature, 306, 229-234

Gill, A.E. (1983)
An estimation of sea-level and surface-current anomalies during the 1972 El Nino, and consequent thermal effects.
J. Phys. Oceanog., 13, 586-606

Gill, A.E. (1985)
An overview of the dynamics of the tropical oceans and global atmosphere.
In: International Conference on the TOGA Scientific Programme.
WCRP Publication Series No. 4. WMO/TD 65. pp1.1-1.12

Gill, A.E. (1985)
Elements of coupled ocean-atmosphere models for the tropics.
In: Coupled Ocean Atmosphere Models (Nihoul ed.),
Elsevier Oceanography Series, Vol.40, pp 303-327

Hirst, A.C. (1986)
Unstable and damped equatorial models in simple coupled ocean-atmosphere models.
J. Atmos. Sci., 43, 606-630.

Lau, K.M. (1981)
Oscillations in a simple equatorial climate system.
J. Atmos. Sci., 38, 248-261

Lukas R., S.P. Hayes & K. Wyrtki (1984)
Equatorial sea level response during the 1982-1983 El Nino.
J. Geophys. Res. 89, 10425-10430

McCreary, J.P. (1983)
A model of tropical ocean-atmosphere interaction.
Mon. Weath. Rev., 111, 370-387

McCreary, J.P. & D.L.T. Anderson (1984)
A simple model of El Nino and the Southern Oscillation.
Mon. Weath. Rev., 112, 934-946

Oceanus 27 (1984) is devoted to El Nino, principally the 1982-83 event.

Philander, S.G.H. (1983)
El Nino Southern Oscillation phenomena.
Nature, 302, 295-301

Philander, S.G.H., T. Yamagata & R.C.Pacanowski (1984)
Unstable air-sea interactions in the tropics.
J. Atmos. Sci., 41, 604-613

Quiroz, R.S. (1983)
The climate of 'El Nino' winter of 1982-83. A season of extraordinary climate anomalies.
Mon. Weath. Rev., 111, 1685-1706

Rasmusson, E.M. & T.H.Carpenter (1982)
Variation in tropical sea surface temperature and surface wind fields associated with the Southern Oscillation/El Nino.
Mon. Weath. Rev., 110, 354-384

Rasmusson, E.M. & J.M. Wallace (1983)
Meteorological aspects of the El Nino/Southern Oscillation.
Science, 222, 1195-1202

Rasmusson, E.M. (1985)
Climate variability and the Southern Oscillation.
In: International Conference on the TOGA Scientific Programme.
WCRP Publication Series No.4. WMO/TD 65. pp 3.11-3.21

Schopf, P.S. & M.J. Suarez (1986)
Vacillations in a coupled tropical ocean-global atmosphere model.
Ocean Modelling Newsletter, 69, 1-6.

Wallace, J.M. (1985)
Atmospheric response to equatorial sea-surface temperature anomalies.
In: International Conference on the TOGA scientific Programme.
WCRP Publication Series No.4. WMO/TD 65. pp 2.1-2.12

Wyrtki,K. (1984)
The slope of sea level along the eqautor during the 1982/83 El Nino.
J. Geophys. Res., 89, 10419-10424

Yamagata, T. (1986)
On the recent development of simple coupled models of ENSO.
J. Ocean. Soc. Jap. (to appear)

Fig. 5.1 Mean surface wind stress for (a) February (b) August
(From Gill 1982)

Fig. 5.2 (a) Mean sea surface temperature for January and July.
(b) Monthly mean sea surface temperature in a section along the equator to 95°W, then to the Peru coast at 8°S, following the line of maximum SST anomalies.
(From Rasmusson 1985)

Fig. 5.3 Mean outgoing longwave radiation for December-February, and June-August.
(From Rasmusson 1985)

Fig. 5.4 Southern Oscillation Index (anomalous Tahiti-Darwin surface pressure difference) is the dashed line. The solid line is a measure of sea surface temperature at Puerto Chicama, Peru. Major ENSO events are shaded. Note particularly 1982-83.
(From Rasmusson 1985)

Fig. 5.5 Typical anomalies during an ENSO event.
(From Rasmusson 1985)

Fig. 5.6 Sea surface temperature anomalies for a composite El Nino.
(From Philander 1983)

Fig. 5.7 Sea surface temperature anomalies along the equator to 95°W, then to Peru at 8°S.
(a) composite for 1957,1965 and 1972 events
(b) the 1982-83 event.
Units are 0.1°C.
(From Rasmusson 1985)

Fig. 5.8 The 1982-83 El Nino:
(a) monthly mean sea surface temperature along the equator to 95°W, then to Peru at 8°S.
(b) monthly mean low level zonal wind anomalies along the equator.
(c) monthly mean outgoing longwave rediation anomalies along the equator
(From Rasmusson 1985)

Fig. 5.9 Sketch of the changes along the Pacific equator from normal to late 1982 conditions.
(From Gill 1985)

Fig. 5.10 Sea surface temperature patterns and the 1982-83 anomaly. Contour internal is 1 C.
(From Wallace 1985)

Fig. 5.11 (a) Zonal wind speed at 850 mb between 5°N and 5°S.
(note that positive values are westward here)
(b) Sea level (dynamic topography relative to 500 db) along the equator. Climatological average (solid) and 1982-83 values (dashed) are shown with units of dynamic centimetres.

Fig. 5.12 A summary of the processes associated with El Nino (from Wallace 1985)

Fig. 5.13 Structure along the equator of Kelvin and Rossby modes in a simple coupled model
(a) model I: local thermal equilibrium
(b) model II: thermal advection limit
(from Hirst 1986)

Fig. 5.14 Horizontal structure of the Kelvin and n=1 Rossby modes in a simple coupled model, showing lower level atmospheric pressure P (solid contours), ocean upper layer depth h (dashed), sea-surface temperature T (dotted), surface wind (solid arrows), and ocean current (dashed arrows). The unit of distance is 250 Km. (From Hirst 1986)

Fig. 5.15 Evolution along the equator of
(a) sea-surface temperature
(b) thermocline depth
(c) zonal wind stress
in the Anderson & McCreary (1985) coupled model.
Warm SST, deep thermocline, and westerly winds occur in the crossed regions.

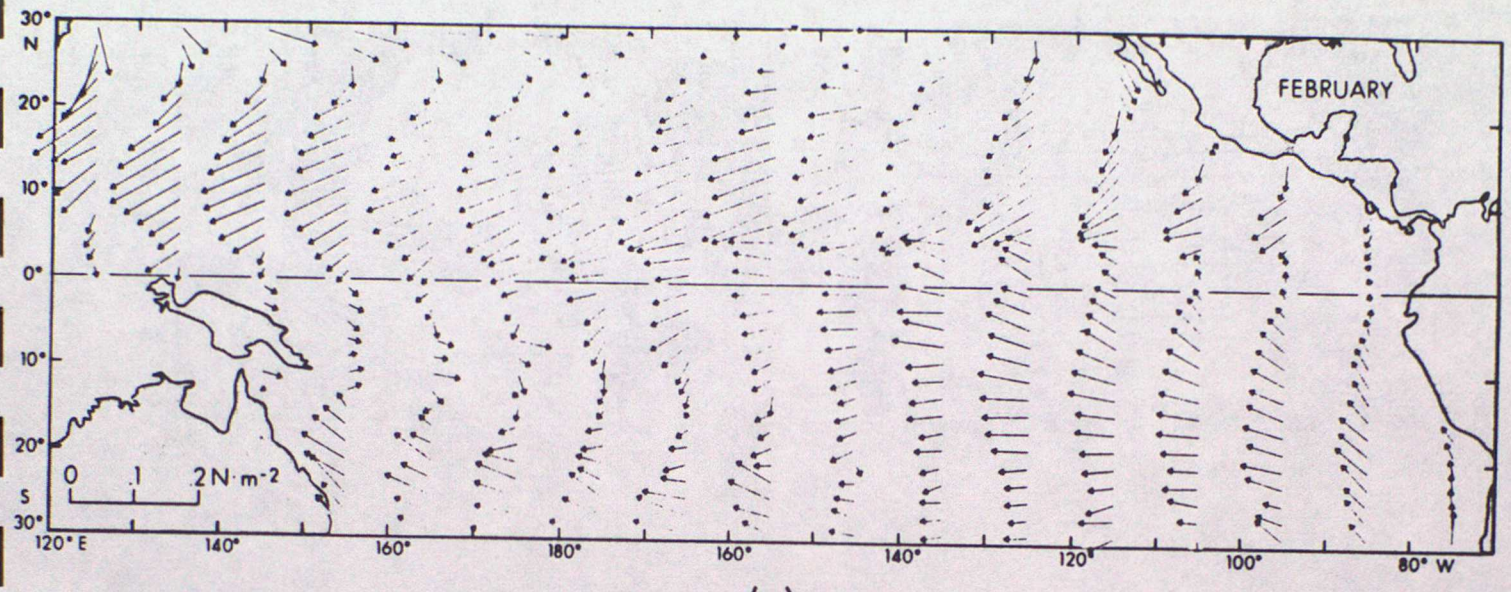

(a)

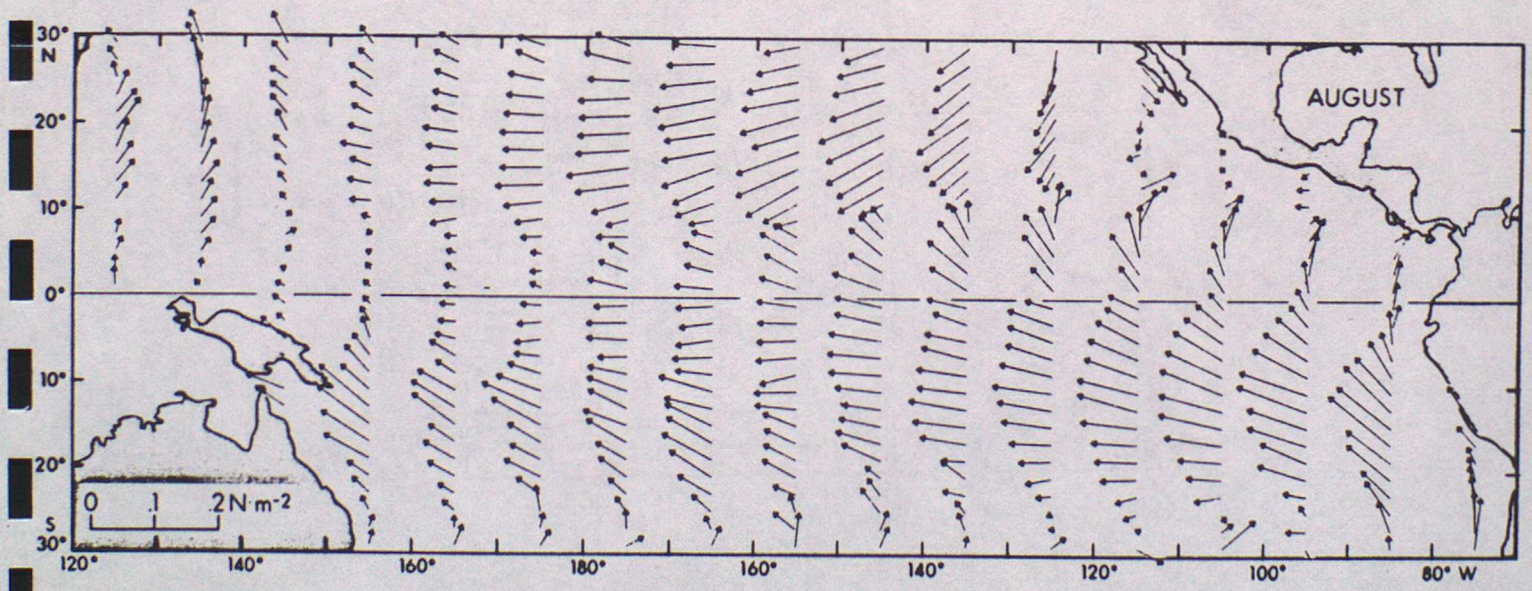

(b)

Fig. 5.1

surface wind stress climatology

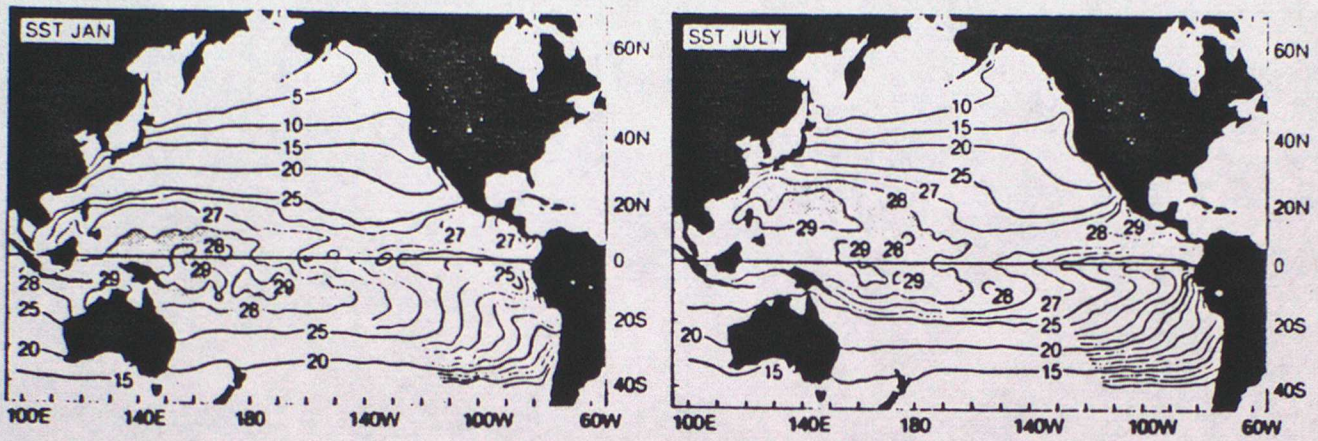

(a)

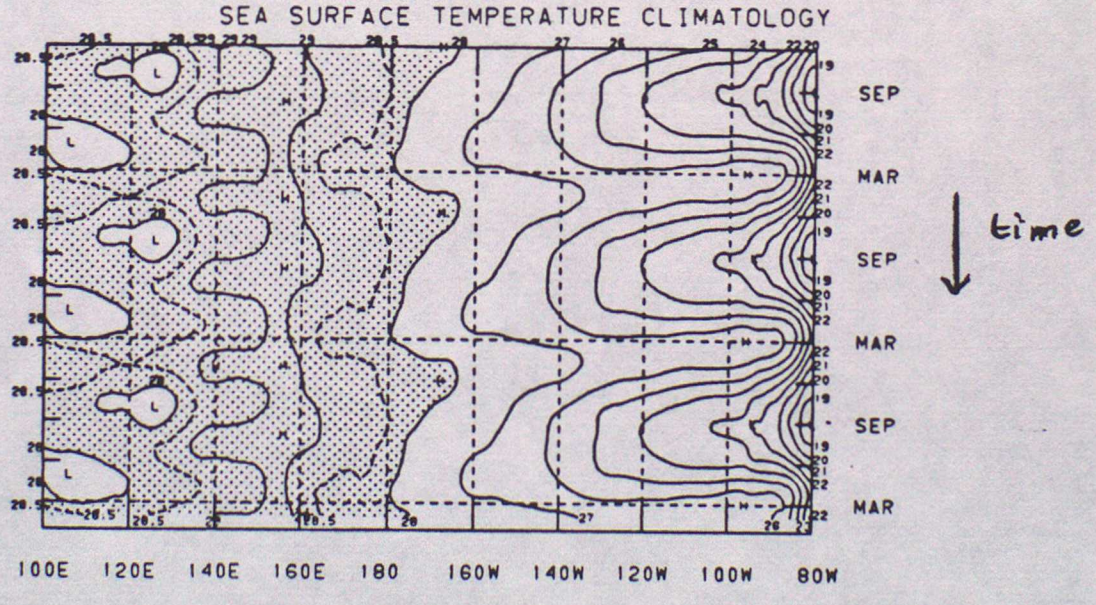

(b)

SST climatology

Fig. 5.2

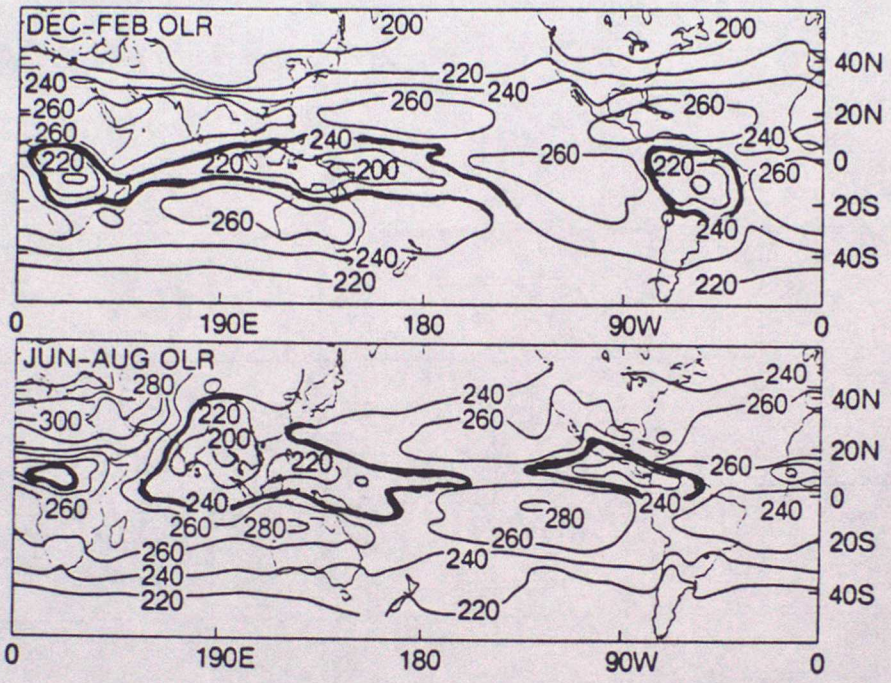

OLR climatology

Fig. 5-3

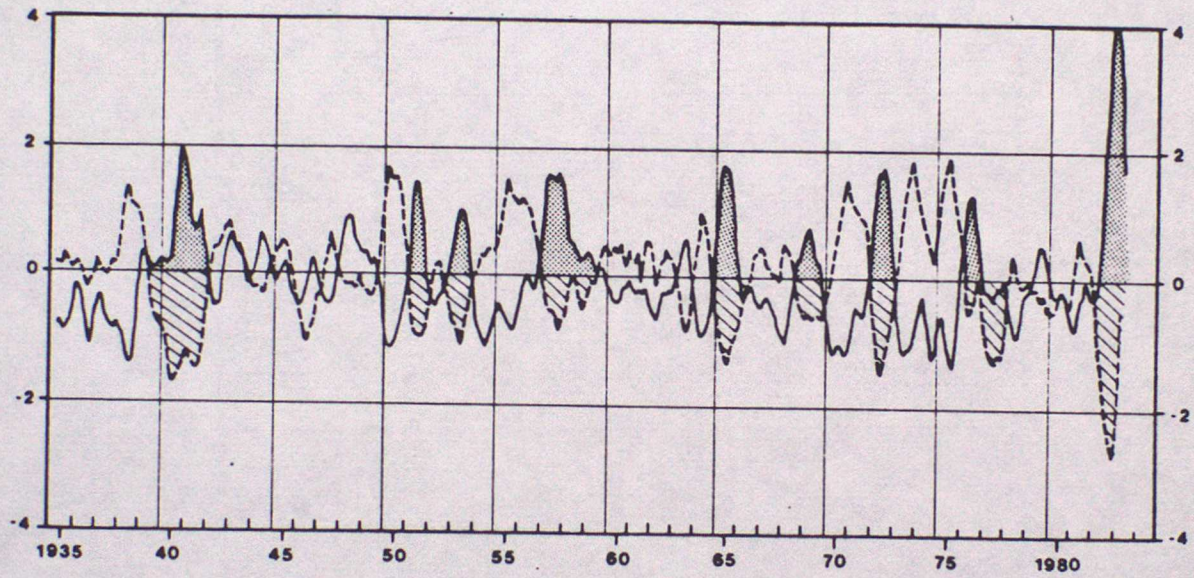

El Nino index ——

SO index - - - -

Fig. 5.4

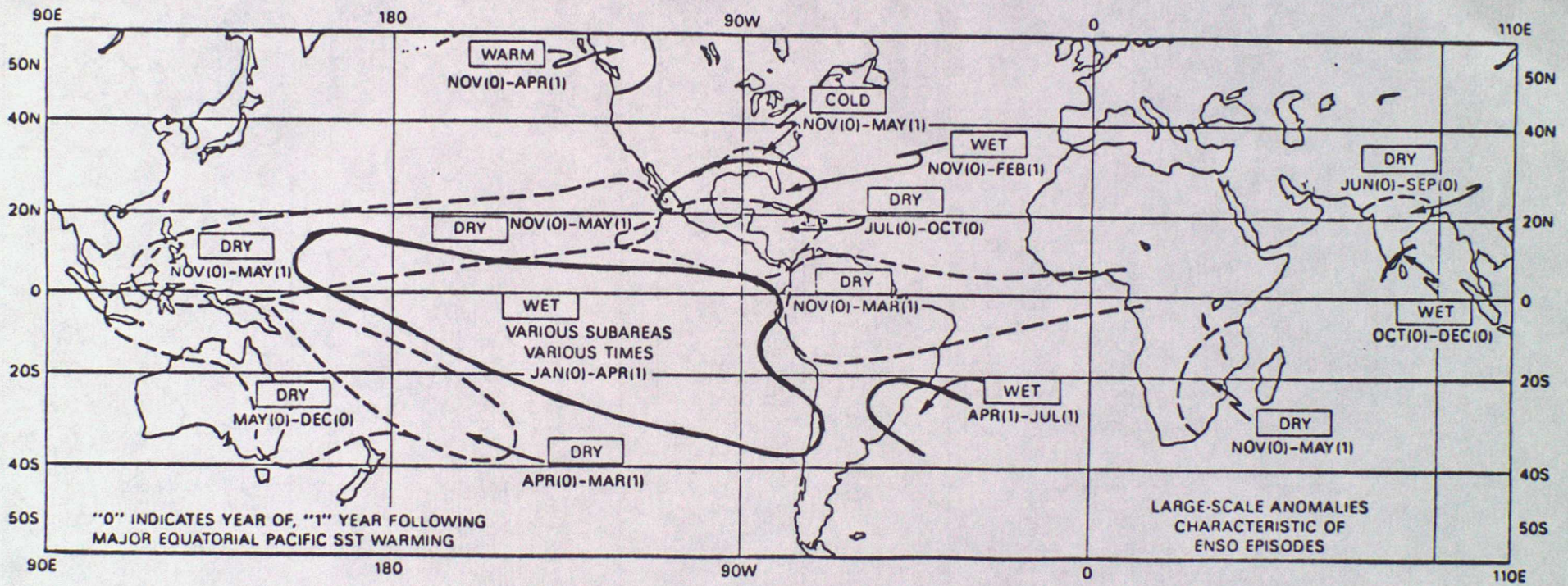
90E
180
90W
0
110E
50N
40N
20N
0
20S
40S
50S
WARM
NOV(0)-APR(1)
COLD
NOV(0)-MAY(1)
WET
NOV(0)-FEB(1)
DRY
JUL(0)-OCT(0)
DRY
NOV(0)-MAY(1)
DRY
NOV(0)-MAY(1)
DRY
NOV(0)-MAR(1)
WET
VARIOUS SUBAREAS
VARIOUS TIMES
JAN(0)-APR(1)
DRY
JUN(0)-SEP(0)
WET
OCT(0)-DEC(0)
DRY
MAY(0)-DEC(0)
DRY
APR(0)-MAR(1)
WET
APR(1)-JUL(1)
DRY
NOV(0)-MAY(1)
"0" INDICATES YEAR OF, "1" YEAR FOLLOWING
MAJOR EQUATORIAL PACIFIC SST WARMING
LARGE-SCALE ANOMALIES
CHARACTERISTIC OF
ENSO EPISODES

Fig. 5.5

March to May year 0

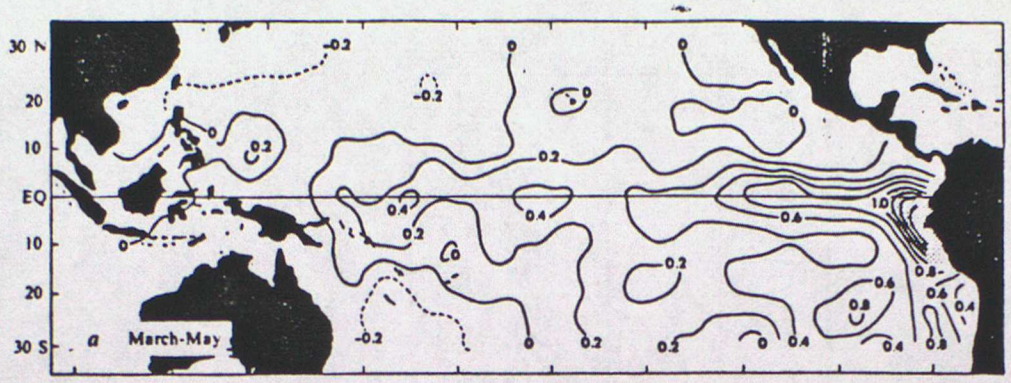

August (0) to October (0)

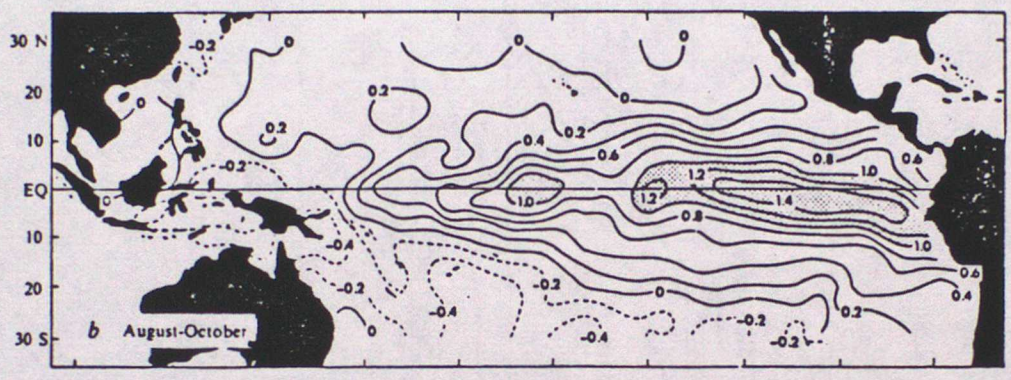

time

December (0) to February (1)

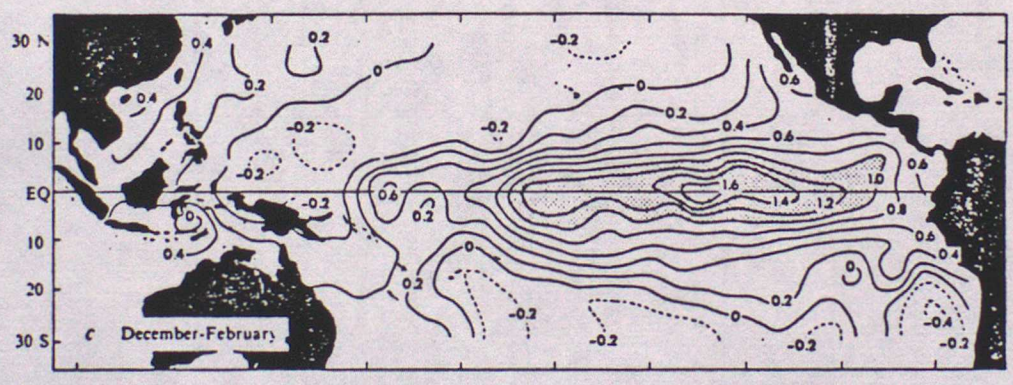

May (1) to July (1)

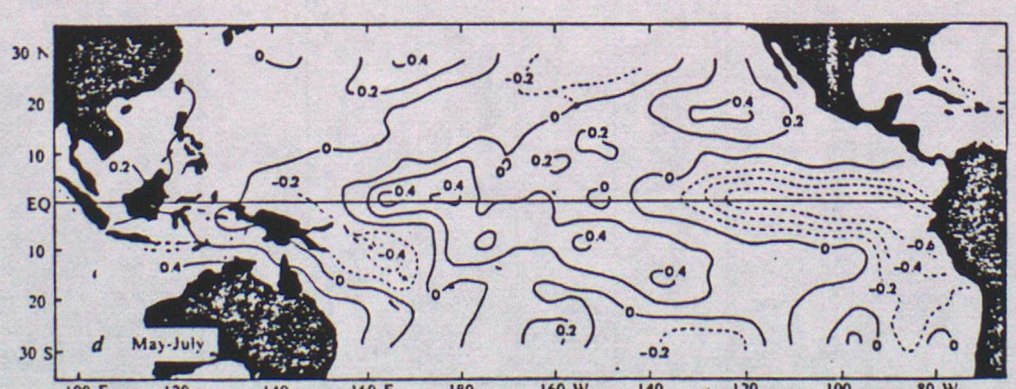

Composite El Nino

Fig. 5.6

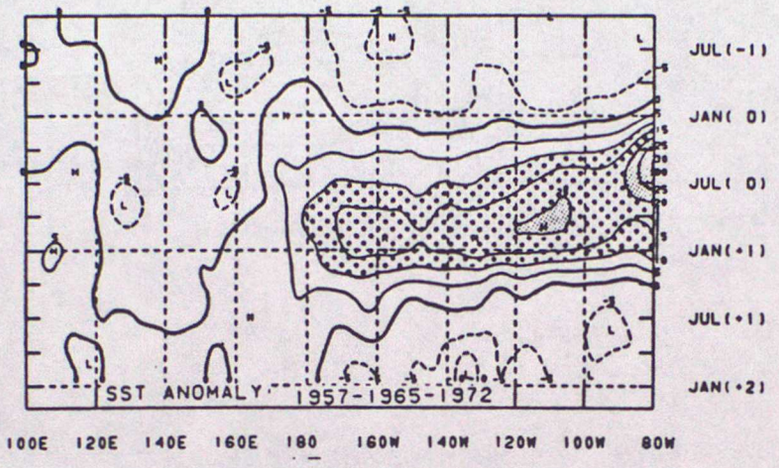

↓ time

(a) Composite El Nino

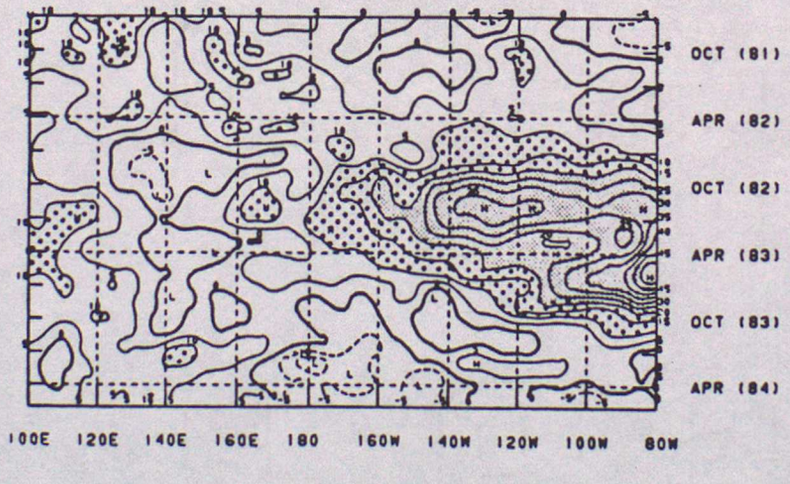

(b) 1982-83 El Nino

Fig. 5.7

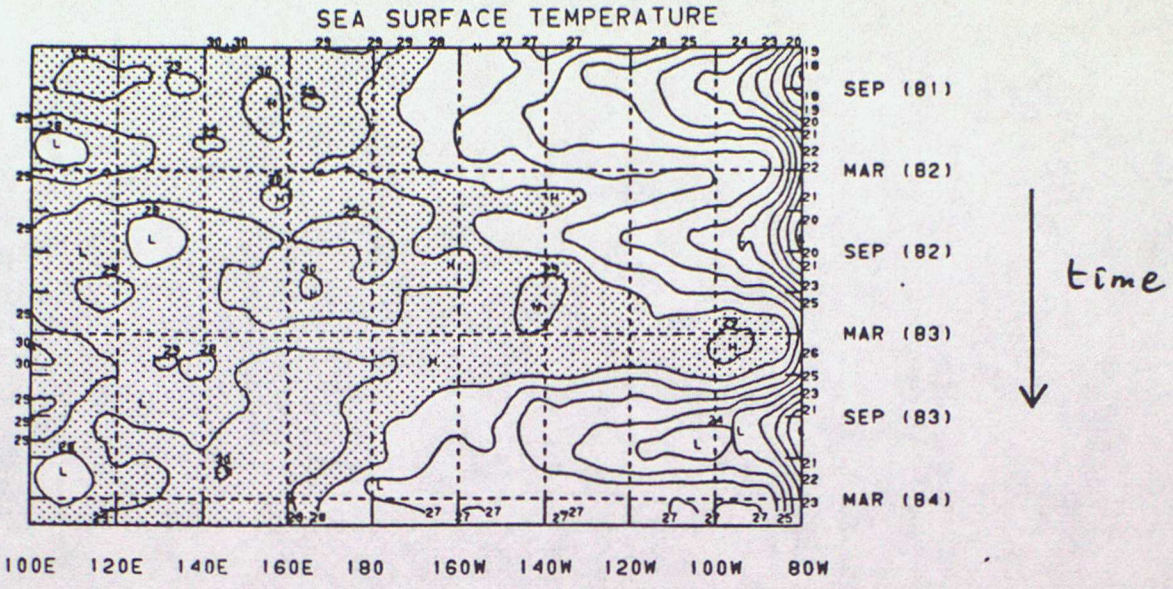
SEA SURFACE TEMPERATURE
SEP (81)
MAR (82)
SEP (82)
MAR (83)
SEP (83)
MAR (84)
time
100E 120E 140E 160E 180 160W 140W 120W 100W 80W

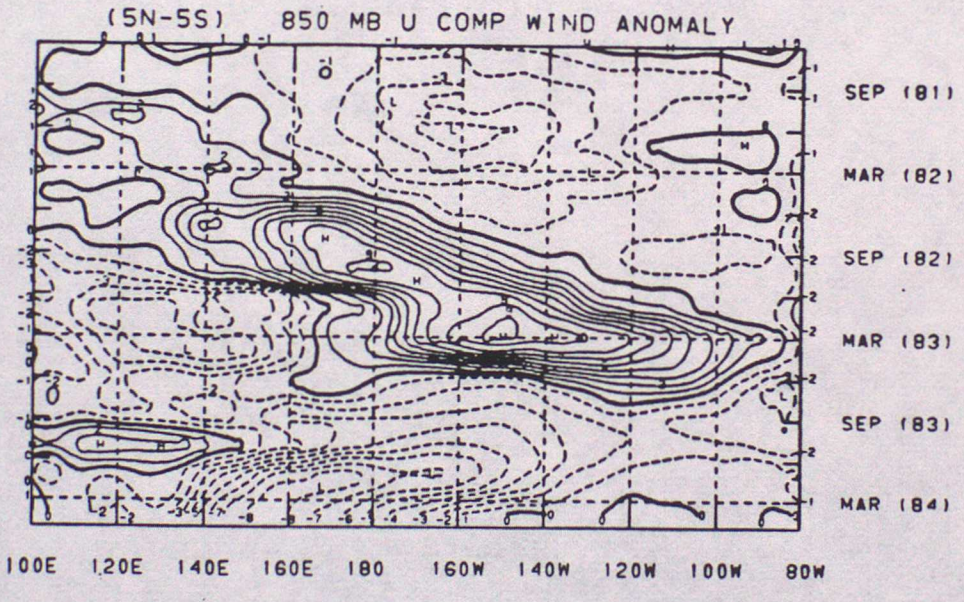
(5N-5S) 850 MB U COMP WIND ANOMALY
SEP (81)
MAR (82)
SEP (82)
MAR (83)
SEP (83)
MAR (84)
100E 120E 140E 160E 180 160W 140W 120W 100W 80W

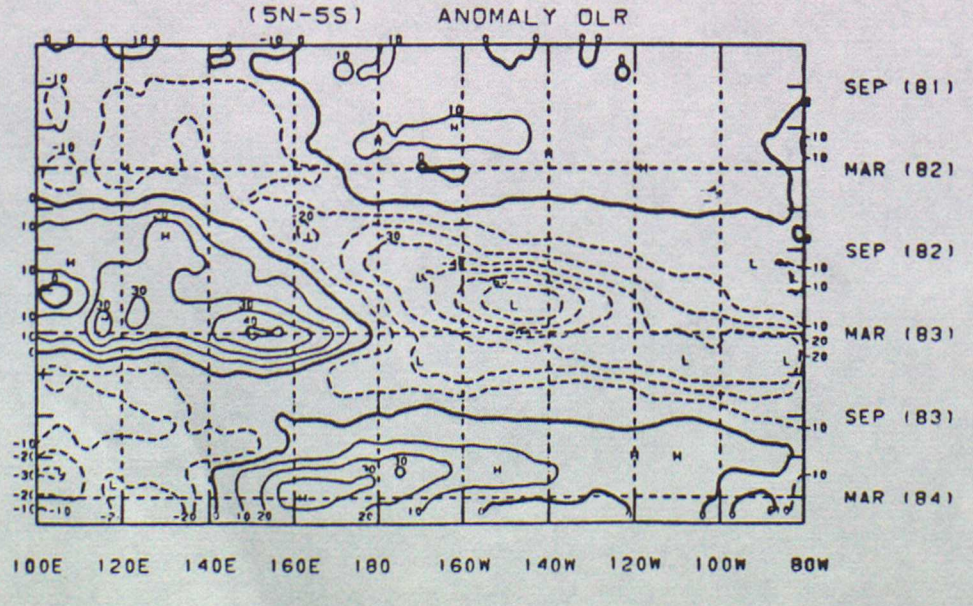
(5N-5S) ANOMALY OLR
SEP (81)
MAR (82)
SEP (82)
MAR (83)
SEP (83)
MAR (84)
100E 120E 140E 160E 180 160W 140W 120W 100W 80W

Fig. 5.

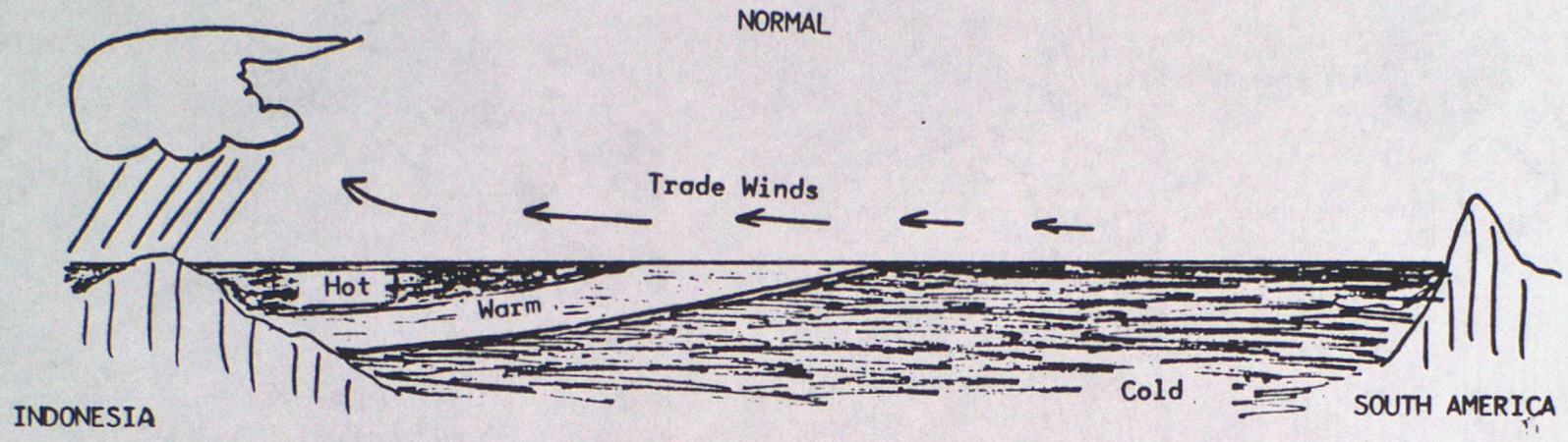
NORMAL
Trade Winds
Hot
Warm
Cold
INDONESIA
SOUTH AMERICA

1982

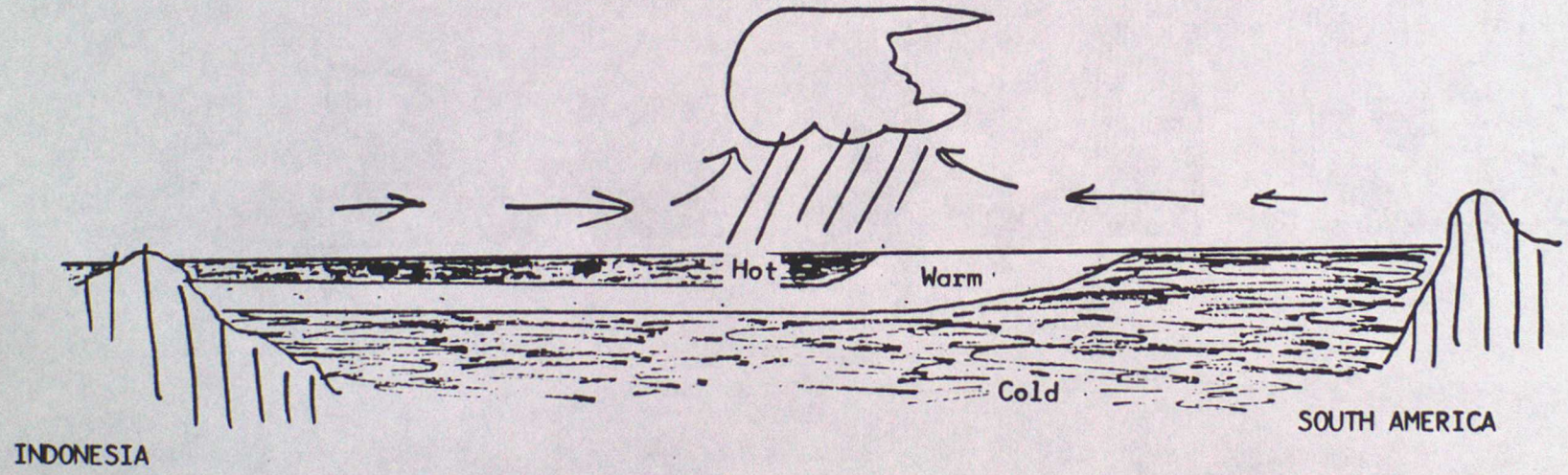
Hot
Warm
Cold
INDONESIA
SOUTH AMERICA

Fig. 5.9

Dec. 1982
to
Feb. 1983

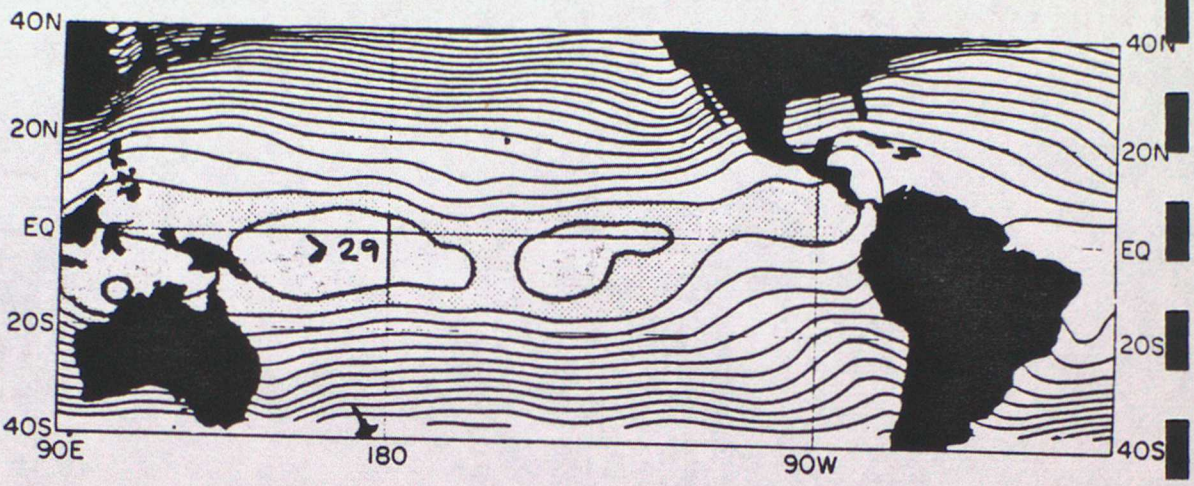

Dec. to Feb.
Climatology

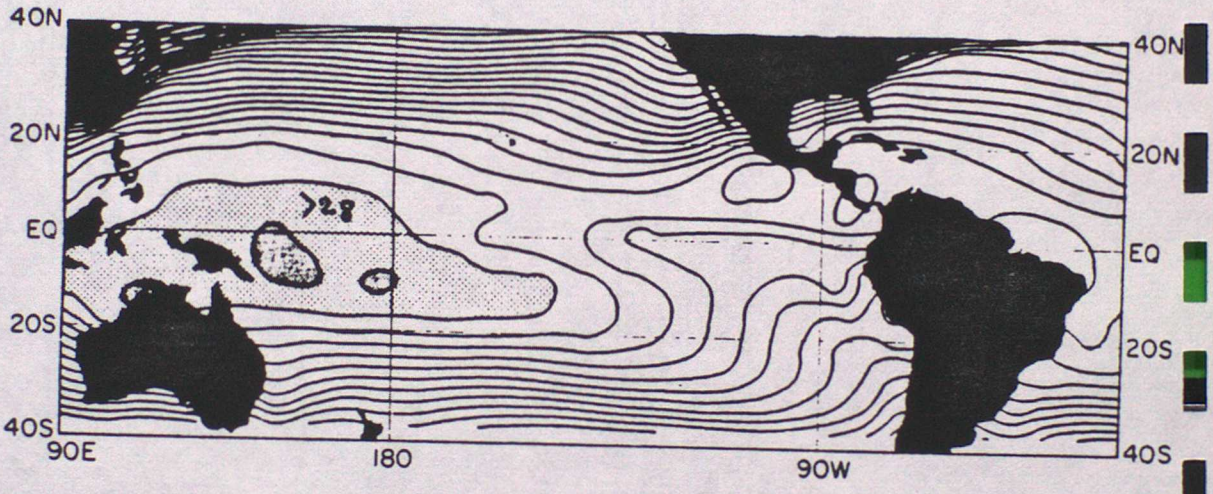

Dec. 1982
to
Feb. 1983

Anomalies

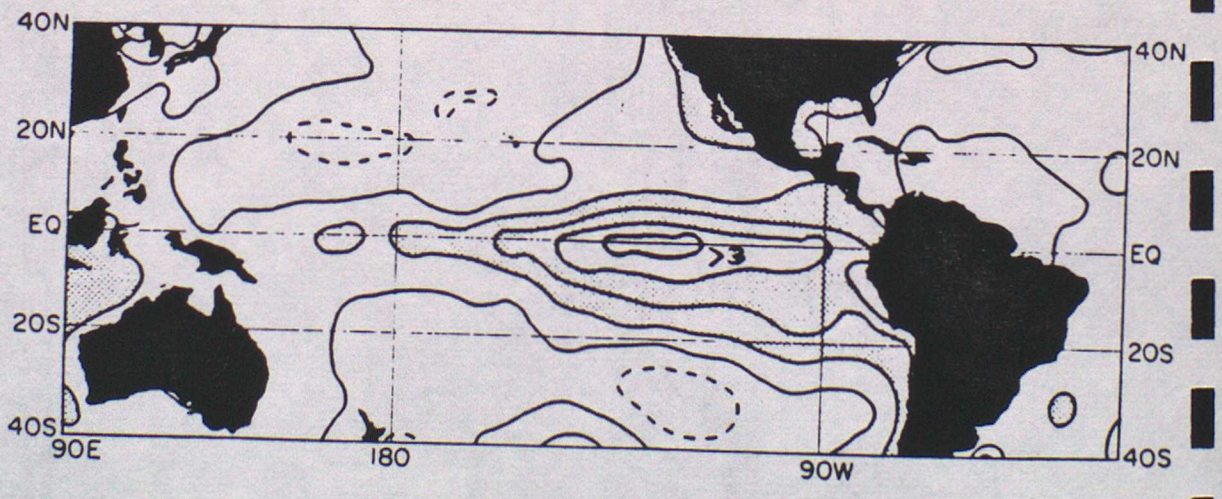

Sea Surface Temperature

Fig. 5.10

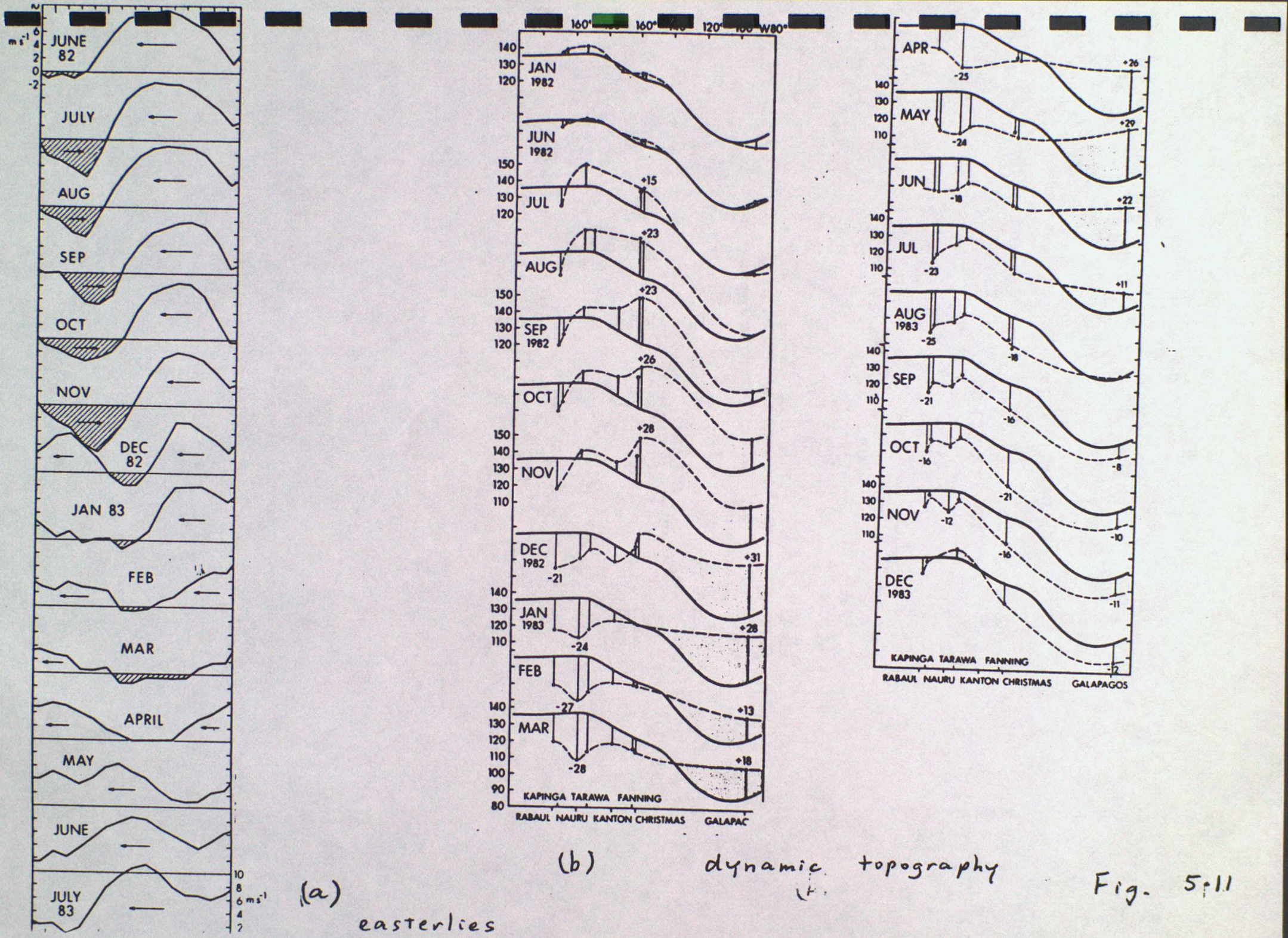

(a) easterlies

(b) dynamic topography

Fig. 5.11

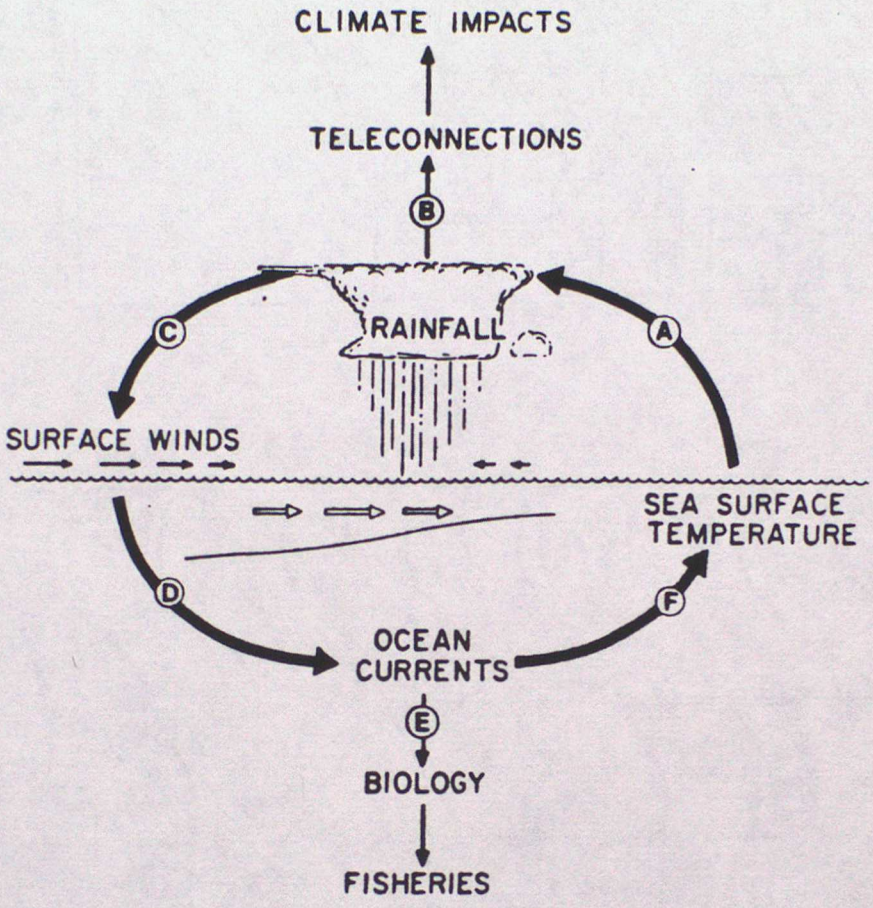

El Nino processes

Fig. 5.12

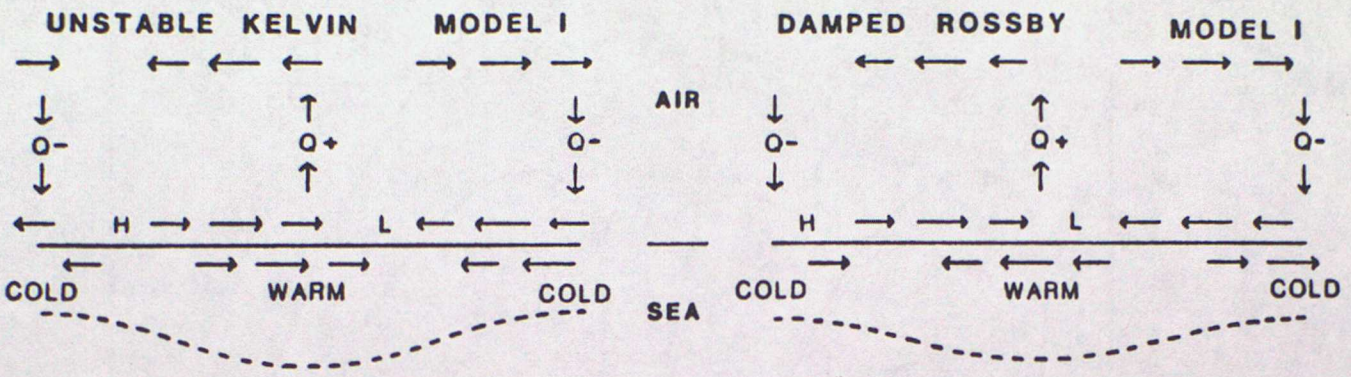
UNSTABLE KELVIN MODEL I
DAMPED ROSSBY MODEL I
AIR
SEA
Q-
Q+
H
L
COLD
WARM
COLD
COLD
WARM
COLD

(a)

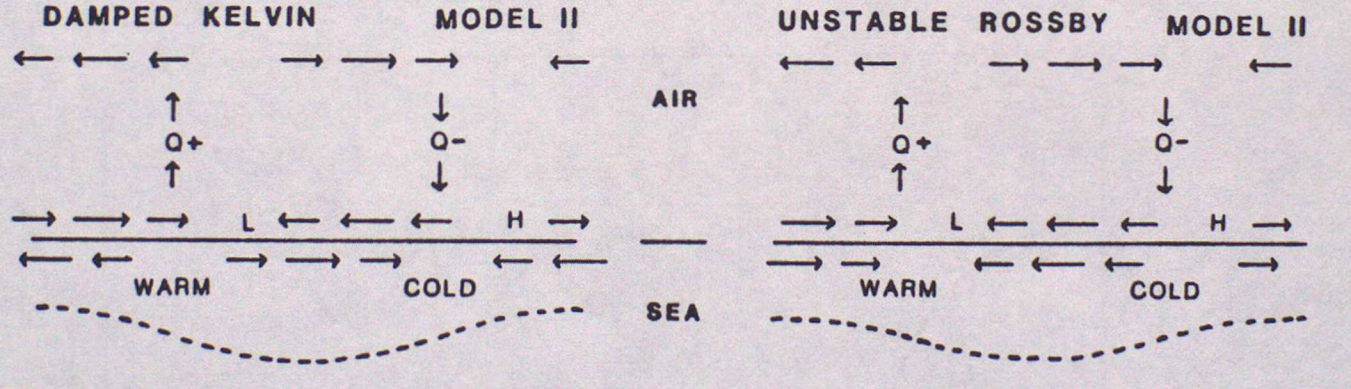
DAMPED KELVIN MODEL II
UNSTABLE ROSSBY MODEL II
AIR
SEA
Q+
Q-
L
H
WARM
COLD
WARM
COLD

(b)

Fig. 5-13

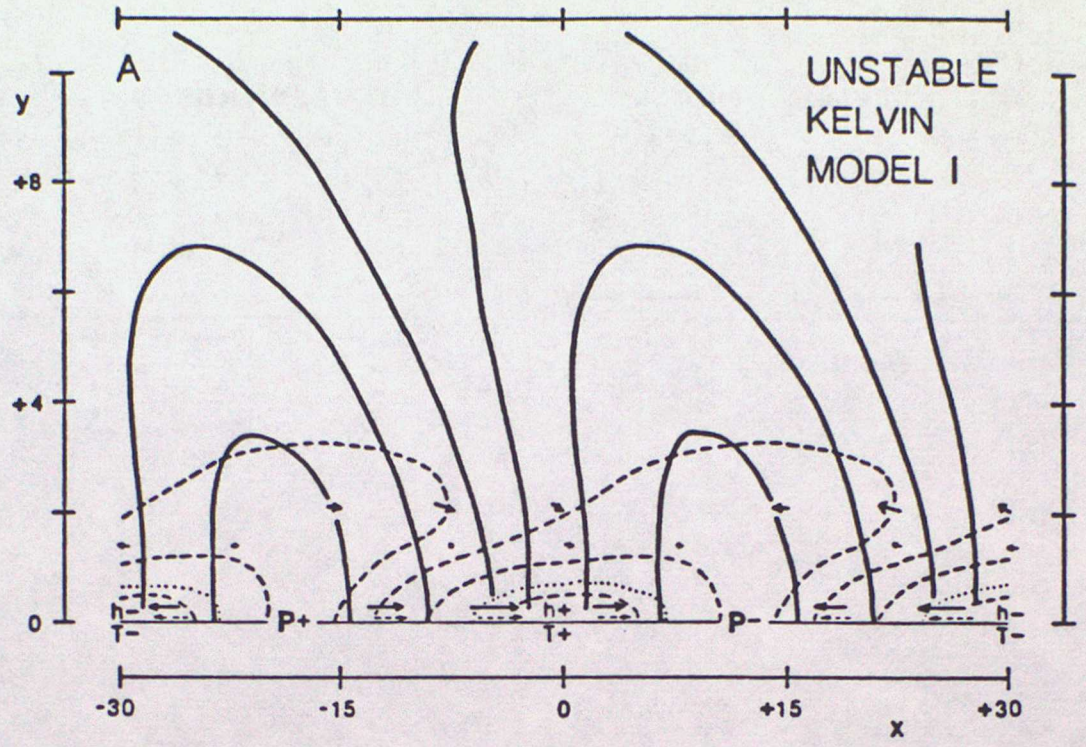
A
UNSTABLE
KELVIN
MODEL I
y
+8
+4
0
h−
T−
P+
h+
T+
P−
h−
T−
-30
-15
0
+15
+30
x

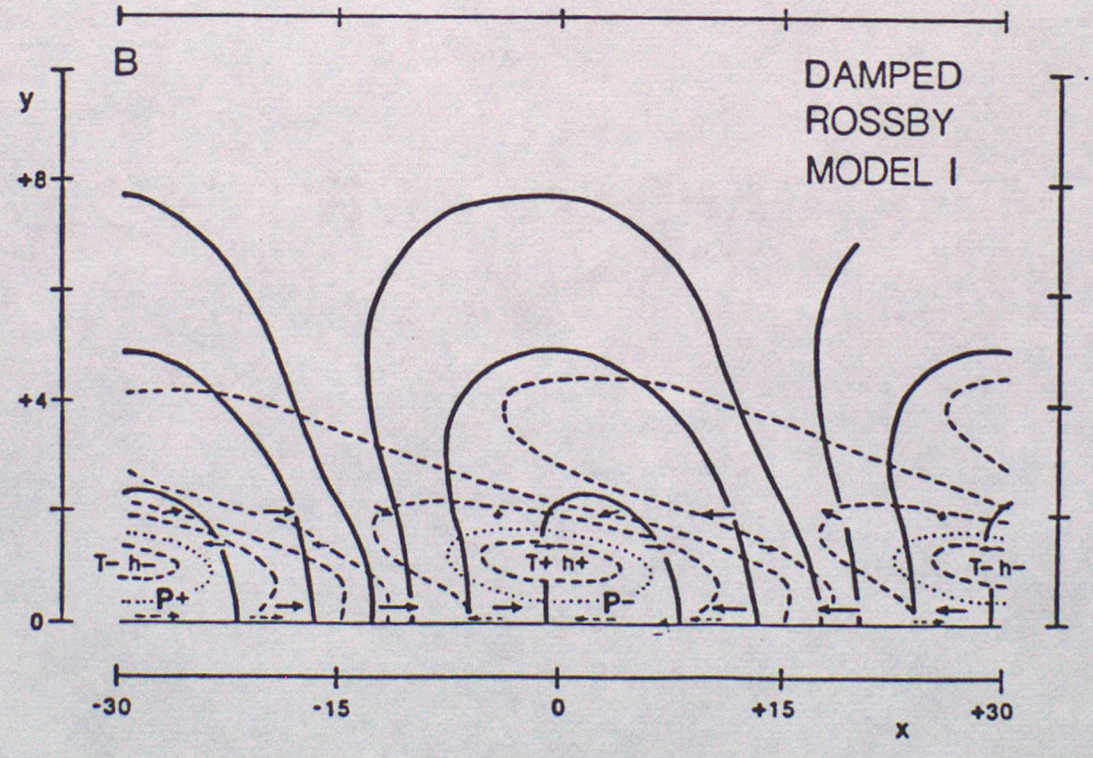
B
DAMPED
ROSSBY
MODEL I
y
+8
+4
0
T− h−
P+
T+ h+
P−
T− h−
-30
-15
0
+15
+30
x

Fig. 5.14

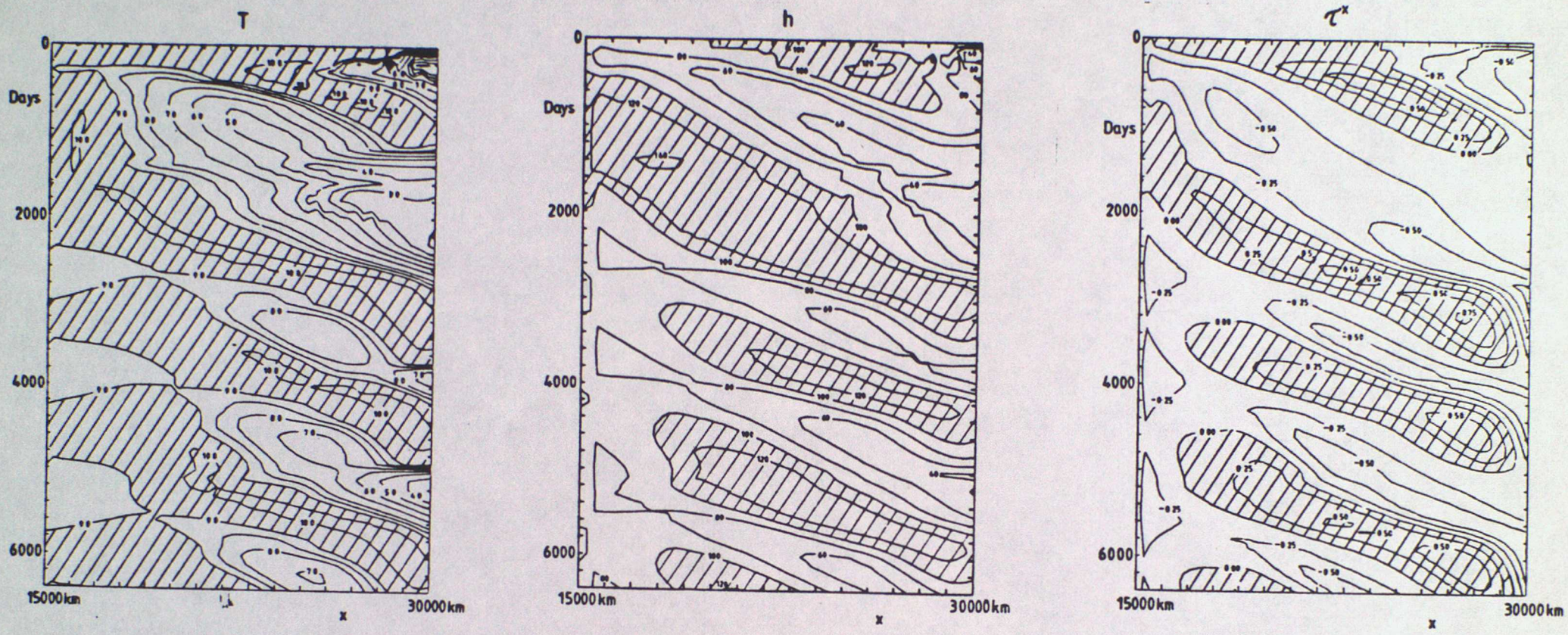

(a) (b) (c)

Fig. 5.15